Digital terrain analysis to predict soil spatial patterns at the Hubbard Brook Experimental Forest

Cody P. Gillin

Thesis submitted to the faculty of the Virginia Polytechnic Institute and State University in partial fulfillment of the requirements for the degree of

Master of Science
In
Forestry

Kevin J. McGuire, Chair
Scott W. Bailey
Stephen P. Prisley

April 26, 2013
Blacksburg, VA

Keywords: digital elevation model, LiDAR, topographic metrics, soil, hydropedology

Digital terrain analysis to predict soil spatial patterns at the Hubbard Brook Experimental Forest

Cody P. Gillin

Abstract: Topographic analysis using digital elevation models (DEMs) has become commonplace in soil and hydrologic modeling and analysis and there has been considerable assessment of the effects of grid resolution on topographic metrics using DEMs of 10 m resolution or coarser. However, examining fine-scale (i.e., 1-10 m) soil and hydrological variability of headwater catchments may require higher-resolution data that has only recently become available, and both DEM accuracy and the effects of different high-resolution DEMs on topographic metrics are relatively unknown. This study has two principle research components. First, an error analysis of two high-resolution DEMs derived from light detection and ranging (LiDAR) data covering the same headwater catchment was conducted to assess the applicability of such DEMs for modeling fine-scale environmental phenomena. Second, one LiDAR-derived DEM was selected for computing topographic metrics to predict fine-scale functional soil units termed hydropedological units (HPUs). HPU development is related to topographic and surface/subsurface heterogeneity resulting in distinct hydrologic flowpaths leading to variation of soil morphological expression. Although the two LiDAR datasets differed with respect to data collection methods and nominal post-spacing of ground returns, DEMs interpolated from each LiDAR dataset exhibited similar error. Grid resolution affected DEM-delineated catchment boundaries and the value of computed topographic metrics. The best topographic metrics for predicting HPUs were the topographic wetness index, bedrock-weighted upslope accumulated area, and Euclidean distance from bedrock. Predicting the spatial distribution of HPUs may provide a more comprehensive understanding of hydrological and biogeochemical functionality of headwater systems.

Acknowledgements

I wish to thank my parents, **Gary and Susan Gillin**, for their love and support. My passion for natural resource management is a direct result of the backpacking trips, fishing excursions, and mountaineering pursuits I've enjoyed with my Dad since I was a wee lad. My love of writing and environmental conservation was passed to me by my Mom, who taught me everything she knows about style, clarity, and caring for the earth. I love them both very much.

Kevin McGuire chaired my committee with a balanced approach – he pushed me to think critically and be self-reliant, but also offered support when I struggled with technology, statistics, or complicated hydrological concepts. His guidance made me a more precise writer and a more creative problem solver. With his help I enjoyed a successful tenure as a Master's Candidate, plan to publish several journal articles, and will embark on a career helping manage and conserve natural resources. I am forever grateful.

Scott Bailey and **Steve Prisley** proved valuable committee members and project collaborators time and again. Scott provided intimate knowledge of my research catchment and devoted many hours examining soil characterizations and DEM analyses. Steve was always available to tackle topographic metric computations and found ways to work around the nuances of spatial analysis software. Both were active during the development of my manuscripts and thesis. Their excitement and involvement in my work is rare among graduate committee members and has not gone underappreciated.

Many thanks to **JP Gannon**, who provided assistance with technology and in the field. Thanks to **Silene Deciucies**, **Geoff Schwaner**, **Rebecca Bourgault**, and **Errin Shoop-Volitis** for their help with field work. Thanks to **Valerie Thomas** for her knowledge of LiDAR data and Merrick Mars software. Thanks to **Mike Sorice** for assistance with logistic regression. Thanks to **Ranjith Gopalakrishnan** for his help with LAS Tools. Thanks to **Patricia Brousseau**, **Margaret Zimmer**, **Margaret Burns**, **Kaitland Harvey**, **Amey Bailey**, **Don Ross**, **and John Campbell** for providing data and for their contribution to the hydropedology project. And many thanks to **Andy Colter** for sharing LiDAR data collected for the White Mountain National Forest.

Financial support was provided by the National Science Foundation Long-Term Ecological Research Network (DEB 1114804) and Hydrologic Sciences (EAR 1014507) programs, as well as the Virginia Lakes and Watersheds Association. LiDAR data were collected as part of the National Center for Airborne Laser Mapping seed award program for the hydropedology project and by Photo Science, Inc. for the White Mountain National Forest. Hubbard Brook Experimental Forest context map data courtesy of the Hubbard Brook Ecosystem Study.

Special thanks to Maura Leveroos – success would not have been possible without her.

Table of Contents

Chapter Four

Appendices

List of Tables

List of Figures

Chapter One

1.0. Background

1.1. Problem context: The importance of headwater catchments

Headwater catchments comprise over 50% of the length of all streams in the United States [*Nadeau and Rains*, 2007], play a critical role in controlling water quality and quantity of downstream water bodies [*Alexander et al.*, 2007; *Nadeau and Rains*, 2007] and set the hydrological, chemical and biological foundation for downstream freshwater systems to which they contribute. Glaciers and snowpack that sustain river flows through dry summer months typically lie in headwater basins. Headwater soils store and transmit water between storm events and sustain baseflow during drought [*Hewlett and Hibbert*, 1963; *Ward and Robinson*, 2000]. The coupling of hydrological, landscape and biogeochemical processes regulate subsurface water storage, flow paths and residence time, as well as the chemical form and transport of solutes to downstream rivers [*Alexander et al.*, 2007]. Furthermore, intermittent, first and second order streams offer a range of habitats for permanent and migrant organisms and contribute to the biodiversity of entire river networks [*Finn et al.*, 2011; *Meyer et al.*, 2007].

The current paradigm of hydrologic science, that small-scale process understanding (such as a stream reach, soil core, or hillslope) may be used to quantify catchment processes, is frequently being challenged [*Troch et al.*, 2008]. While researchers have gained a comprehensive understanding of the behavior of small, homogenous systems over short time periods, more research is needed to understand system and process complexities and heterogeneity at the catchment-scale [*Wagener et al.*, 2010]. One promising method for enhancing an understanding of hydrological and biogeochemical pattern complexity in headwater catchments is through examination of soil spatial heterogeneity using a process-based framework. The movement and

distribution of water was long ago recognized as a major driver of pedogenesis [*Jenny*, 1941]. Hydrological processes control soil composition/morphology [*Daniels et al.*, 1975; *Knuteson et al.*, 1989] and affect the distribution of secondary metal compounds in a landscape [*McDaniel et al.*, 1992]. While traditional pedology conceptualizes vertical percolation through the landscape, recent research recognized lateral components to subsurface flow [*Park and Burt*, 2002; *Sommer and Schlichting*, 1997] leading to the development of distinct soil units [*Sommer et al.*, 2000]. Yet much soil data in headwater catchments comes from taxonomical soil surveys of coarse resolution that may not offer sufficient information about fine-scale (1-10 m) hydrological and biogeochemical functionality that provide signatures at hillslope and catchment scales.

1.2. Organization of thesis

This document is organized around two journal articles that will be submitted for publication in peer-reviewed scientific journals. The focus of the work centers on analyzing error associated with light detection and ranging (LiDAR) data and high-resolution digital elevation models (DEMs) interpolated from LiDAR data, as well as the applicability of such DEMs for predicting the distribution of fine-scale hydropedologial units (HPUs) in forested headwater catchments. Chapter one provides a comprehensive literature review to set the problem context, provide examples of methodologies reported in pertinent literature, and highlight previous work involving digital terrain modeling with pedologic and hydrologic emphases. Chapter two contains an article evaluating LiDAR and DEM error using topographic metrics, field observations, and detailed total station ground surveys. Chapter three contains an article using topographic metrics to predict soil spatial patterns. When viewed jointly, these manuscripts offer guidance for using high-resolution LiDAR-derived DEMs for the evaluation and prediction of fine-scale soil and hydrological phenomena. Chapter four provides a brief summary of the investigations, offers overall conclusions that may be interpreted from research findings, and suggests recommendations for future research. An appendix of supporting documentation, including tables, figures, digital terrain analysis procedures, and computer code comprises the final section of the document.

Section 2

Gillin, C.P., McGuire, K.J., Bailey, S.W., and Prisley, S.P. 2013. Evaluation of high-resolution LiDAR-derived DEMs through terrain analysis and field comparison. To be submitted to *Photogrammetric Engineering and Remote Sensing*.

Section 3

Gillin, C.P., McGuire, K.J., Bailey, S.W., and Prisley, S.P. 2013. Topographic metrics to predict hydropedologic spatial patterns. To be submitted to *Hydrological Processes* or *Catena*.

1.3. Literature review

1.3.1. Hydrologic processes as a driver of pedogenesis: From pedon to catchment

There are an array of factors that affect soil development, but none is more important than the abundance, flux, flowpath, and distribution of water in a landscape [*Daniels and Hammer*, 1992; *Jenny*, 1941; *Zaslavsky and Rogowski*, 1969]. Hydrologic properties and processes were long ago recognized as factors of soil development. These factors may be considered on a range of scales from pedon to catchment. Regionally, climate controls the amount of precipitation falling on a landscape, and at the catchment scale topography plays a major role in the process and rate by which water penetrates the soil surface and moves through the subsurface [*Jenny*, 1941]. At the soil unit and pedon scales, soil moisture has been shown to control soil composition and morphology [*Daniels et al.*, 1975; *Knuteson et al.*, 1989; *Zaslavsky and Rogowski*, 1969]. In some areas soil moisture is a dominant factor in the soil forming process [*Norris*, 1972; *Zhu et al.*, 2001]. Duration of soil saturation shows a relationship with observed color [*Franzmeier et al.*, 1983] and redoximorphic features [*Brouwer and Fitzpatrick*, 2002; *Morgan and Stolt*, 2006]. Soil chemical properties may also be modified by site hydrologic conditions. Eluviation and illuviation (transport and subsequent deposition of organic matter, silicate clays and certain weathered minerals across soil horizon boundaries) are water-assisted processes. Furthermore, the distribution of secondary metal compounds in a landscape indicates field-scale water movement [*McDaniel et al.*, 1992].

1.3.2. Lateral soil development processes

Traditional pedology tends to characterize water and solute transport through soils as vertical in nature [*Zaslavsky and Rogowski*, 1969]. Even where horizontal water movement is recognized, scientists contend that soil horizons change vertically [*Daniels and Hammer*, 1992].

Thus, a typical representation of a soil profile reflects vertical percolation and translocation of minerals and organic material leading to horizontal layering. The process by which dissolved organic matter precipitates with aluminum (Al) and iron (Fe) from an A or E soil horizon to a B horizon is called podzolization. Spodosols are the soil order exhibiting the most intense podzolization characteristics [*Sauer et al*. 2007; *Sommer et al*. 2000]. These are the dominant soils of the boreal zone in the northern hemisphere but also occur in temperate humid forests with high annual precipitation.

Several recent studies documented lateral components to solute transport and water flow through soils [*McDaniel et al.*, 1992], podzolization [*Sommer et al.*, 2000] and pedogenic processes in general [*Park and Burt*, 2002; *Sommer and Schlichting*, 1997]. In steep topography or mountainous regions, where subsurface heterogeneities facilitate lateral water movement through soils, vertical podzolization tends to occur at the pedon scale, whereas lateral podzolization tends to occur at the hillslope or catena scale [*Sauer et al.*, 2007]. Lateral translocation results in distinct soil morphology and composition and could provide the basis for enhanced understanding of hydrologic and pedogenic processes and patterns at the landscape (catchment) level. It may be the case that soil scientists acknowledge that water moves both vertically and laterally in sloping landscapes, but that lateral processes are not well understood and thus pedologic implications are ignored [*Sommer*, 2006] or underreported.

1.3.3. The evolution of digital soil mapping

Hudson [1992] argued that the basis for soil surveys, including conventional surveys, is a coupling of the five factors of soil formation [*Jenny*, 1941] and soil-landscape relationships. Soils have traditionally been mapped in the field by identifying landscape attributes or other environmental features which are believed to contain similar soil groups [*Hudson*, 1992] and

supported with extensive field sampling along transects. This approach is outlined in the *Soil Survey Manual* used within the National Resources Conservation Service [*Soil Survey Division Staff,* 1993]. While conventional soil surveys map taxonomic units (soil series) based on multiple properties, soil-landscape modeling also allows mapping of functional units using a small set of soil attributes or even a single attribute. The soil-landscape model can be used to map the spatial distribution of soil units at a finer resolution than those delineated in most conventional surveys. Soil-landscape modeling techniques offer quantitative, digital approaches for predicting the spatial distribution of soil properties based on the variability of environmental correlates (i.e. the five soil formative factors), and in particular topography and hydrology [*Thompson et al.*, 2006]. Quantifiable approaches to soil mapping are more objective than conventional surveys that rely on expert knowledge, which varies from one soil surveyor to the next.

Quantifiable, statistical approaches to soil unit delineation have been explored for several decades. *Troeh* [1964] found a strong statistical correlation between landscape shape and soil drainage class, albeit for a narrowly defined study that did not consider variation in slope gradient or slope length. *Norris and Loveday* [1971] discovered greater consistency of soil profiles classified objectively using multivariate discriminate analysis than those classified subjectively by soil surveyors, noting that the results of surveyors working without the aid of multivariate analysis were consistent when using data with which they are familiar but more variable when using unfamiliar data. Several additional analyses suggested that soil units classified by discriminant functions were more compact (i.e., similar) and better separated than the final maps created by soil surveyors [*Webster and Burrough,* 1972; 1974].

Statistical approaches to soil mapping using the soil-landscape relationship continued to evolve through the 1980s and 1990s. *Shovic and Montagne* [1985] developed a model for

recognizing soil-landscape relationships intended not to replace soil surveyor knowledge and experience, but rather to update existing surveys, provide initial data for new surveys adjacent to old surveys, and to perform tracking functions that would consume a survey staff's time and resources. Much like the aforementioned statistical approaches to soil mapping, the soil-landscape models derived by *Bell et al.* [1992; 1994] demonstrated that spatial patterns of soil drainage class could be predicted using spatial patterns of topography (slope gradient and shape), proximity to surface drainage features, and/or parent material.

Advancements in computation, remote sensing, and geospatial information technology have facilitated a continued evolution of soil mapping with new digital approaches presented in recent years. The most common digital soil mapping (DSM) strategies fall under the broad umbrella of spatial inference models and generally require observed soil data and some sort of ancillary data related to one or more of the soil forming factors. *McBratney et al.* [2003] provide a detailed inventory of these models. Spatial inference models can be categorized into data mining approaches such as multiple regression models [*Moore et al.*, 1993] or classification trees [*Bell et al.*, 1992], geostatistical approaches such as regression kriging [*Odeh et al.*, 1994], and approaches utilizing the knowledge of soil surveyors with expertise in a given region [*Lagacherie et al.*, 1995; *Zhu et al.*, 1996].

Some DSM methods combine the *surveyor* approach with either the *geostatistical* or *data mining* approach. One such method aims to integrate the soil-landscape concept, GIS and remote sensing technologies, and inferred knowledge from existing soil surveys into a soil land inference model [*Zhu et al.*, 1997; *Zhu et al.*, 2001]. An advantage of this integration is the development of a geographic information system that includes environmental covariates related to soil development. Such information system databases can vary from area to area due to

differences in pedogenesis and common environmental factors that affect it [*Yang et al.*, 2011]. Another combination approach uses cluster analysis methods to decrease inter-group variability and increase intra-group variability, thus homogenizing soil units [*Young and Hammer*, 2000].

Yet another approach to DSM involves the use of logistic regression models to predict the probability of occurrence of soil units across the landscape. For example, *Campling et al.* [2002] used a logistic model to predict the probability of six soil drainage classes in southeastern Nigeria. *Kempen et al.* [2009] used multinomial logistic regression and ancillary environmental data to update conventional soil survey maps for the Dutch province of Drenthe where significant land use change has altered soil distribution since the original soil surveys. Logistic regression models offer numerous benefits. They can incorporate one or more predictor variables, the regressors may be continuous or categorical, and accuracy can be assessed by cross-validating the model against a set of data not used during model development. Unlike multiple linear regression models, logistic regression may recognize non-linear relationships in soil-landscape associations. Logistic regression is also less demanding than other non-linear models in terms of normality of the underlying data [*Real et al.*, 2006].

1.3.4. Topography and hydrologic analysis

The effects of topography on hydrologic processes and soil development have been recognized for many years [*Jenny*, 1941]. Scientists first acknowledged the influence of vertical and horizontal slope curvature (i.e., profile and planform curvature) on soil moisture in an agricultural environment, characterizing their effect on moisture and pedogenesis in qualitative terms [*Aandahl*, 1948]. Delineation of hillslopes by topographic position such as summits, shoulders, backslopes, footslopes, and toeslopes [*Ruhe*, 1960] is still commonly used in estimating forest productivity related to the availability of soil moisture using the Forest Site

Quality Index (FSQI) [*Smith and Burkhart*, 1976], as a foundation for land element classifications [*MacMillan et al.*, 2000; *Pennock et al.*, 1987; *Schmidt and Hewitt*, 2004], and in soil sampling protocols [*Schoenberger et al.*, 2011].

In the mid-1960s a quantitative assessment of hillslope morphology was introduced [*Troeh*, 1964]. This involved a description of land elements using three-dimensional equations to estimate plan curvature, profile curvature, and gradient. When topographical maps were superimposed over soil survey maps, *Troeh* [1964] noted that breaks in topography correlated well with soil type boundaries. Results of his work indicated a strong relationship between surface geometry and soil drainage class, which led him to the conclusion that soil moisture regime is a major driver of pedogenesis.

Numerous studies have expanded on the work of *Troeh* [1964], focusing on the influence of hillslope geometry on the movement and distribution of water. The variable source area concept presented by *Hewlett and Hibbert* [1967] argued that a strong relationship existed between hydrologic flowpaths and landform. *Zaslavsky and Rogowski* [1969] postulated that water (saturated, unsaturated, or overland flow) would tend to diverge at convex land elements and converge at concave elements, and that increased soil moisture at convergent land elements leads to enhanced soil development. Similar results were obtained by other researchers [*Anderson and Burt*, 1978; *Pennock et al.*, 1987]. Curvature has been correlated with soil properties at least partially attributable to soil moisture regimes such as depth of A horizon and presence of eluviated or gleyed layers [*Pennock et al.*, 1987]. Many studies have found subsurface flow following surface topography [*Burt and Butcher*, 1985; *Seibert et al.*, 1997], but evidence also suggests mixed results when estimating subsurface flow and soil moisture using topographic metrics [*Moore and Thompson*, 1996].

Recently, light detection and ranging (LiDAR) has emerged as a valuable technology for acquiring high-quality DEMs via interpolation of accurate, high-density point data [*Lefsky et al.*, 2002; *Wehr and Lohr*, 1999]. LiDAR sensors emit laser pulses, and the time delay between emission and detection of a reflected pulse can be used to compute the range of the object causing the reflection [*Wehr and Lohr*, 1999]. LiDAR data produces DEMs of greater accuracy and reliability at a higher resolution than DEMs created using photogrammetric methods [*Guo et al.*, 2010]. As technological advancements decrease the cost of acquiring LiDAR-derived DEMs, their use for topographic spatial analysis is becoming increasingly commonplace.

In pedogenic and geomorphologic applications topographic analyses are typically used as representations of spatial variation of hydrological processes and conditions [*Guntner et al.*, 2004; *Merot et al.*, 1995]. Information derived from DEMs (those derived from LiDAR data as well as other data sources) that support the evaluation and use of topographic data are referred to as topographic metrics [*Beier et al.*, 2008]. A variety of metrics have been developed and can generally be categorized into three groups: 1) Local-elevation metrics such as slope, curvature, aspect and elevation; 2) Metrics determined using more distant elevations such as distance from stream, distance from a specified land element or upslope accumulated area, and 3) Compound metrics that combine metrics from the above two categories.

The topographic wetness index (TWI = $\ln(a/\tan\beta)$ [*Beven and Kirkby*, 1979] is a combination of upslope accumulated area (drainage area per unit contour length a, which indicates the amount of area sloping toward a specific location, and the local slope β, which is a measure of the potential drainage from an area). It has been used in diverse research ranging from spatial effects on runoff response and routing [*Beven et al.*, 1988; *Robson et al.*, 1992; *Sivapalan and Wood*, 1987] to characterization of vegetation patterns [*Zinko et al.*, 2005].

Since the TWI was introduced in 1975 [*Kirkby*, 1975], researchers have sought to improve computational approaches [*Quinn et al.*, 1995; *Tarboton*, 1997] and relax theoretical assumptions that form the foundation of the models that employ the index [*Ambroise et al.*, 1996; *Saulnier et al.*, 1997a; *Saulnier et al.*, 1997b]. While the TWI has been a useful tool for hydrologic modelers, many processes that drive variability of soil moisture distribution in a landscape are not fully captured by the index [*Grayson et al.*, 1997]. For instance, *Jordan* [1994] discovered that in a catchment where infiltration excess overland flow [*Horton*, 1933] predominates during large storm events, the location of contributing areas was difficult to determine from the TWI. *Moore and Thompson* [1996] reported a weak correlation between observed and modeled point distributions of water table depth. *Burt and Butcher* [1985] also reported a weak correlation between observed and modeled changes in soil moisture distribution. Soon after the TWI's introduction, *Speight* [1980] argued that both the upslope accumulated area and downslope dispersal area influence water drainage from a given point on the landscape, and downslope controls have since been strongly linked to soil characteristics [*Crave and Gascuel-Odoux*, 1997].

To address the limitations of the TWI in capturing hydrologic processes that control changing spatial patterns of soil moisture distribution in hillslopes, *Hjerdt et al.* [2004] developed a new algorithm for calculating gradient that is used as the local slope parameter in TWI computations. Their downslope index ($DI = \tan \alpha_d = d/L_d$, where L_d is the horizontal distance to a point with an elevation d meters below the elevation of the starting cell) estimates the hydraulic gradient for a given point in a DEM by stepping down the flow path in the steepest descent (i.e., least resistance) until a user-specified vertical drop has been achieved. Unlike other slope parameters commonly used with the TWI, the DI considers the enhancement or impedance

of drainage by local downslope steepness. However, the DI does not consider variation in downslope convexity, so the full effect of downslope topography has not yet been captured. In their analysis, *Hjerdt et al.* [2004] found DI values to be less affected by changes in DEM resolution than local slope.

1.3.5. Effects of DEM resolution on topographic metrics

Topographic analysis using digital elevation models (DEMs) has become commonplace in soil and hydrologic modeling, and there has been considerable assessment of the effects of DEM resolution on extracted topographic metrics [*Quinn et al.*, 1991; *Sorenson and Seibert*, 2007]. However, much research examined such effects at coarse resolutions offered by early DEMs derived from topographic maps created using aerial photos, largely limiting analyses to river basins and watersheds covering thousands of hectares. Examining fine-scale (i.e., 1-10 m) soil and hydrological variability of small headwater catchments may require higher-resolution data that has only recently become available through advancements in remote sensing technology, and both DEM accuracy and the effects of different high-resolution DEMs on important topographic metrics are relatively unknown.

Examples of topographic metric comparison between DEMs are abundant in the literature. For example, *Isaacson and Ripple* [1990] observed that slope values extracted from 3 arc second (100 m) DEMs were generally lower than those extracted from 7.5 minute (10 m) DEMs. *Jenson* [1991] examined slope values extracted from 10 arc minute, 30 arc second, and 3 arc second DEMs covering the Delaware River region and found that slope decreased with DEM coarsening. Many studies have reported TWI values increasing with DEM grid cell size [*Hancock*, 2005; *Quinn et al.*, 1991; *Saulnier et al.*, 1997c; *Wolock and Price*, 1994; *Wolock and McCabe*, 2000; *Wu et al.*, 2008]. *Zhang and Montgomery* [1994] observed a decrease in slope

value and increase in UAA with DEM coarsening. Variation in topographic metric values are a result of discretization effects when the size of DEM grid cells is altered (which can affect the algorithm used to compute a topographic metric) and the loss of terrain detail (smoothing) that occurs through DEM coarsening [*Gallant and Hutchinson*, 1996].

The aforementioned studies chiefly considered the effects of DEM resolution at scales greater than 10 m; most made comparisons of DEMs covering thousands of hectares, and all used elevation data derived from topographic maps. Over the past few years DEMs interpolated from LiDAR data have become increasingly accessible for digital terrain analysis. Such elevation models are typically available at resolutions of 1 m, facilitating their application to finer-scale analysis. For example, *Zimmer et al*. [2012] observed reductions in variation of surface water solute concentration associated with greater UAA calculated from a 5 m DEM aggregated from an original 1 m LiDAR-derived DEM for a 42 ha watershed at the Hubbard Brook Experimental Forest (HBEF) in New Hampshire. *Bailey et al.* [in review] found UAA differences correlated with soil variability in the same Hubbard Brook catchment using the same 5 m LiDAR-derived DEM for terrain analysis.

LiDAR data used to interpolate DEMs are subject to sensor and systematic error propagated to DEMs, and the nominal post-spacing (average ground spacing between postings) is believed to be a major contributor to vertical error in a LiDAR-derived DEM [*Hodgson et al.*, 2004]. Yet these uncertainties are rarely considered during soil and hydrologic analysis. *Shi et al.* [2012] compared DEMs interpolated from a LiDAR dataset with those developed using topographic maps for knowledge-based digital soil mapping, evaluating the performance of each DEM in calculating field-determined slope gradient for a 350 ha watershed in Vermont, United States. Slope values computed from 1 m and resampled 5 m LiDAR-derived DEMs more closely

matched field measurements than a 10 m DEM interpolated from a USGS 7.5 minute topographic map. *Vaze et al.* [2010] found that elevations from LiDAR-derived DEMs were more representative of the actual ground surface than elevations from DEMs created using contour maps.

Comparison of variation in topographic metric values extracted from a range of high-resolution (10 m or less) LiDAR-derived DEMs is also sparse in the literature. *Sorensen and Seibert* [2007] used a 5 m LiDAR-derived DEM to generate coarser models of 10 m, 25 m, and 50 m resolutions. The range of slope values decreased as DEM resolution decreased (steeper became less steep and gentle became steeper). Minimum, maximum, mean, and median TWI and specific upslope area values increased with DEM grid cell size. *Vaze et al.* [2010] observed a decrease in maximum slope values across five LiDAR-derived DEMs as resolution decreased from 1 m to 25 m. Additionally, they noted changes in DEM-delineated watershed boundary and stream network across DEM resolutions.

Variation in DEM-delineated watershed boundary and stream network when using DEMs of different resolution was observed nearly two decades ago [*Quinn et al.*, 1995]. DEM resolution impacts, to varying degrees, the value of computed topographic metrics. Yet the modeler rarely considers how the effects of DEM resolution on catchment features and topographic metrics will influence model outputs. Furthermore, investigations have not focused explicitly on the accuracy and limitations of high-resolution LiDAR-derived DEMs and better guidance must be developed for their utility in evaluating fine-scale environmental phenomena in small headwater catchments.

1.3.7. Hydropedology: Integration of hydrology, soil science, and spatial analysis

Researchers have long recognized the connections between the movement and distribution of water in a landscape and soil development and morphology [*Aandahl*, 1948; *Horton*, 1933; *Jenny*, 1941]. Recently, it has been suggested that incorporating disciplines such as hydrology, pedology, and geomorphology when studying catchments might advance an understanding of controls on catchment-scale hydrological processes [*Sivapalan*, 2005]. Furthermore, researchers argue that a lack of understanding of heterogeneity and system complexities across space and time and an inability of watershed hydrologists to extrapolate findings and make predictions across regions and spatial scales might be remedied through the integration of hydrology with ecology and other related disciplines [*McDonnell et al.*, 2007]. Indeed, interdisciplinary approaches are emerging in the form of a new field called hydropedology [*Lin*, 2011; *Lin et al.*, 2006].

While hydrologists have typically been concerned with watershed-scale processes, pedologists have traditionally focused their study of soils at the pedon level. Hydropedology seeks to examine the interface of hydrology and soil science as well as other geo- and bio-sciences [*Lin*, 2011] and link phenomena occurring at a variety of spatial and temporal scales [*Lin*, 2003]. A hydropedological approach to studying catchments may offer a useful framework for studying the earth's critical zone and contribute to an enhanced understanding of pressing environmental issues related to water and soil quality, watershed management, and climate change.

In addition to a call for trans-disciplinary efforts, hydrologists have cited a need for the following specific advances in hydrologic science (from *Lin et al.* [2011; 2006]):

1. Where, when, and how water moves through landscapes and its impacts on soil development, evolution, function, and distribution.
2. Enhancement of soil survey interpretations for flow and transport characteristics in different soils and landscapes, including soil categorizations that differentiate various soil hydrologic units.
3. The influence of soil architecture and soil distribution on hydrological processes as well as biogeochemical and ecological dynamics across spatio-temporal scales.

There exists tremendous heterogeneity and complexity in landscape properties, making prediction of hydrologic response to natural and anthropogenic forcing an immense challenge. Researchers contend that there is also structure and organization within the landscape that when understood helps explain catchment complexity and functionality. This complexity may be better understood when examined through the lens of hydropedology.

For example, hydropedology permits the delineation of soils into functional units based on morphological characteristics resulting from distinctive topography and hydrologic flowpaths. These functional units are also associated with distinct landscape features and biogeochemical signatures. The use of functional soil units delineated using a hydropedological framework can offer insight into the movement and distribution of water in a landscape, biogeochemical hotspots that transform solutes, and landscape locations contributing to streamflow generation. Thus, the prediction of functional soil units developed using a hydropedological framework may be an important step toward an enhanced understanding of catchment complexity and functionality.

1.4. Research objectives

This study has three principal objectives:

1. Compare watershed delineation and examine differences in topographic metrics computed from 1 m DEMs interpolated from two different LiDAR datasets, as well as DEMs aggregated from the original 1 m resolution to coarser models of 3 m, 5 m, and 10 m, and make suggestions for DEM application to modeling functional soil units.
2. Evaluate each LiDAR dataset through comparison with field-determined slope measurements and detailed total station ground surveys.
3. Predict the spatial distribution of process-based functional soil units across a 42 ha forested headwater catchment.

Soils of the HBEF hydrologic reference catchment, watershed three (WS3), may be grouped into five functional units, referred to henceforth as hydropedological units (HPUs). Preliminary data suggest that each HPU is affected by topography and substrate resulting in distinctive hydrologic flowpaths through the landscape. It is hypothesized that these HPUs occur in a pattern related to topographical features and substrate which in turn affect the pathway by which water flows through the subsurface [*Bailey et al.*, in review]. Therefore, field observations of soil morphology, a geographic information system (GIS), and a statistical model were used to predict HPU occurrence across a small headwater catchment in the HBEF, New Hampshire.

1.5. Broader impacts

It is clear that hydrological processes play a major role in soil development and the patterns of soil distribution. Mapping the distribution of HPUs in WS3 will provide an enhanced understanding of the functionality of headwater catchments by elucidating pedon-, hillslope-, and catchment-scale hydrologic flowpaths and the location of biogeochemical hotspots that lead to solute transformation and streamflow generation. This study will also be the first to develop an HPU predictive model. Examination of headwater catchments from the perspective of system functionality is critical for several reasons:

1. The importance of headwater catchments in controlling downstream water quantity [*Alexander et al.,* 2007] and mitigating floods [*Bradshaw et al.,* 2007; *Shankman,* 1996] is well-established. This study is part of a larger research project aimed at understanding headwater catchment hydrologic dynamics that may be incorporated into regional flood forecasting in the face of a changing climate and increasing development pressure.
2. Headwater catchments also play a crucial role in controlling downstream water quality [*Alexander et al.,* 2007; *Evans et al.,* 2006]. HBEF soils contain stores of soil organic matter [*Dittman et al.,* 2007; *McDowell and Wood,* 1984] and may be susceptible to dissolved organic carbon (DOC) export due to changes in acid deposition, rising temperatures, and increases in atmospheric CO_2 concentrations described by *Evans et al.* [2006]. Although headwater catchments typically contain low levels of DOC that do not affect water quality, fine-scale HPU mapping in WS3 may serve as a foundation for similar mapping efforts in other regions that will indicate the location of soils containing larger stores of soil organic carbon that may be considered during future land and watershed management planning intended to enhance water quality.

3. Headwater catchments are known to enhance biodiversity of larger basins [*Finn et al.*, 2011; *Meyer et al.*, 2007]. The same variation in surface water chemistry found in the entire Hubbard Brook Valley [*Likens and Buso*, 2006] has been documented in a single 42 ha watershed within the HBEF [*Zimmer et al.*, 2012]. Chemical variability may contribute to biological diversity by accommodating species with specific ecological requirements.
4. Soils represent the largest pool of terrestrial carbon [*Jobbagy and Jackson*, 2000; *Schlesinger*, 1997]. HPU maps will indicate fine-scale variability of soil attributes, including carbon stocks. Such maps could be a valuable tool for researchers and land managers interested in the effects of a changing climate on carbon sequestration and carbon flux within headwater catchments.
5. Finally, the White Mountain National Forest (WMNF) is the last US National Forest to have its soils mapped, an effort that is yet unfinished. Conventional soil surveys, which are often used to develop management strategies on US forestlands that include or exclude activities such as timber harvest, stand to benefit from hydropedologic information. Incorporation of topographic metrics and hydropedologic information into traditional taxonomic soil surveys offers a more comprehensive representation of system structure and organization through the perspective of landscape-level process and functionality. This will aid in the development of holistic forest and watershed management within the WMNF and, in the future, other physiographic regions.

1.6. References

Aandahl, A. R. (1948), The characterization of slope positions and their influence on the total nitrogen content of a few virgin soils of western Iowa, Soil Science Society of America Proceedings, 13, 449-454.

Alexander, R. B., E. W. Boyer, R. A. Smith, G. E. Schwarz, and R. B. Moore (2007), The role of headwater streams in downstream water quality, Journal of the American Water Resources Association, 43, 41-59.

Ambroise, B., K. Beven, and J. Freer (1996), Toward a generalization of the TOPMODEL concepts: Topographic indices of hydrological similarity, Water Resources Research, 32, 2135-2145.

Anderson, M. G., and T. P. Burt (1978), The role of topography in controlling throughflow generation, Earth Surface Processes, 3, 331-344.

Bailey, S. W., P. A. Brousseau, K. J. McGuire, and D. S. Ross (in review), Influence of hillslope position and shallow water table dynamics on soil development and carbon distribution in a steep, headwater catchment, Geoderma.

Beier, P., D. R. Majka, and W. D. Spencer (2008), Forks in the road: Choices in procedures for designing wildland linkages, Conservation Biology, 22, 836-851.

Bell, J., R. Cunningham, and M. Havens (1992), Calibration and validation of a soil-landscape model for predicting soil drainage class, Soil Science Society of America Journal, 56, 1860-1866.

Bell, J., R. Cunningham, and M. Havens (1994), Soil drainage class probability mapping using a soil-landscape model, Soil Science Society of America Journal, 58, 464-470.

Beven, K., and M. Kirkby (1979), A physically based, variable contributing area model of basin hydrology, Hydrological Sciences Bulletin, 24, 43-69.

Beven, K., E. Wood, and M. Sivapalan (1988), On hydrological heterogeneity — Catchment morphology and catchment response, Journal of Hydrology, 100, 353-375.

Bradshaw, C. J. A., N. S. Sodhi, K. S. H. Peh, and B. W. Brook (2007), Global evidence that deforestation amplifies flood risk and severity in the developing world, Global Change Biology, 13, 2379-2395.

Brouwer, J., and R. W. Fitzpatrick (2002), Restricting layers, flow paths and correlation between duration of soil saturation and soil morphological features along a hillslope with an altered soil water regime in western Victoria, Australian Journal of Soil Research, 40, 927-946.

Burt, T. P., and D. P. Butcher (1985), Topographic controls of soil moisture distributions, Journal of Soil Science, 36, 469-486.

Campling, P., A. Gobin, and J. Feyen (2002), Logistic modeling to spatially predict the probability of soil drainage classes, Soil Science Society of America Journal, 66, 1390-1401.

Crave, A., and C. Gascuel-Odoux (1997), The influence of topography on time and space distribution of soil surface water content, Hydrological Processes, 11, 203-210.

Daniels, R. B., and R. D. Hammer (1992), Soil Geomorphology, 236 pp., John Wiley and Sons, Inc., New York.

Daniels, R. B., S. Gamble, S. Buol, and H. Bailey (1975), Free iron sources in an aquult-udult sequence from North Carolina, Soil Science Society of America Proceedings, 39, 335-340.

Dittman, J. A., C. T. Driscoll, P. M. Groffman, and T. J. Fahey (2007), Dynamics of nitrogen and dissolved organic carbon at the Hubbard Brook Experimental Forest, Ecology, 88, 1153-1166.

Evans, C. D., P. J. Chapman, J. M. Clark, D. T. Monteith, and M. S. Cresser (2006), Alternative explanations for rising dissolved organic carbon export from organic soils, Global Change Biology, 12, 2044-2053.

Finn, D. S., N. Bonada, C. Murria, and J. M. Hughes (2011), Small but mighty: headwaters are vital to stream network biodiversity at two levels of organization, Journal of the North American Benthological Society, 30, 963-980.

Franzmeier, D. P., J. E. Yahner, G. C. Steinhardt, and H. R. Sinclair (1983), Color patterns and water table levels in some Indiana soils, Soil Science Society of America Journal, 47, 1196-1202.

Gallant, J. C., and M. F. Hutchinson (1996), Towards and understanding of landscape scale and structure, paper presented at Third International Conference/Workshop on Integrating GIS and Environmental Modeling, Santa Fe, NM, January 21-26, 1996.

Grayson, R., A. Western, F. Chiew, and G. Bloschl (1997), Preferred states in spatial soil moisture patterns: Local and nonlocal controls, Water Resources Research, 33, 2897-2908.

Guntner, A., J. Seibert, and S. Uhlenbrook (2004), Modeling spatial patterns of saturated areas: An evaluation of different terrain indices, Water Resources Research, 40(5).

Guo, Q., W. Li, H. Yu, and O. Alvarez (2010), Effects of Topographic Variability and Lidar Sampling Density on Several DEM Interpolation Methods, Photogrammetric Engineering & Remote Sensing, 76.

Hancock, G. R. (2005), The use of digital elevation models in the identification and characterization of catchments over different grid scales, Hydrological Processes, 19, 1727-1749.

Hewlett, J. D., and A. R. Hibbert (1963), Moisture and energy conditions within a sloping soil mass during drainage, Journal of Geophysical Research, 68(4), 1081-1087.

Hewlett, J. D., and A. R. Hibbert (1967), Factors affecting the response of small watersheds to precipitation in humid areas, in International Symposium on Forest Hydrology, edited by W. E. Sopper and H. W. Lull, pp. 275-291, Pergamon Press, New York.

Hjerdt, K. N. (2004), A new topographic index to quantify downslope controls on local drainage, Water Resources Research, 40, doi: W05602.

Hodgson, M. E., X. Li, and Y. Cheng (2004), A parameterization model for transportation feature extraction, Photogrammetric Engineering & Remote Sensing, 12, 1399-1404.

Horton, R. E. (1933), The role of infiltration in the hydrologic cycle, Transactions, American Geophysical Union, 446-460.

Hudson, B. (1992), The soil survey as paradigm-based science, Soil Science Society of America Journal, 56, 836-841.

Isaacson, D. L., and W. J. Ripple (1990), Comparison of 7.5-minute and 1-degree digital elevation models, Photogrammetric Engineering & Remote Sensing, 56, 1523-1527.

Jenny, H. (1941), Factors of soil formation: A system of quantitative pedology, 320 pp., McGraw-Hill, New York.

Jenson, S. K. (1991), Applications of hydrologic information automatically extracted from digital elevation models, Hydrological Processes, 5, 31-44.

Jobbagy, E. G., and R. B. Jackson (2000), The vertical distribution of soil organic carbon and its relation to climate and vegetation, Ecological Applications, 10(2), 423-436.

Jordan, J. P. (1994), Spatial and temporal variability of stormflow generation processes on a Swiss catchment, Journal of Hydrology, 153, 357-382.

Kempen, B., D. Brus, G. Heuvelink, and J. Stoorvogel (2009), Updating the 1:50,000 Dutch soil map using legacy soil data: A multinomial logistic regression approach, Geoderma, 151, 311-326.

Kirkby, M. J. (1975), Hydrograph modelling strategies, in Processes in Physical and Human Geography, edited by R. F. Peel, M. D. Chisholm and P. Haggett, Heinemann, London, UK.

Knuteson, J., J. Richardson, D. Patterson, and L. Prunty (1989), Pedogenic carbonates in a calciaquoll associated with a recharge wetland, Soil Science Society of America Journal, 53, 495-499.

Lagacherie, P., J. P. Legros, and P. A. Burrough (1995), A soil survey procedure using the knowledge of soil pattern established on a previously mapped reference area, Geoderma, 65, 283-301.

Lefsky, M. A., W. B. Cohen, G. G. Parker, and D. J. Harding (2002), Lidar remote sensing for ecosystem studies, Bioscience, 52, 19-30.

Likens, G. E., and D. C. Buso (2006), Variation in streamwater chemistry throughout the Hubbard Brook Valley, Biogeochemistry, 78(1), 1-30.

Lin, H. S. (2003), Hydropedology: Bridging disciplines, scales, and data, Vadose Zone, 2(1), 1-11.

Lin, H. S. (2011), Hydropedology: Towards new insights into interactive pedologic and hydrologic processes across scales, Journal of Hydrology, 406, 141-145.

Lin, H. S., J. Bouma, Y. Pachepsky, A. Western, J. Thompson, R. van Genuchten, H. Vogel, and A. Lilly (2006), Hydropedology: Synergistic integration of pedology and hydrology, Water Resources Research, 42, W05301.

MacMillan, R. A., W. W. Pettapiece, S. C. Nolan, and T. W. Goddard (2000), A generic procedure for automatically segmenting landforms into landform elements using DEMs, heuristic rules and fuzzy logic, Fuzzy Sets and Systems, 113, 81-109.

McBratney, A. B., M. L. Mendonça Santos, and B. Minasny (2003), On digital soil mapping, Geoderma, 117, 3-52.

McDaniel, P. A., G. R. Bathke, S. W. Buol, D. K. Cassel, and A. L. Falen (1992), Secondary manganese iron ratios as pedochemical indicators of field-scale throughflow water-movement, Soil Science Society of America Journal, 56, 1211-1217.

McDonnell, J. J., et al. (2007), Moving beyond heterogeneity and process complexity: A new vision for watershed hydrology, Water Resources Research, 43, W07301.

McDowell, W. H., and T. Wood (1984), Podzolization - soil processes control dissolved organic-carbon concentrations in stream water, Soil Science, 137, 23-32.

Merot, P., B. Ezzahar, C. Walter, and P. Aurousseau (1995), Mapping waterlogging of soils using digital terrain models, Hydrological Processes, 9(1), 27-34.

Meyer, J. L., D. L. Strayer, J. B. Wallace, S. L. Eggert, G. S. Helfman, and N. E. Leonard (2007), The contribution of headwater streams to biodiversity in river networks, Journal of the American Water Resources Association, 43, 86-103.

Moore, I. D., P. E. Gessler, G. A. Nielsen, and G. A. Petersen (1993), Soil attribute prediction using terrain analysis, Soil Science Society of America Journal, 57, 443-552.

Moore, R. D., and J. C. Thompson (1996), Are water table variations in a shallow forest soil consistent with the TOPMODEL concept?, Water Resources Research, 663-669.

Morgan, C. P., and M. H. Stolt (2006), Soil morphology-water table cumulative duration relationships in southern New England, Soil Science Society of America Journal, 70, 816-824.

Nadeau, T. L., and M. C. Rains (2007), Hydrological connectivity between headwater streams and downstream waters: How science can inform policy, Journal of the American Water Resources Association, 43, 118-133.

Norris, J. M. (1972), The application of multivariate analysis to soil studies: Soil variation, Journal of Soil Science, 23, 62-75.

Norris, J. M., and J. Loveday (1971), The application of multivariate analysis to soil studies II: The allocation of soil profiles to established groups: A comparison of soil survey and computer methods, Journal of Soil Science, 22, 395-400.

Odeh, I., A. McBratney, and D. Chittleborough (1994), Spatial prediction of soil properties from landform attributes derived from a digital elevation model, Geoderma, 63, 197-214.

Park, S. J., and T. P. Burt (2002), Identification and characterization of pedogeomorphological processes on a hillslope, Soil Science Society of America Journal, 66, 1897-1910.

Pennock, D. J., B. J. Zebarth, and E. Dejong (1987), Landform classification and soil distribution in hummocky terrain, Saskatchewan, Canada, Geoderma, 40, 297-315.

Quinn, P., K. Beven, and R. Lamb (1995), The in(a/tan/β) index: How to calculate it and how to use it within the topmodel framework, Hydrological Processes, 9, 161-182.

Quinn, P., K. Beven, P. Chevallier, and O. Planchon (1991), The prediction of hillslope flow paths for distriubted hydrological modelling using digital terrain models, Hydrological Processes, 5, 59-79.

Real, R., A. M. Barbosa, and J. M. Vargas (2006), Obtaining environmental favourability functions from logistic regression, Environmental and Ecological Statistics, 13, 237-245.

Robson, A., K. Beven, and C. Neal (1992), Towards identifying sources of subsurface flow: A comparison of components identified by a physically based runoff model and those determined by chemical mixing techniques, Hydrological Processes, 6, 199-214.

Ruhe, R. V. (1960), Elements of the soil landscape, in Transactions of the 7th International Congress on Soil Science, edited, pp. 165-170, Madison, WI.

Sauer, D., H. Sponagel, M. Sommer, L. Giani, R. Jahn, and K. Stahr (2007), Podzol: Soil of the year 2007. A review on its genesis, occurrence, and functions, Journal of Plant Nutrition and Soil Science, 170, 581-597.

Saulnier, G. M., K. Beven, and C. Obled (1997a), Including spatially variable effective soil depths in TOPMODEL, Journal of Hydrology, 202, 158-172.

Saulnier, G. M., C. Obled, and K. Beven (1997b), Analytical compensation between DTM grid resolution and effective values of saturated hydraulic conductivity within the TOPMODEL framework, Hydrological Processes, 11, 1331-1346.

Saulnier, G. M., K. Beven, and C. Obled (1997c), Digital elevation analysis for distributed hydrological modeling: Reducing scale dependence in effective hydraulic conductivity values, Water Resources Research, 33, 2097-2101.

Schmidt, J., and A. Hewitt (2004), Fuzzy land element classification from DTMs based on geometry and terrain position, Geoderma, 121, 243-256.

Schlesinger, W. H. (1997), Biogeochemistry, an analysis of global change, Academic Press, San Diego, California, USA.

Schoenberger, P. J., D. A. Wysocki, and E. C. Benham (2011), Field book for describing and sampling soils, Version 3.0, Natural Resources Conservation Service, National Soil Survey Center, Lincoln, NE.

Seibert, J., K. H. Bishop, and L. Nyberg (1997), A test of TOPMODEL's ability to predict spatially distributed groundwater levels, Hydrological Processes, 11, 1131-1144.

Shankman, D. (1996), Stream channelization and changing vegetation patterns in the U.S. Coastal Plain, Geographical Review, 86(2), 216.

Shi, X., L. Girod, R. Long, R. DeKett, J. Philippe, and T. Burke (2012), A comparison of LiDAR-based DEMs and USGS-sourced DEMs in terrain analysis for knowledge-based digital soil mapping, Geoderma, 170, 217-226.

Shovic, H., and C. Montagne (1985), Application of a statistical soil-landscape model to an order-III wildland soil survey, Soil Science Society of America Journal, 49, 961-968.

Sivapalan, M. (2005), Pattern, process and function: elements of a unified theory of hydrology at the catchment scale, in Encyclopedia of Hydrologic Sciences, edited by M. G. Anderson, pp. 193-220, John Wiley and Sons, Inc., Chichester, UK.

Sivapalan, M., and E. F. Wood (1987), A multidimensional model of nonstationary space-time rainfall at the catchment scale, Water Resources Research, 23, 1289-1299.

Smith, W. D., and H. E. Burkhart (1976), Forest resource management plan: Philpott Lake comlex, Smith River, Virginia, edited, p. 59, Department of Forestry and Forest Products, Virginia Polytechnic Institute and State University, Blacksburg, Virginia.

Soil Survey Division Staff (1993), Soil survey manual, Soil Conservation Service, US Department of Agriculture Handbook 18.

Sommer, M. (2006), Influence of soil pattern on matter transport in and from terrestrial biogeosystems—A new concept for landscape pedology, Geoderma, 133, 107-123.

Sommer, M., and E. Schlichting (1997), Archetypes of catenas in respect to matter - A concept for structuring and grouping catenas, Geoderma, 76, 1-33.

Sommer, M., D. Halm, U. Weller, M. Zarei, and K. Stahr (2000), Lateral podzolization in a granite landscape, Soil Science Society of America Journal, 64, 1434-1442.

Sorensen, R., and J. Seibert (2007), Effects of DEM resolution on the calculation of topographical indices: TWI and its components, Journal of Hydrology, 347, 79-89.

Speight, J. (1980), The role of topography in controlling throughflow generation: A discussion, Earth Surface Processes, 5, 187-191.

Tarboton, D. G. (1997), A new method for the determination of flow directions and upslope areas in grid digital elevation models, Water Resources Research, 33, 309-319.

Thompson, J. A., E. M. Pena-Yewtukhiw, and J. H. Grove (2006), Soil–landscape modeling across a physiographic region: Topographic patterns and model transportability, Geoderma, 133, 57-70.

Troch, P. A., G. A. Carrillo, I. Heidbuchel, S. Rajagopal, M. Switanek, T. H. M. Volkmann, and M. Yaeger (2008), Dealing with landscape heterogeneity in watershed hydrology: A review of recent progress toward new hydrological theory, Geography Compass, 2, 1-18.

Troeh, F. R. (1964), Landform parameters correlated to soil drainage, Soil Science Society of America Proceedings, 28, 808-812.

Vaze, J., J. Teng, and G. Spencer (2010), Impact of DEM accuracy and resolution on topographic indices, Environmental Modelling & Software, 25, 1086-1098.

Wagener, T., M. Sivapalan, P. A. Troch, B. L. McGlynn, C. J. Harman, H. V. Gupta, P. Kumar, P. S. C. Rao, N. B. Basu, and J. S. Wilson (2010), The future of hydrology: An evolving science for a changing world, Water Resources Research, 46, W05301.

Ward, R. C., and M. Robinson (2000), Principles of Hydrology, Fourth edition, 365 pp., McGraw-Hill, New York.

Webster, R., and P. Burrough (1972), Computer-based soil mapping of small areas from sample data: I. Multivariate classification and ordination, Journal of Soil Science, 23, 210-221.

Webster, R., and P. Burrough (1974), Multiple discriminant analysis in soil survey, Journal of Soil Science, 25, 120-134.

Wehr, A., and U. Lohr (1999), Airborne laser scanning - An introduction and overview, ISPRS Journal of Photogrammetry and Remote Sensing, 54, 68-82.

Wolock, D. M., and C. V. Price (1994), Effects of digital elevation model map scale and data resolution on a topography-based watershed model, Water Resources Research, 30, 3041-3052.

Wolock, D. M., and G. J. McCabe (2000), Differences in topographic characteristics computed from 100- and 1000-m resolution digital elevation model data, Hydrological Processes, 14, 987-1002.

Wu, S., J. Li, and G. H. Huang (2008), A study on DEM-derived primary topographic attributes for hydrologic applications: Sensitivity to elevation data resolution, Applied Geography, 28, 210-223.

Yang, L., Y. Jiao, S. Fahmy, A. X. Zhu, S. Hann, J. E. Burt, and F. Qi (2011), Updating conventional soil maps through digital soil mapping, Soil Science Society of America Journal, 75, 1044.

Young, F. J., and R. D. Hammer (2000), Defining geographic soil bodies by landscape position, soil taxonomy, and cluster analysis, Soil Science Society of America Journal, 64, 989-998.

Zaslavsky, D., and A. S. Rogowski (1969), Hydrologic and morphologic implications of anisotropy and infiltration in soil profile development, Soil Science Society of America Proceedings, 33, 594-599.

Zhang, W., and D. R. Montgomery (1994), Digital elevation model grid size, landscape presentation, and hydrologic simulation, Water Resources Research, 30, 1019-1028.

Zhu, A. X., L. E. Band, B. Dutton, and T. J. Nimlos (1996), Automated soil inference under fuzzy logic, Ecological Modelling, 90, 123-145.

Zhu, A. X., L. E. Band, R. Vertessy, and B. Dutton (1997), Derivation of soil properties using a soil land inference model (SoLIM), Soil Science Society of America Journal, 61, 523-533.

Zhu, A. X., B. Hudson, J. Burt, K. Lubich, and D. Simonson (2001), Soil mapping using GIS, expert knowledge, and fuzzy logic, Soil Science Society of America Journal, 65, 1463-1472.

Zimmer, M. A., S. W. Bailey, K. J. McGuire, and T. D. Bullen (2012), Fine scale variations of surface water chemistry in an ephemeral to perennial drainage network, Hydrological Processes, doi: 10.1002/hyp.

Zinko, U., J. Seibert, M. Dynesius, and C. Nilsson (2005), Plant species numbers predicted by a topography-based groundwater flow index, Ecosystems, 8, 430-441.

Chapter Two

2.0. Evaluation of LiDAR-derived DEMs through terrain analysis and field comparison

Abstract: Topographic analysis using digital elevation models (DEMs) has become commonplace in soil and hydrologic modeling and analysis and there has been considerable assessment of the effects of grid resolution on topographic metrics using DEMs of 10 m resolution or coarser. However, examining fine-scale (i.e., 1-10 m) soil and hydrological variability of headwater catchments may require higher-resolution data that has only recently become available, and both DEM accuracy and the effects of different high-resolution DEMs on topographic metrics are relatively unknown. We evaluated two high-resolution DEMs derived from light detection and ranging (LiDAR) data covering the same headwater catchment to assess the applicability of such DEMs for modeling fine-scale environmental phenomena related to soil development and hydrological processes. Each native 1 m DEM was coarsened to 3 m, 5 m, and 10 m resolutions and treated with a low-pass smoothing filter yielding 16 DEMs for comparison. Watershed boundaries were delineated and slope, plan curvature, upslope accumulated area, and the topographic wetness index were computed for each DEM resolution/filter combination. Additionally, we compared DEM slope values with field measurements, and evaluated LiDAR classification/interpolation errors using total station surveys. Results indicate that 3 m and 5 m filtered/unfiltered DEMs were most appropriate for boundary delineation and topographic metric extraction. Conversely, 1 m DEMs were sensitive to potentially misclassified elevations and 10 m DEMs demonstrated greater variability of watershed area and boundary. DEMs provided a good estimate of slope values, particularly when grid resolution reflected field methods. Total station surveys indicated that LiDAR classification algorithms mitigate the classification non-ground surface features as ground points.

Keywords: topographic metrics, LiDAR, digital elevation model, total station

2.1. Introduction

Topographic analysis using digital elevation models (DEMs) has become commonplace in soil and hydrologic modeling, and there has been considerable assessment of the effects of DEM resolution on extracted topographic metrics [e.g., *Quinn et al.*, 1991; *Sorenson and Seibert*, 2007]. However, much research examined such effects at coarse resolutions of 10 m or greater offered by early DEMs derived from topographic maps and aerial photos [*Isaacson and Ripple*, 1990; *Jenson and Domingue*, 1988; *Quinn et al.*, 1991; *Wolock and Price*, 1994], largely limiting analyses to river basins and watersheds covering thousands of hectares. Examining soil and hydrological variability of small headwater catchments requires higher-resolution data that has only recently become available through LiDAR technology, and both DEM accuracy and the effects of different high-resolution DEMs on important topographic metrics are relatively unknown.

Isaacson and Ripple [1990] observed that slope values extracted from 3 arc second (100 m) DEMs were generally lower than those extracted from 7.5 minute (10 m) DEMs. *Jenson* [1991] examined slope values extracted from 10 arc minute, 30 arc second, and 3 arc second DEMs covering the Delaware River region and found that coarser DEMs generated lower slope values. Many studies examining differences in topographic metric values computed from DEMs of 10 m resolution and greater have reported higher topographic wetness index (TWI = $\ln(a/\tan\beta)$, where a = upslope accumulated area (UAA) and β = local slope; [*Beven and Kirkby*, 1979]) value for coarser DEMs [e.g., *Hancock*, 2005; *Quinn et al.*, 1991; *Saulnier et al.*, 1997; *Wolock and Price*, 1994; *Wolock and McCabe*, 2000]. *Zhang and Montgomery* [1994] observed both lower slope values and larger UAA for coarser DEMs. Variation in topographic metric values is a result of discretization effects when the size of DEM grid cells is altered (which can

affect the algorithm used to compute a topographic metric) and the loss of terrain detail (smoothing) that occurs through DEM coarsening [*Gallant and Hutchinson*, 1996].

Previous studies chiefly considered the effects of DEM resolution at scales greater than 10 m; most made comparisons of DEMs covering thousands of hectares, and all used elevation data derived from topographic maps. Over the past few years DEMs interpolated from light detection and ranging (LiDAR) data have become increasingly accessible for digital terrain analysis. Such elevation models are often at resolutions of 1 m, facilitating their application to smaller land areas and more complex terrain. For example, *Zimmer et al.* [2012] observed reductions in surface water solute variation associated with greater UAA calculated at a 5 m resolution for a 42 ha watershed at the Hubbard Brook Experimental Forest in New Hampshire. *Bailey et al.* [in review] found UAA differences correlated with fine-scale soil variability in the same Hubbard Brook catchment, and that a 5 m DEM resampled from a 1 m LiDAR-derived DEM resulted in more realistic UAA and better correlations with soil morphological variability, raising the question of whether there is a limitation to the utility of higher-resolution elevation data.

High-resolution DEMs may offer a level of detail and landscape roughness greater than that controlling surface/near surface flow pathways, and may interfere with the computation of some topographic metrics, including those related to hydrological processes. In such situations a DEM may be coarsened to a lower resolution, which has the effect of smoothing landscape roughness. Common methods for DEM coarsening include nearest neighbor, bilinear or cubic convolution resampling and cell aggregation [e.g., *Band and Moore*, 1995; *Sorensen and Seibert*, 2007; *Wu et al.*, 2008].

Another approach to smoothing landscape roughness is filtration. Unlike cell aggregation or resampling methods, smoothing filters mitigate landscape roughness [*Lillesand and Kiefer*, 2000] without generating a coarser DEM, thus maintaining greater topographic detail. Filtration is a common technique for smoothing DEMs, but a comparison of topographic metrics extracted from filtered and coarsened DEMs is absent in the literature. Smoothing filters and DEM coarsening methods may facilitate the use of high-resolution surface models as representations of surface or subsurface hydrologic dynamics and distribution.

LiDAR data used to interpolate DEMs are subject to sensor and systematic error leading to misinterpolation of elevations and misclassification of returns from non-ground features as ground [*Höhlea and Höhle*, 2009]. The resulting errors are propagated to DEMs. Furthermore, the nominal post-spacing (average ground spacing between postings) has been shown to contribute to vertical error in a LiDAR-derived DEM [e.g., *Aguilar et al.*, 2005; *Hodgson et al.*, 2004; *Hu et al.*, 2009]. Yet these uncertainties are rarely considered during soil and hydrologic analysis. *Shi et al.* [2012] compared DEMs interpolated from a LiDAR dataset with those developed using topographic maps for knowledge-based digital soil mapping, evaluating the performance of each DEM in calculating field-determined slope gradient for a 350 ha watershed in Vermont, United States. Slope values computed from 1 m and resampled 5 m LiDAR-derived DEMs more closely matched field measurements than a 10 m DEM interpolated from a USGS 7.5 minute topographic map. *Vaze et al.* [2010] found that elevations from LiDAR-derived DEMs were more representative of the actual ground surface than elevations from DEMs created using contour maps.

Comparison of variation in topographic metric values extracted from a range of high-resolution (10 m or less) LiDAR-derived DEMs is also sparse in the literature. *Sorensen and*

Seibert [2007] used a 5 m LiDAR-derived DEM to generate coarser models of 10 m, 25 m, and 50 m resolutions. The range of slope values decreased as DEM resolution decreased (steeper became less steep and gentle became steeper). Minimum, maximum, mean, and median TWI and specific upslope area values increased with DEM grid cell size. *Vaze et al.* [2010] observed a decrease in maximum slope values across five LiDAR-derived DEMs as resolution decreased from 1 m to 25 m. Additionally, they noted changes in DEM-delineated watershed boundary and stream network across DEM resolutions.

Variation in DEM-delineated watershed boundary and stream network when using DEMs of different resolution was observed nearly two decades ago [*Quinn et al.*, 1995]. DEM resolution impacts, to varying degrees, the value of computed topographic metrics. Yet the modeler rarely considers how the effects of DEM resolution on catchment features and topographic metrics will influence model outputs that rely on terrain characterization. Furthermore, investigations have not focused explicitly on the accuracy and limitations of high-resolution LiDAR-derived DEMs and better guidance must be developed for their utility in evaluating soil and hydrologic phenomena occurring over scales less than 10 m in small headwater catchments.

This study has two principal objectives. First, we compare watershed delineation and examine trends in topographic metrics computed from 1 m DEMs interpolated from each of two LiDAR datasets, as well as DEMs aggregated from the original 1 m resolution to coarser models of 3 m, 5 m, and 10 m resolutions and treated with a low-pass smoothing filter. Second, we evaluate the accuracy of each LiDAR dataset through comparison with detailed total station ground surveys and the ability of LiDAR-derived DEMs to characterize topography by comparison with field-determined slope measurements.

2.2. Study location

The Hubbard Brook Experimental Forest (HBEF) (Figure 2.1), located in the White Mountains of New Hampshire (43°56'N, 71°45'W), is maintained by the United States Forest Service (USFS), Northern Research Station and is part of the National Science Foundation Long-Term Ecological Research (NSF LTER) network. Watershed Three (WS3), the hydrologic reference catchment, is underlain by mica schist of the Silurian Rangeley formation [*Barton et al.*, 1997] and covered by glacial tills of varying thickness. Soils are predominantly Spodosols of sandy loam texture developed in glacial till parent material [*Likens and Bormann*, 1995]. Elevation ranges from 527 m to 732 m. The western side of the catchment is characterized by steep spurs flanking intermittent and perennial streams, while the eastern portion exhibits little or no evidence of channel formation. Bedrock outcrops are found in the upper portion of the catchment.

Climate at the HBEF is humid continental. Winters tend to be long and cold with an average January temperature of -9°C. Summers are mild with July temperatures averaging 19°C (temperature averages recorded at 450 m elevation). Annual precipitation averages 1400 mm, with about 30% falling as snow. Streamflow is high in the spring (nearly half of the 870 mm average annual runoff occurs during snowmelt) and very low in late summer/early autumn [*Bailey et al.*, 2003].

The catchment is dominated by second-growth northern hardwood forest including sugar maple (*Acer saccharum*), American beech (*Fagus grandifolia*), and yellow birch (*Betula alleghaniensis*) with shallow-to-bedrock areas dominated by red spruce (*Picea rubens*) and balsam fir (*Abies balsamea*) interspersed with mountain white birch (*Betula cordifolia*). The

forest was harvested from 1880 to 1920 and damaged by a hurricane in 1938 [*Likens and Bormann*, 1995].

2.3. Methods

2.3.1. LiDAR data collection and DEM interpolation

Two LiDAR datasets were evaluated. The first was obtained by the National Center for Airborne Laser Mapping (NCALM) in November 2009 as part of their Seed Proposal program, and the second by Photo Science Inc. in April 2012 for the USFS White Mountain National Forest (WMNF). Both datasets were collected during leaf-off and snow-free conditions and were used to interpolate a 1 m DEM from returns classified as ground. A comparison of LiDAR data collection and DEM interpolation methodologies is in Table 2.1.

2.3.2. DEM aggregation, filtration, and sink filling

We produced 14 DEMs from the original 1 m DEMs by cell aggregation and low-pass filtering for a total of 16 DEMs. Coarsening was achieved via the mean cell aggregation approach, which computes the mean of all cells in a desired neighborhood size and applies that value to a new cell equal to the size of the neighborhood. Each 1 m DEM was aggregated to coarser resolutions of 3 m, 5 m, and 10 m. Then, a simple low-pass filter was applied to each DEM. To accommodate the best possible comparison with our cell aggregation approach to DEM coarsening, we selected a mean filtering technique. This method computes the mean elevation value in a 3x3 cell neighborhood moving window and applies that value to the cell at the neighborhood center.

Cells representing elevations where every surrounding cell is characterized by a higher elevation value are called sinks. Although sinks occur naturally in a landscape, their presence in a DEM may interfere with the computation of topographic metrics related to water flow

pathways (e.g., flow accumulation algorithms). Furthermore, while DEM coarsening and filtration effectively smooth landscape roughness they may not eliminate all sinks in a dataset. To calculate flow direction, we applied a sink-filling algorithm to each DEM resolution/filter combination. Sink-filling routines developed by *Planchon and Darboux* [2001] and *Wang and Liu* [2006] have been modified in the System for Automated Geoscientific Analyses (SAGA) software (version 2.1.0) to include a parameter aimed at preserving downward gradient. This prevents flow accumulation from dead-ending in flat areas, which can result in the manifestation of broken stream channels. We selected the *Wang and Liu* [2006] algorithm as it prevented broken channels with the lowest minimum gradient value possible, whereas the alternate option required increasing the gradient to maintain hydrologic connectivity and thus could have a greater impact on subsequent DEM computations.

2.3.3. Watershed boundary delineation

All DEM-delineated watershed boundaries were established with ArcGIS software (ArcMap version 10.1, ESRI 2012, Redlands, CA) for each DEM resolution/filter combination using a differentially corrected GPS point collected at a weir marking the watershed outlet. The single flow direction algorithm [*Jenson and Domingue,* 1988] was used for the flow direction parameter during delineation. To ensure that the point denoting the catchment weir was located in the DEM-delineated main stream channel, flow accumulation was also computed for each DEM resolution/filter combination to identify the channel network. If the weir point did not fall in the channel for a given DEM, we applied the Snap Pour Point tool to locate the nearest stream cell and used this location to delineate the watershed boundary. Subsequent watershed outlet locations were never more distant than a cell adjacent to the cell containing the weir point. Each watershed polygon was buffered to a distance of 20 m to mitigate edge effects during

topographic metric computation. Finally, each DEM was clipped to the corresponding buffered watershed boundary polygon. Watershed boundaries delineated from each DEM resolution/filter combination were assessed visually for differences in shape as previous research found that a qualitative/visual assessment is an important early step when comparing catchment morphology [*Hancock et al.*, 2002]. Then, differences in boundary area between DEM resolution/filter combinations were compared quantitatively. DEM-derived watershed boundaries were compared with a boundary determined using standard surveying techniques when HBEF experimental watersheds were first established in the 1950s.

2.3.4. Topographic metric computation

DEMs were used to compute slope, UAA, TWI, and planform curvature layers. All topographic metric computation was completed using SAGA. Slope was calculated using the maximum slope algorithm [*Travis et al.*, 1975]. Planform curvature was calculated using equation described by *Zevenbergen and Thorne* [1987]. UAA was calculated using the multiple triangular flow direction algorithm [*Seibert and McGlynn*, 2007]. TWI was calculated using the triangular multiple flow direction algorithm for the a parameter and maximum slope for the tan β parameter. Planform curvature was selected as a fourth topographic metric as it affects convergence or divergence of flow across a cell and thus is an indicator of soil wetness and soil drainage class [*Troeh*, 1964], which has been shown to affect soil development and morphology [*Pennock et al.*, 1987; *Zaslavsky and Rogowski*, 1969]. Positive values indicate the surface is convex in the across-slope direction (divergent), negative values indicate the surface is concave in the across-slope direction (convergent), and a value of zero indicates the surface is linear.

To compare topographic metrics across DEM resolution/filter combinations, we generated random points for topographic metric value extraction. Point generation was

constrained by a 20 m negative buffer polygon created using the NCALM 1 m watershed boundary polygon. Visual inspection provided confirmation that the negative buffer was contained within each watershed boundary polygon for all resolution/filter combinations; thus all random points were also contained within each watershed boundary. To avoid spatial autocorrelation, which commonly occurs in spatial data, we generated 421 random points. This value was established by computing area within each watershed boundary polygon, determining the number of 10 m grid cells that could fit in each polygon, then calculating 10% of the mean number of 10 m grid cells across all watershed polygons. The resulting random point density was 10 points per ha or 1 point per 1000 m^2. Slope, planform curvature, and TWI values from each DEM resolution/filter combination were extracted to the random points. Boxplots provided an evaluation of differences in topographic metric distribution statistics across changes in DEM resolution and filtration. Additionally, UAA maps were created using the WMNF DEMs for unfiltered 1 m, 3 m, 5 m, and 10 m resolutions to demonstrate how DEM resolution affects UAA values for each grid cell.

2.3.5. Comparison of field and DEM slope measurements

One way to test DEM accuracy is through field validation. We compared 75 field slope measurements with DEM-derived slope values. At each location percent slope was measured with a clinometer 5 m upslope and 5 m downslope from soil characterization pits and groundwater wells along the line of maximum slope. We collected GPS locations for each pit/well location using a Trimble Geo XT 2005 GPS unit equipped with a Trimble Hurricane Antenna. Data were differentially-corrected using Trimble Pathfinder software and Continuously Operating Reference Station (CORS) data from the National Geodetic Survey to obtain circa-one meter precision of horizontal positions.

The steeper of the upslope/downslope clinometer measurements was compared with DEM-derived percent slope values computed using the maximum slope algorithm [*Travis et al.*, 1975]. The maximum slope algorithm and 5 m DEM resolution represent the best digital simulation of field slope measurement methods. Both 1 m and 5 m resolution (unfiltered and filtered) DEM slopes were compared with field slope measurements to examine how grid cell size and filtration affects differences between DEM and field gradient. Differences between DEM and field slope values were compared using frequency histograms. Eight 2-sample t-tests were performed to compare field slope measurements with slope values extracted from each filtered/unfiltered 1 m and 5 m DEM.

2.3.6. Total station ground surveys

While LiDAR technology has provided detailed models of the land surface, both the classification of raw data into ground and off-terrain points and their interpolation to generate a gridded representation of the ground surface are subject to errors [*Höhlea and Höhle*, 2009]. Classification errors occur when non-ground surface features (e.g., fallen tree boles, boulders, low-lying vegetation) are classified as ground. Interpolation errors are inherent in the DEM generation process when point elevations are gridded to create a raster bare earth model.

To investigate potential classification and interpolation errors, four detailed elevation ground surveys were conducted in WS3 during the spring of 2012 using a Sokia SET 610 total station. Survey sites were selected to incorporate diverse topography, surface features, variation in density of shrub cover, and presence/absence of canopy cover. Three sites were located entirely under the forest canopy (UpperK, LowerK, SO2) while the fourth site was located in a forest clearing extending into the canopy (RG5) (Figure 2.2).

At each site an arbitrary benchmark was established as the plot center and located via GPS to horizontal accuracy circa-one meter. The total station was placed directly over the benchmark and leveled to an XY planar accuracy of 10 seconds. Data were collected at 3 m intervals along transects established prior to each survey. Transects at UpperK, LowerK, and S02 survey sites radiated outward 20 m to 30 m from the benchmark (much like spokes radiating from the central hub of a bicycle wheel). A grid of dimensions 40 m x 30 m was set up at the RG5 survey site with perpendicular transects laid out across-slope and down-slope. When a surface feature was encountered, data points were collected adjacent to and on the feature, often resulting in greater point densities at these locations. Vertical (relative elevation), horizontal, and slope distances, as well as horizontal angle (azimuth in degrees) were recorded for each point.

Elevation values were extracted from the unfiltered/unfilled NCALM and WMNF 1 m DEMs for each survey point. Relative elevation differences between each benchmark and survey points indicated by each DEM were subtracted from the relative elevation differences between each benchmark and survey points indicated by the total station. The absolute value of the resulting values constitutes overall error (Figure 2.3). To quantify observed errors, we calculated Root Mean Square Error ($RMSE_{Observed\text{-}DEM} = \sqrt{Sum}\ (Z_{Survey} - Z_{DEM})^2/n$). RMSE offers a common empirical assessment of LiDAR-derived DEM accuracy [*Raber et al.*, 2007]. RMSE values were calculated for locations with/without surface features and for locations under/not under forest canopy.

2.4. Results

2.4.1. Watershed boundary delineation

In general, boundaries were most similar to the field-surveyed boundary when delineated from 3 m and 5 m resolution DEMs, regardless of whether a filter was applied (Figure 2.2). The

NCALM unfiltered 1 m DEM excluded a 1 ha region (approximately 2% of the total watershed area) in the southeastern portion of the catchment that was included in the field-surveyed boundary, while the WMNF filtered 10 m DEM included a 1 ha area in this same region that was not included in the field-surveyed boundary.

Watershed areas were also compared for each DEM resolution/filter combination and to the field-surveyed boundary. Areas ranged from 41.4 ha (unfiltered NCALM 1 m) to 43.0 ha (unfiltered WMNF 10 m) (Table 2.2). The mean of watersheds delineated using NCALM DEMs was 42.0 ha, the mean of watersheds delineated using WMNF DEMs was 42.2 ha, and the overall mean watershed area was 42.1 ha. Coarse (10 m) and fine (1 m) DEMs tended to generated watersheds containing areas least similar to the field-surveyed boundary. The mean watershed area of NCALM unfiltered/filtered 3 m and 5 m DEMs was 42.1 ha and the mean watershed area of WMNF unfiltered/filtered 3 m and 5 m DEMs was 42.1 ha.

2.4.2. Topographic metric computation

Boxplots were used to compare the distributions of topographic metric values computed for each DEM resolution/filter combination (Figure 2.4). No noteworthy or statistically significant differences were observed between DEMs derived from the NCALM or WMNF LiDAR datasets, so for ease of visualization only WMNF distributions are shown (Figure 2.4). Filtration and DEM coarsening increased minimum slope values while maximum slope values decreased. Median slope values decreased from 30% to 27% with the application of the low-pass filter and cell aggregation (Figure 2.4). Variance decreased with filtration and DEM coarsening, and interquartile range (IQR) decreased with coarsening from 0.17 to 0.07 for the WMNF DEMs.

Median plan curvature did not change with filtration or cell aggregation (Figure 2.4). No clear trend was observed for the IQR across DEM resolution/filter combinations. Variance was consistently lower for the filtered version of each DEM resolution. Distributions tended to be skewed toward positive (convex/divergent) curvature values. With the exception of values outside the whiskers (whiskers contain over 99% of the data) distributions were within a range of +/- 100 for all resolution/filter combinations. The 3 m and 5 m DEMs tended to produce plan curvature values with the narrowest distributions (Figure 2.4).

Median UAA values increased from 173.6 m^2 and 19.1 m^2 to 3077.7 m^2 and 1215.7 m^2, respectively (Figure 2.4). UAA maps indicated that for finer-resolution DEMs the catchment is dominated by grid cells with small UAAs (Figure 2.5). As DEMs are coarsened, UAA values become larger.

Minimum, maximum, and median TWI values increased with filtration and cell aggregation (Figure 2.4). The greatest increase occurred from the filtered 1 m DEM to the unfiltered 3 m DEM. Only a slight increase occurred from the filtered 3 m to unfiltered 5 m DEMs, and no notable changes occurred with filtration for the 3 m or 5 m DEMs. Overall, median TWI increased from 4.1 to 8.4 when calculated using the NCALM and WMNF DEMs (Figure 2.4). TWI distributions computed using the 3 m DEMs and 5 m DEMs, regardless of filtration, exhibited the greatest similarity.

2.4.3. Comparison of field and DEM slope measurements

The difference between slope values measured in the field versus computed using filtered/unfiltered 1 m and 5 m DEMs for both datasets were assessed using frequency histograms. Slope values computed from each DEM were subtracted from corresponding field measurements. Resulting difference values were placed into difference classes where each class

(or bin) represents 5% for a total of 20 difference classes. Differences follow a normal distribution for each field-DEM pair and most differences are within +/- 10% of 0 (where 0 represents no difference). A majority of DEM slope values were within +/- 12.5% of corresponding field measurements for the 1 m DEMs and +/- 7.5% for the 5 m DEMs (Figure 2.6). Variances are greater for 1 m DEMs than for 5 m DEMs. In general, 1 m DEM slope differences within +/- 7.5% of 0 (i.e. bins adjacent to center bin) tend to be negative or are equally positive and negative, while positive differences occur more frequently than negative differences for the 5 m DEMs within +/- 7.5% of 0 (Figure 2.6). Two-sample t-tests comparing field slope measurements with DEM-computed slope values indicated no significant differences between the means ($\alpha = 0.05$).

2.4.4. Total station ground surveys

DEM errors generated during LiDAR-to-DEM interpolation are propagated to computed topographic metrics. Therefore, we adapted a method for quantifying and assessing DEM and LiDAR classification error [*Raber et al.*, 2007] using RMSE related to surface features and canopy cover. Relative elevation differences between each survey benchmark and the survey points were compared with relative elevation differences derived from unfiltered 1 m DEMs for both datasets. Interpolation errors, inherent in the LiDAR-to-DEM interpolation process when ground returns are connected to create a digital land surface, are expected to be random. Such errors should decrease in the absence of canopy cover as the density of LiDAR pulses striking the ground surface (termed nominal post-spacing) increases. To determine the magnitude of interpolation errors present, we compared error in forest clearings (RMSE of 1.06 m and 0.80 m for NCALM and WMNF DEMs, respectively) versus error under forest canopy (RMSE of 1.32 m and 1.29 m for NCALM and WMNF DEMs, respectively) (Table 2.3).

Classification errors, which occur when LiDAR returns from non-ground features are classified as ground returns, were also assessed using RMSE values. Locations on or adjacent to surface features (e.g., boulders, tree boles, vegetation) exhibited an RMSE of 1.49 meters for the NCALM DEM and 1.40 meters for the WMNF DEM, while locations without surface features exhibited an RMSE of 1.03 meters for the NCALM DEM and 0.99 meters for the WMNF DEM (Table 2.3).

Greater RMSE values were observed for both datasets at locations with surface features than non-feature survey points. In most cases, the total station measurements yielded a greater relative elevation difference than the DEM between benchmark and surface feature survey locations.

2.5. Discussion

2.5.1. Watershed boundary varies with DEM resolution and landscape roughness

Each DEM generated a different watershed boundary. Watersheds are delineated following the direction of flow upslope from one pixel to the next originating at a user-selected pour point until maximum elevation is reached for each possible flow path. Differences in grid cell elevation affect the selected flow direction algorithm and thus DEMs interpolated from different elevation datasets and DEMs from the same dataset but differing in resolution and filtration are likely to exhibit variations in watershed boundary.

A visual comparison of watershed boundaries suggested that areas of rougher terrain generated similar boundaries. However, along the southeast portion of WS3, which is characterized by smoother terrain (little to no channel formation and no steep spurs) than much of the rest of the catchment, boundary differences were substantial. This was especially true for the unfiltered NCALM 1 m DEM (which excluded nearly 1 ha more area than the field-surveyed

boundary) and the unfiltered WMNF 10 m DEM (which included nearly 1 ha more area than the field-surveyed boundary) (Table 2.2). The filtered 10 m DEMs from both datasets contained nearly 1 ha less area than the field-surveyed boundary. The area excluded or included for these four watershed boundaries was chiefly located in the southeastern portion of WS3. Variation in watershed boundary and flow accumulation (i.e., stream channel) across DEM resolutions is consistent with previous observations [*Quinn et al.,* 1995; *Vaze et al.,* 2010]. It is likely that small elevation differences for just a few pixels resulted in the southeast boundary disparity. Such results demonstrate that care should be taken when using LiDAR-derived DEMs for watershed delineation, especially in regions where delineation of small headwater catchments is challenging due to subtle topography.

2.5.2. Topographic metric value variation with DEM resolution

The tendency for slope values to become more intermediate (decreased maximum values and increased minimum values) with DEM coarsening is consistent with previous observations [*Band and Moore,* 1995; *Sorensen and Seibert,* 2007; *Vaze et al.,* 2010]. Slope values can be expected to become more intermediate when finer-resolution grid cell neighborhoods are averaged into larger cells through DEM coarsening via mean cell aggregation. Decreases in slope variance and IQR observed in this study are also consistent with previous investigations [*Sorensen and Seibert,* 2007; *Vaze et al*., 2010]. Our observation that the filtered version of a given DEM resolution exhibited a smaller variance than the unfiltered version for plan curvature suggests that low-pass filtration has a greater impact on plan curvature distribution statistics than DEM coarsening by mean cell aggregation.

Minimum, maximum, and median TWI values tended to increase with DEM coarsening and filtration, consistent with previous investigations [*Quinn et al.,* 1991; *Sorensen and Seibert,*

2007; *Wolock and Price*, 1994] but extended to a finer scale in this study. TWI values can be expected to increase when slope values used to calculate TWI decrease and/or UAA values used to calculate TWI increase. In this case, we observed no significant change in mean/median slope values and an increase in minimum slope values with DEM coarsening. We also observed increases in median UAA values with DEM coarsening (Figure 2.4) consistent with previous observations [*Zhang and Montgomery*, 1994].

The 4.2 and 4.1 unit differences in mean TWI values (Table 2.2) computed from unfiltered 1 m and filtered 10 m DEMs derived from NCALM and WMNF LiDAR datasets, respectively, are significant from the perspective of the hydrological modeler. This disparity is equivalent to approximately two orders of magnitude difference in subsurface flow when following TOPMODEL theory [*Beven and Kirkby*, 1979] and using the hydraulic conductivity distribution with depth observed for WS3 [*Detty and McGuire*, 2010]. The parameterization of TOPMODEL and other hydrologic models is often independent of topography. However, small differences (less than 10 m) in DEM resolution have implications for computed topographic metric values (e.g., the mean) that affect hydrologic information derived from such models.

Increases in minimum, mean, and median TWI values with DEM coarsening appear to be controlled by increases in UAA values. Minimum slope values increased and mean/median slope values were unchanged with DEM coarsening and thus cannot explain the observed increases in TWI values. However, UAA maps indicated increasing values with DEM coarsening (Figure 2.5), and must therefore offset observed changes in slope value when calculating TWI. Maximum slope value decreases, in addition to UAA increases, may at least partially explain TWI maximum value increases with DEM coarsening. Note also that the 1 m DEMs generated very small UAA values throughout much of the catchment (Figure 2.5) that are not likely

reflective of real-world hydrological processes, indicating that such fine-scale DEMs offer too much topographic detail and landscape roughness for accurate modeling of soil and hydrological phenomena occurring at the hillslope or catchment scale.

2.5.3. Agreement between DEM and field slope values

DEM-computed slope values were similar to field-measured slope values. The tendency for 1 m DEM differences to be negative and 5 m DEM differences to be positive indicates that DEM slope values tend to be greater than field slope measurements when computed at the 1 m resolution and lower than field slope measurements when computed at the 5 m resolution. This is an artifact of DEM coarsening and filtration, which had the effect of decreasing maximum slope values and increasing minimum slope values. Therefore, intermediate resolutions result in the best agreement between field and DEM slope measurements.

2.5.4. Classification and interpolation error

The tendency for total station relative elevation differences to be greater than DEM relative elevation difference indicates that either the LiDAR pulses tended to miss small surface features or, more likely, that DEM interpolation algorithms recognized and smoothed such features, thus mitigating classification errors, but also possibly biasing the DEM against areas of hummocky terrain or rougher ground surfaces.

RMSE was lower in forest clearings than under canopy for both NCALM and WMNF datasets. This is expected, as the density of LiDAR ground returns used during DEM interpolation should increase in the absence of forest canopy. Higher LiDAR ground return density facilitates the interpolation of more accurate DEMs – thus clearings are presumed to suffer fewer DEM interpolation errors than regions with a canopy and therefore exhibit a lower RMSE. It also indicates that interpolation errors – which occur inherently in the DEM generation

process – are indeed present in the WMNF LiDAR dataset, and that they differ according to canopy cover.

The forest clearing surrounding RG5 is dominated by subtle topography and contains few notable surface features apart from one boulder of dimensions 2 m x 3 m x 1.5 m and a bedrock outcropping. Comparison of RG5 total station surveys with DEM elevation data provides a good estimate of error associated with 1 m DEMs derived from high-density LiDAR datasets under ideal conditions. DEM interpolation algorithms appear to recognize non-ground surface features classified as ground and filter prior to interpolation, but vertical accuracy is compromised by about 0.3 m to 0.5 m (Table 2.3) under dense canopy even when collected during leaf-off conditions. These factors should be considered when determining DEM resolution to perform digital terrain analyses and whether or not a smoothing filter should be applied to the DEM to mitigate landscape roughness that may interfere with the accuracy of computed topographic metrics.

It is also worth highlighting that the two LiDAR datasets contain different ground return densities in WS3; the NCALM dataset contains a density of 3.27 ppsm while the WMNF dataset contains a density of 1.16 ppsm (Table 2.1) – a difference of 2.09 ppsm. Yet the datasets generated very similar DEMs in terms of raw elevations, and the DEMs generated similar watershed boundaries (especially when coarsened to 3 m and 5 m resolutions). Furthermore, the distribution of topographic metrics computed from filtered/unfiltered coarser DEMs derived from the original 1 m resolution for each dataset were similar (Table 2.2; Figure 2.4). Density of nominal post-spacing has been shown to affect DEM error [e.g., *Aguilar et al.*, 2005; *Hodgson et al.*, 2004; *Hu et al.*, 2009] although several studies also indicated that LiDAR sampling density can be reduced by up to 50% with no degradation of DEM accuracy [*Anderson et al.*, 2006; *Liu*

et al., 2007a]. Denser post-spacing can be achieved by using a higher pulse rate, lower altitude over-flight, narrower scan angle, or some combination of these variables [*Raber et al.*, 2007]. The WMNF dataset contains less dense nominal post-spacing and was collected from a higher altitude than the NCALM dataset. Similar DEM elevations, computed topographic metrics, and delineated watershed boundaries for each dataset investigated in this study do not reflect previous reports that differences in such variables should result in DEM error differences.

2.6. Conclusions

High-resolution DEMs derived from LiDAR data are a useful tool for soil and hydrologic modeling. They may be particularly useful when the phenomena being modeled occur over small land areas at the catchment or hillslope scale. However, accuracy of LiDAR-derived DEMs when used in the context of soil and hydrologic processes has been sparsely investigated. This study aimed to evaluate LiDAR and DEM errors through field validation and comparison of DEMs derived from different LiDAR datasets.

DEM elevation differences resulted in unique watershed boundaries generated by each DEM, although boundary differences were most severe in regions of subtler topography and between the coarsest and finest DEMs. The most similar boundaries both within and across datasets were delineated from filtered/unfiltered 3 m and 5 m DEMs. Boundaries delineated from 3 m and 5 m DEMs were also most similar to the field-surveyed boundary. Care must be taken when selecting appropriate DEM resolution for delineating watershed boundaries.

We also compared topographic metrics extracted from high-resolution 1 m, 3 m, 5 m, and 10 m DEMs, including a version of each DEM treated with a low-pass smoothing filter. Grid resolution and low-pass filtration clearly affects values of computed topographic metrics and should be carefully considered when modeling hydrological and soil processes and patterns. As

expected, application of a low-pass filter resulted in a DEM with a level of topographic detail lower than the unfiltered DEM of the same resolution but greater than a DEM with a coarser resolution and may be useful when a DEM of decreased landscape roughness without reduced grid cell resolution is desired. In general, topographic metrics stabilized (i.e., reduction in magnitude of change from one DEM resolution to the next) at the 5 m filtered DEM. Therefore, we recommend resolution/filter combination as a good starting point for modeling fine-scale (i.e., less than 10 m) environmental phenomena related to soils and hydrologic processes in steep, forested headwater catchments.

Field observations proved a useful method for evaluating LiDAR/DEM error. Our comparison of field and DEM slope values indicates that DEMs provide a good estimate of field slope gradients so long as the DEM resolution and slope algorithm selected represent a close approximation of field methods. Total station surveys provided evidence for algorithmic mitigation of classification errors as well as decreased interpolation errors in the absence of canopy cover. RMSE differences between canopy/non-canopy locations and feature/non-feature locations were less than 0.5 meters, suggesting that even under canopy cover and in rough terrain characterized by surface features LiDAR still can produce DEMs useful for analysis of soil and hydrologic analyses.

Finally, we noted differences in LiDAR data collection methods and ground return density for two datasets used to interpolate different DEMs. According to previous reports, this should have resulted in differences in DEM error. However, the similarities we observed in watershed boundaries and topographic metrics computed from each DEM, as well as a set of coarsened and filtered DEMs generated from the original datasets, suggest that differences in LiDAR collection methods and ground return densities we studied were not sufficient to create

tangible DEM error differences. Methods for increasing accuracy, such as increasing return densities through sensor enhancements, lowering over-flight altitude, and narrowing the scan angle, all increase the cost of LiDAR acquisition as well as personnel time and data processing/storage requirements. Our observations suggest that these costs can be reduced while generating DEMs as accurate as those developed with more monetary and time inputs.

2.7. Acknowledgements

Financial support was provided by the National Science Foundation Long-Term Ecosystem Research (DEB 1114804) and Hydrologic Sciences (EAR 1014507) programs. LiDAR data were collected as part of the National Center for Airborne Laser Mapping seed award program for the hydropedology project and by Photo Science, Inc. for the White Mountain National Forest. Hubbard Brook Experimental Forest (HBEF) context map data courtesy of the Hubbard Brook Ecosystem Study. The HBEF is operated and maintained by the USDA Forest Service Northern Research Station and is part of the NSF Long-Term Ecological Research network.

Table 2.1. LiDAR data collection and DEM interpolation methodologies for datasets acquired from the National Center for Airborne Laser Mapping (NCALM) and the White Mountain National Forest (WMNF). Information provided by post-project reports and personal communication with representatives of NCALM and Photo Science, Inc.

Data Collection/Processing Method	NCALM	WMNF
LiDAR flight and processing	NCALM	Photo Science, Inc. (ground control/calibration points located by the James W. Sewell Company)
Area of survey	Hubbard Brook Valley (about 42 sq. km)	White Mountain National Forest (about 484 sq. km)
Date of LiDAR collection	November 2009	November 2010, April 2012
Ground conditions	Leaf-off, snow-free	Leaf-off, snow-free
LiDAR collection system	Optech GEMINI Airborne Laser Terrain Mapper (ALTM)	Optech GEMINI Airborne Laser Terrain Mapper (ALTM)
Approximate altitude above sea level	1600 meters	1800 meters
Swath width	400 meters	550 meters
Overlap	50%	30%
Laser PRF	100 kHz	N/A
Scan frequency	40 kHz	N/A
Scan angle (+/- degrees)	21	N/A
Scan angle cutoff (degrees)	3	N/A
Horizontal datum	NAD83 UTM zone 19N, meters	NAD83 UTM zone 19N, meters
Vertical datum	NAVD88 (NGS GEOID03), meters	NAVD88 (NGS GEOID09), meters
Classified file type/size	LAS, 1000m x 500m tiles	LAS 1.2, 2000m x 2000m tiles
Ground Return Density (over WS3 only) (ppsm = points per square meter)	3.27 ppsm	1.16 ppsm
Vertical RMSE	0.0720 meters	0.124 meters
Ground control stations	3 (Hubbard Brook Valley only)	37 (entire WMNF)
Final DEM resolution	1 meter	1 meter
Smoothed Best Estimate of Trajectory (SBET) development software (from GNSS and inertial data)	POSProc	Applanix POSPac MMS
Point-cloud development software	Optech	Optech
Automated data classification, manual cleanup, and bare earth generation	TerraSolids	TerraSolids

Table 2.2. Catchment area and mean topographic metrics for each DEM resolution/filter combination (LP denotes the application of a low-pass filter). Mean topographic metric values are based on a random sampling of 10% of 10 m grid cells that would fit into each boundary. Area of the field-surveyed boundary is 42.3 ha.

LiDAR Dataset	**DEM resolution/filter**	**Area (ha)**	**Slope (%)**	**Plan Curvature (radians/m)**	**UAA (m^2)**	**TWI ($ln(m^2)$)**
NCALM	1m	41.4	31	2.8	188	4.3
NCALM	1mLP	42.3	29	0.9	161	4.8
NCALM	3m	41.9	29	0.4	571	6.4
NCALM	3mLP	42.1	29	0.1	791	6.6
NCALM	5m	42.1	29	0.4	1621	7.2
NCALM	5mLP	42.0	28	0.2	1594	7.3
NCALM	10m	42.2	28	-0.5	3287	8.2
NCALM	10mLP	41.5	27	-0.3	3411	8.5
WMNF	1m	42.4	30	2.4	174	4.4
WMNF	1mLP	42.3	29	0.9	202	4.9
WMNF	3m	42.3	29	1.4	859	6.4
WMNF	3mLP	41.8	28	0.0	938	6.6
WMNF	5m	42.3	29	-0.5	1669	7.2
WMNF	5mLP	42.1	28	0.1	1540	7.4
WMNF	10m	43.0	28	-0.2	2623	8.2
WMNF	10mLP	41.6	27	-0.6	3098	8.5

Table 2.3. RMSE for locations under canopy and in forest clearings as well as for locations with and without surface features. Relative elevation differences between total station survey benchmark/survey locations and corresponding DEM benchmark/survey locations were used to compute RMSE.

Point Type	**Number of Points**	**RMSE NCALM (meters)**	**RMSE WMNF (meters)**
No Canopy	151	1.06	0.80
Canopy	614	1.32	1.29
No Feature	403	1.03	0.99
Feature	362	1.49	1.40

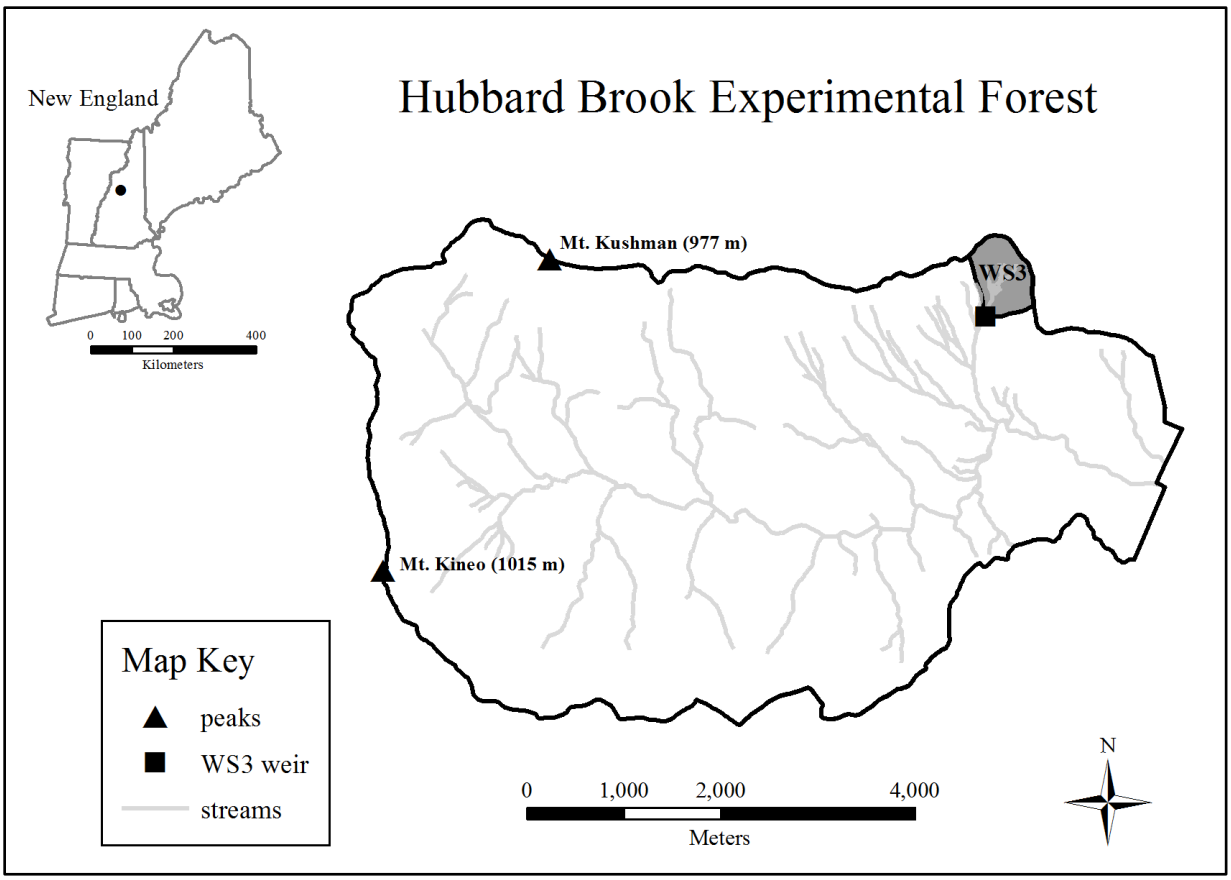

Figure 2.1. Map of Hubbard Brook Experimental Forest, WS3, and location within New England, United States. GIS data provided courtesy of the Hubbard Brook Ecosystem Study (public domain).

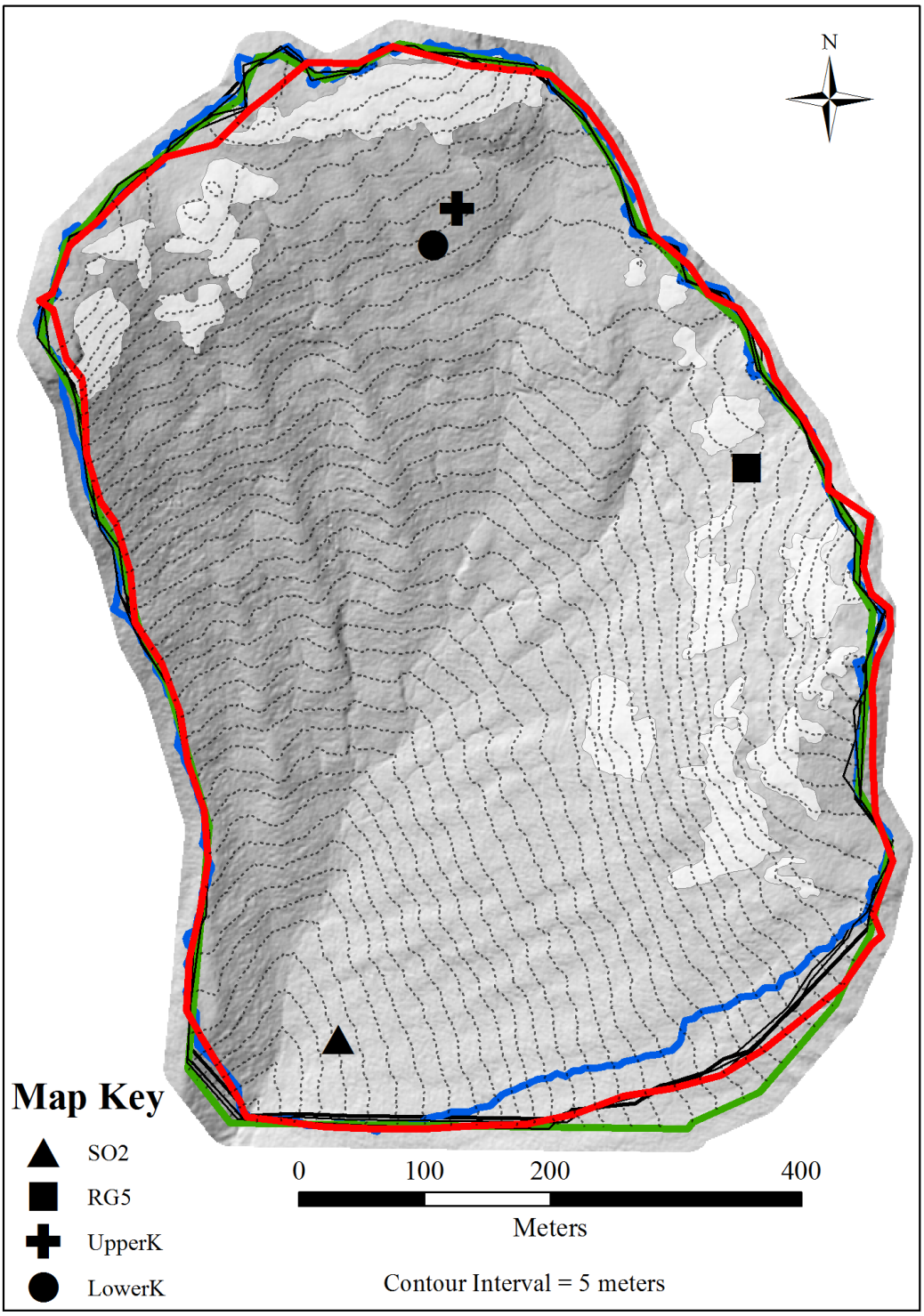

Figure 2.2. Catchment hillshade map with 5 m contour lines, total station surveys (filled symbols), DEM-delineated catchment boundaries, and bedrock outcroppings (light grey areas). Red line represents the field-surveyed boundary, the blue line denotes the NCALM 1 m boundary, the green line represents the WMNF 10 m boundary, and the black lines represent NCALM and WMNF 3 m and 5 m boundaries.

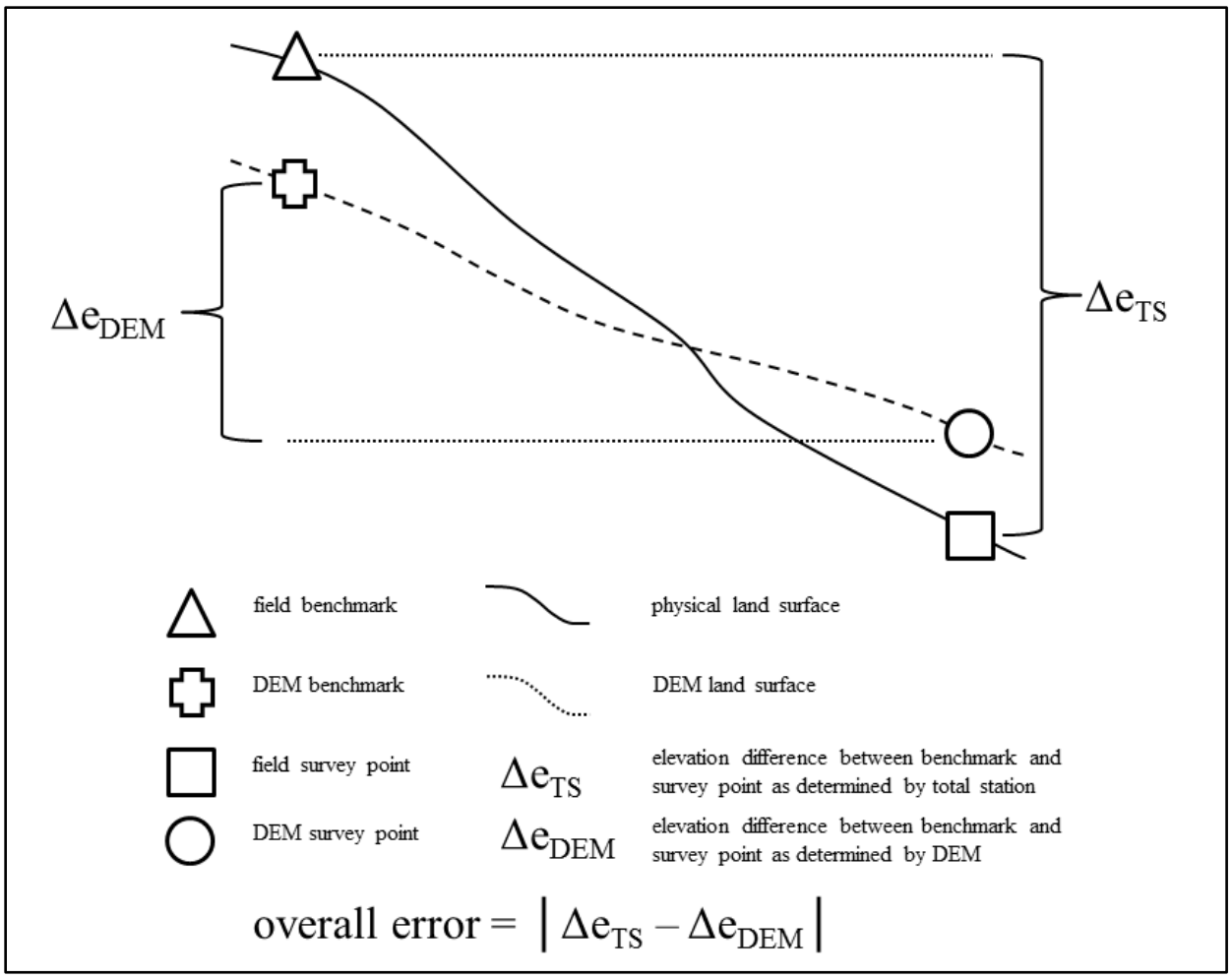

Figure 2.3. Conceptual diagram indicating method for determining DEM elevation error using total station surveys. Resulting errors were used to calculate RMSE for locations with/without surface features (boulders, tree boles) and locations under/not under forest canopy. RMSE values were used to interpret LiDAR classification and interpolation errors.

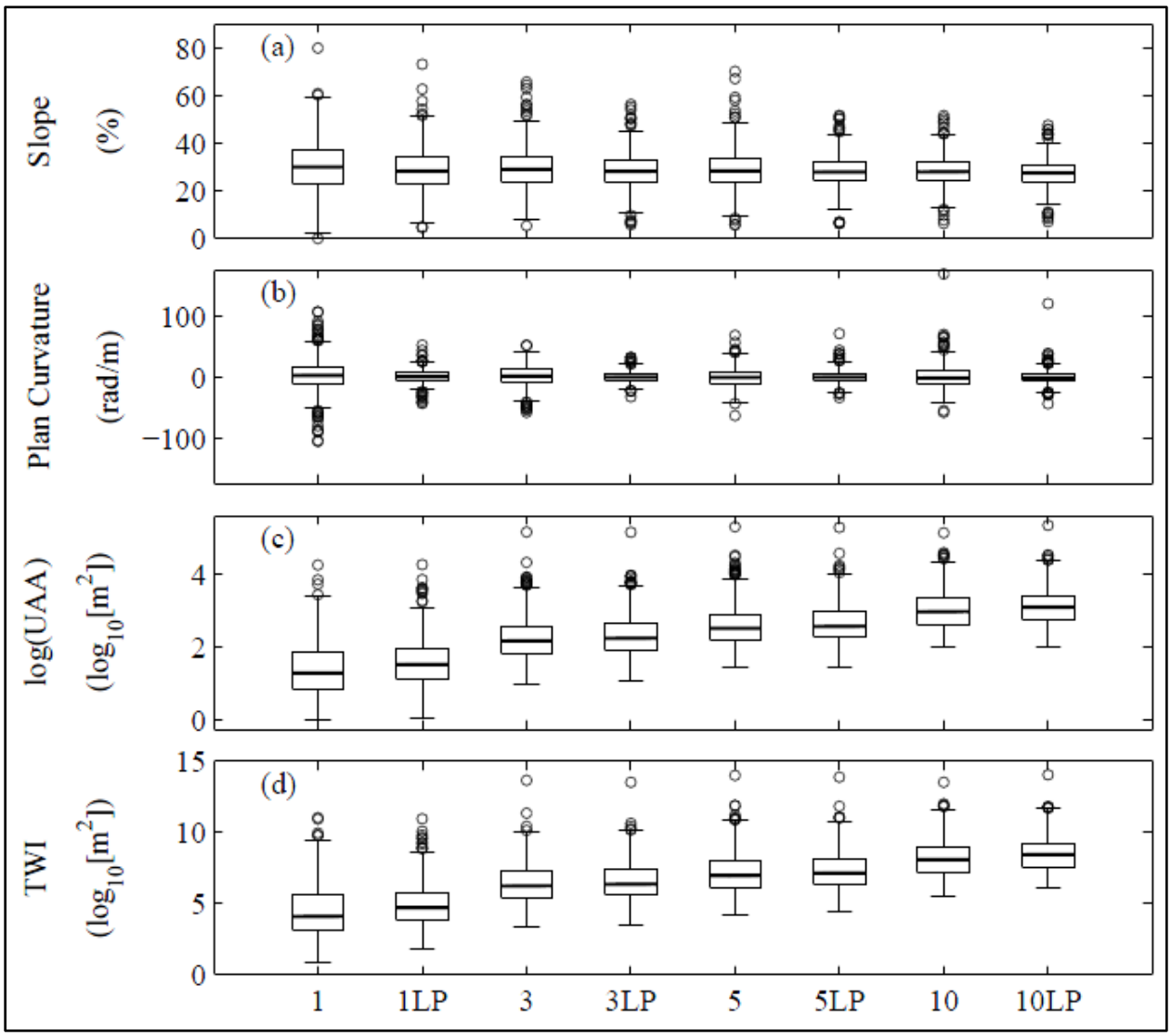

Figure 2.4. Box and whisker plots indicate variation in distribution of topographic metrics for WMNF slope (a), plan curvature (b), UAA (c), and TWI (d). Median values are represented by the thick black line, boxes represent the interquartile range, whiskers extend 1.5 times the interquartile range beyond the interquartile range box and contain approximately 99.3% of the data, and circles indicate points outside 99.3% of the data. Topographic metrics were computed for each DEM and values were extracted to 421 random points generated inside the WS3 boundary.

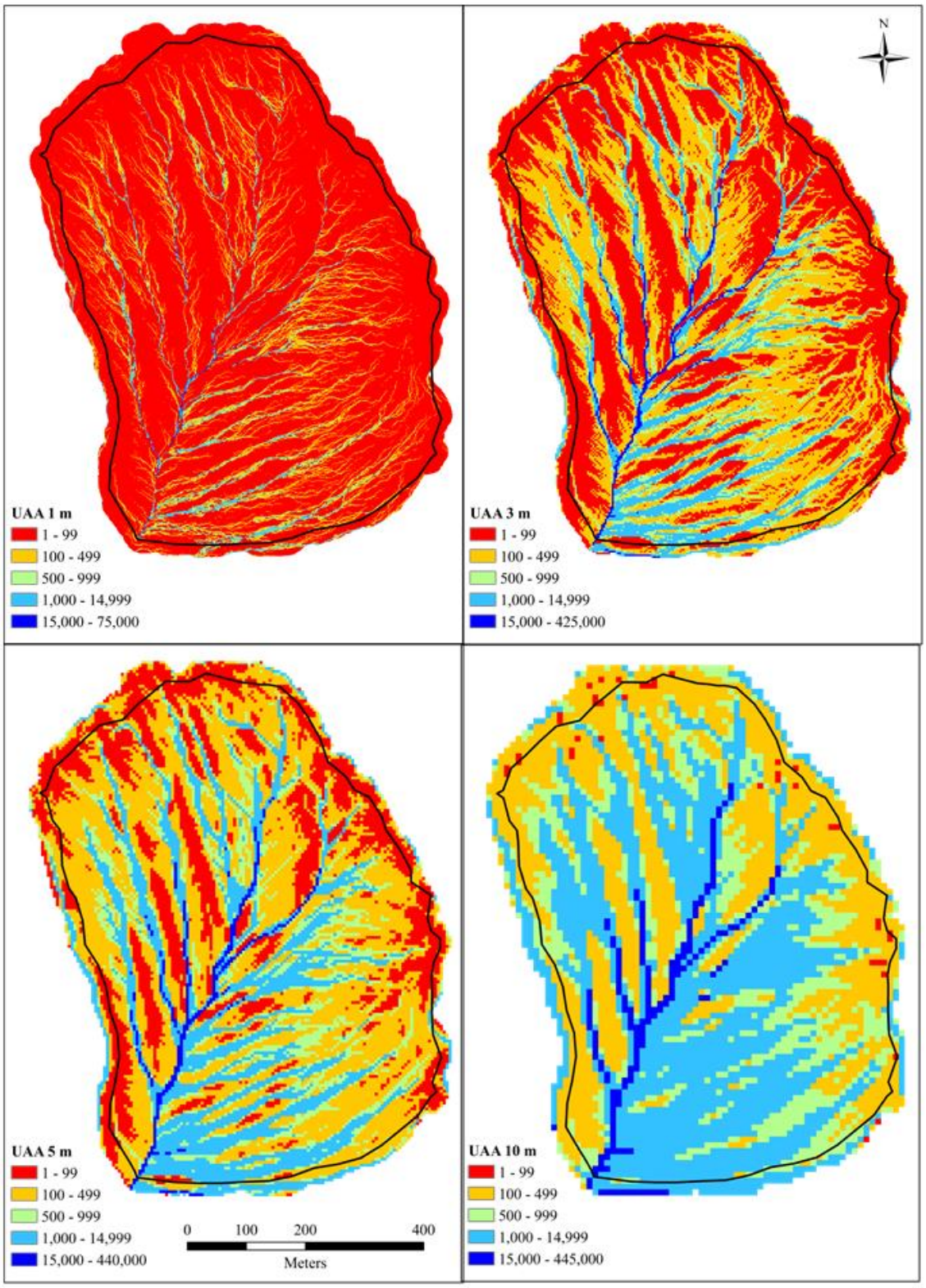

Figure 2.5. UAA computed for 1 m, 3 m, 5 m, and 10 m WMNF DEMs. Black line denotes the field-surveyed catchment boundary.

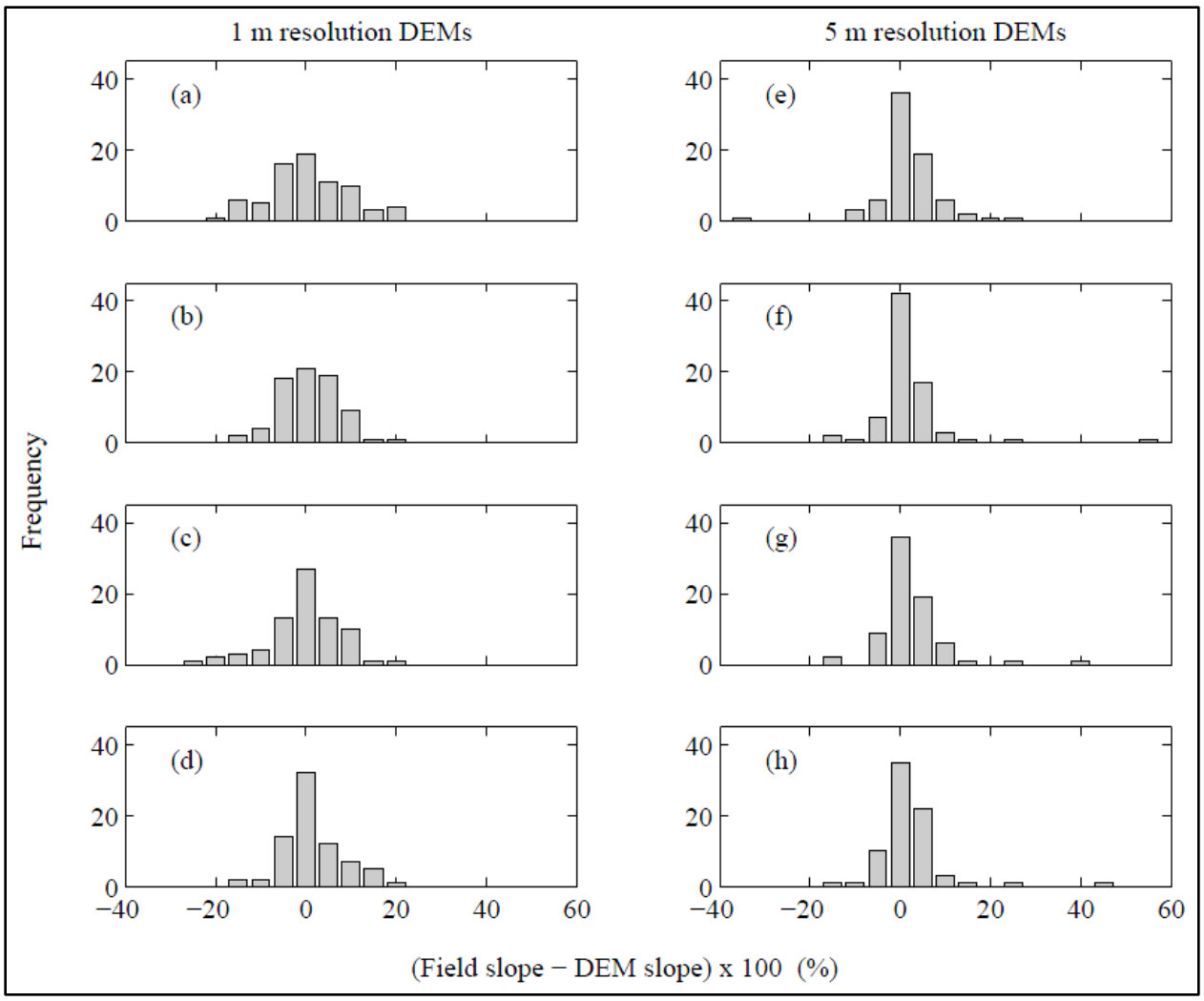

Figure 2.6. Field slope values measured with a clinometer compared with DEM-derived slope values computed using the maximum slope algorithm for NCALM 1 m (a), 1 m LP (b), 5 m (e), 5 m LP (f), and WMNF 1 m (c), 1 m LP (d), 5 m (g), and 5 m LP (h) DEMs. Slopes were measured for 75 locations corresponding with soil pits and shallow subsurface wells. The x-axis denotes DEM difference from field slope in percent (%).

2.8. References

Aguilar, F. J., F. Aguera, M. A. Aguilar, and C. Fernando (2005), Effects of terrain morphology, sampling density, and interpolation methods on grid DEM accuracy, Photogrammetric Engineering & Remote Sensing, 71, 805-816.

Anderson, E. S., J. Thompson, D. A. Crouse, and R. E. Austin (2006), Horizontal resolution and data density effects on remotely sensed LiDAR-based DEM, Geoderma, 132, 406-415.

Bailey, A. S., J. W. Hornbeck, J. L. Campbell, and C. Eagar (2003), Hydrometeorological database for Hubbard Brook Experimental Forest: 1955-2000Rep., 36 pp, USDA Forest Service, Northeastern Research Station.

Bailey, S. W., P. A. Brousseau, K. J. McGuire, and D. S. Ross (in review), Influence of hillslope position and shallow water table dynamics on soil development and carbon distribution in a steep, headwater catchment, Geoderma.

Band, L. E., and I. D. Moore (1995), Scale: Landscape attributes and geographical information systems, Hydrological Processes, 9, 401-422.

Barton, C. C., R. H. Camerlo, and S. W. Bailey (1997), Bedrock geologic map of Hubbard Brook Experimental Forest and maps of fractures and geology in roadcuts along Interstate-93, Grafton County, New Hampshire, Sheet 1, Scale 1:12,000; Sheet 002, Scale 001:200, US Geological Survey, Miscellaneous Investigations Series, Map I-2562.

Beven, K., and M. Kirkby (1979), A physically based, variable contributing area model of basin hydrology, Hydrological Sciences Bulletin, 24, 43-69.

Detty, J. M., and K. J. McGuire (2010), Threshold changes in storm runoff generation at a till-mantled headwater catchment, Water Resources Research, 46, W07525.

Gallant, J. C., and M. F. Hutchinson (1996), Towards and understanding of landscape scale and structure, paper presented at Third International Conference/Workshop on Integrating GIS and Environmental Modeling, Santa Fe, NM, January 21-26, 1996.

Hancock, G. R. (2005), The use of digital elevation models in the identification and characterization of catchments over different grid scales, Hydrological Processes, 19, 1727-1749.

Hancock, G. R., G. R. Willgoose, and K. G. Evans (2002), Testing of the SIBERIA landscape evolution model using the Tin Camp Creek, Northern Territory, Australia, field catchment, Earth Surface Processes and Landforms, 27, 125-143.

Hodgson, M. E., X. Li, and Y. Cheng (2004), A parameterization model for transportation feature extraction, Photogrammetric Engineering & Remote Sensing, 12, 1399-1404.

Höhlea, J., and M. Höhle (2009), Accuracy assessment of digital elevation models by means of robust statistical methods, ISPRS Journal of Photogrammetry and Remote Sensing, 64, 398-406.

Hu, P., X. Liu, and H. Hu (2009), Accuracy assessment of digital elevation models based on approximation theory, Photogrammetric Engineering & Remote Sensing, 75, 49-56.

Isaacson, D. L., and W. J. Ripple (1990), Comparison of 7.5-minute and 1-degree digital elevation models, Photogrammetric Engineering & Remote Sensing, 56, 1523-1527.

Jenson, S. K. (1991), Applications of hydrologic information automatically extracted from digital elevation models, Hydrological Processes, 5, 31-44.

Jenson, S. K., and J. O. Domingue (1988), Extracting topographic structure from digital elevation data for geographic information system analysis, Photogrammetric Engineering and Remote Sensing, 54, 1593-1600.

Likens, G. E., and F. H. Bormann (1995), Biogeochemistry of a forested ecosystem, 159 pp., Springer-Verlag, New York.

Lillesand, T. M., and R. W. Kiefer (2000), Remote Sensing and Image Interpretation, Fourth ed., John Wiley and Sons, Inc., New York.

Liu, X., Z. Zhang, J. Peterson, and S. Chandra (2007a), The effect of LiDAR data density on DEM accuracy, paper presented at Proceedings of the International Congress on Modelling and Simulation (MODSIM07), Christchurch, New Zealand.

Pennock, D. J., B. J. Zebarth, and E. Dejong (1987), Landform classification and soil distribution in hummocky terrain, Saskatchewan, Canada, Geoderma, 40, 297-315.

Planchon, O., and F. Darboux (2001), A fast, simple and versatile algorithm to fill the depression of digital elevation models, Catena, 46, 159-176.

Quinn, P., K. Beven, and R. Lamb (1995), The in(a/tan/β) index: How to calculate it and how to use it within the topmodel framework, Hydrological Processes, 9, 161-182.

Quinn, P., K. Beven, P. Chevallier, and O. Planchon (1991), The prediction of hillslope flow paths for distriubted hydrological modelling using digital terrain models, Hydrological Processes, 5, 59-79.

Raber, G. T., J. R. Jensen, M. E. Hodgson, J. A. Tullis, B. A. Davis, and J. Berglund (2007), Impact of Lidar Nominal Post-spacing on DEM Accuracy and Flood Zone Delineation, Photogrammetric Engineering & Remote Sensing, 73, 793-804.

Saulnier, G. M., K. Beven, and C. Obled (1997), Digital elevation analysis for distributed hydrological modeling: Reducing scale dependence in effective hydraulic conductivity values, Water Resources Research, 33, 2097-2101.

Seibert, J., and B. L. McGlynn (2007), A new triangular multiple flow direction algorithm for computing upslope areas from gridded digital elevation models, Water Resources Research, 43, W04501.

Shi, X., L. Girod, R. Long, R. DeKett, J. Philippe, and T. Burke (2012), A comparison of LiDAR-based DEMs and USGS-sourced DEMs in terrain analysis for knowledge-based digital soil mapping, Geoderma, 170, 217-226.

Sorensen, R., and J. Seibert (2007), Effects of DEM resolution on the calculation of topographical indices: TWI and its components, Journal of Hydrology, 347, 79-89.

Travis, M. R., G. H. Elsner, W. D. Iverson, and C. G. Johnson (1975), VIEWIT: computation of seen areas, slope, and aspect for land-use planning, in USDA General Technical Report PSW-11/1975, edited, Berkely, California, USA.

Troeh, F. R. (1964), Landform parameters correlated to soil drainage, Soil Science Society of America Proceedings, 28, 808-812.

Vaze, J., J. Teng, and G. Spencer (2010), Impact of DEM accuracy and resolution on topographic indices, Environmental Modelling & Software, 25, 1086-1098.

Wang, L., and H. Liu (2006), An efficient method for identifying and filling surface depressions in digital elevation models for hydrologic analysis and modelling, International Journal of Geographical Information Science, 20, 193-213.

Wolock, D. M., and C. V. Price (1994), Effects of digital elevation model map scale and data resolution on a topography-based watershed model, Water Resources Research, 30, 3041-3052.

Wolock, D. M., and G. J. McCabe (2000), Differences in topographic characteristics computed from 100- and 1000-m resolution digital elevation model data, Hydrological Processes, 14, 987-1002.

Wu, S., J. Li, and G. H. Huang (2008), A study on DEM-derived primary topographic attributes for hydrologic applications: Sensitivity to elevation data resolution, Applied Geography, 28, 210-223.

Zaslavsky, D., and A. S. Rogowski (1969), Hydrologic and morphologic implications of anisotropy and infiltration in soil profile development, Soil Science Society of America Proceedings, 33, 594-599.

Zevenbergen, L. W., and C. R. Thorne (1987), Quantitative analysis of land surface topography, Earth Surface Processes and Landforms, 12, 47-56.

Zhang, W., and D. R. Montgomery (1994), Digital elevation model grid size, landscape presentation, and hydrologic simulation, Water Resources Research, 30, 1019-1028.

Zimmer, M. A., S. W. Bailey, K. J. McGuire, and T. D. Bullen (2012), Fine scale variations of surface water chemistry in an ephemeral to perennial drainage network, Hydrological Processes, doi: 10.1002/hyp.

Chapter Three

3.0. Topographic metrics to predict hydropedologic spatial patterns

Abstract: Recent literature has advocated the application of hydropedology, or the integration of hydrology and pedology, to better understand hydrologic flowpaths and soil spatial heterogeneity in a landscape. Hydropedology can be used to describe soil units affected by distinct topography and hydrological processes. Such an approach has not been applied to digital soil mapping in the context of spatial variations in hydrological and biogeochemical function. The purpose of this study is to use field observations of soil morphology and geospatial information technology to predict the distribution of five hydropedological units (HPUs) across a 42 ha forested headwater catchment in New England. Watershed 3 (WS3) serves as the hydrologic reference catchment for the Hubbard Brook Experimental Forest and was selected as the test site due to known variations in sub-catchment surface water, subsurface water, and soil chemistry. 172 soil characterization pits were located throughout the catchment and HPU was identified based on the presence and thickness of genetic soil horizons. Results indicate that each HPU occurs under specific topographic settings that influence subsurface hydrologic conditions. The most important metrics for predicting HPUs were Euclidean distance from bedrock outcrop, the topographic wetness index, and bedrock-weighted upslope accumulated area. This study is unique in that it delineates high-resolution soil units using a process-based morphological approach rather than a taxonomical method taken by conventional soil surveys. Hydropedological predictor models can be a valuable tool for informing watershed management and soil carbon accounting.

Keywords: hydropedology, digital elevation model, topographic wetness index, Hubbard Brook Experimental Forest

3.1. Introduction

Recently, it has been suggested that incorporating disciplines such as hydrology, pedology, and geomorphology and emphasizing observed patterns when studying catchment basins might advance an understanding of controls on catchment-scale hydrological processes [*Sivapalan*, 2005]. Lack of understanding of heterogeneity and system complexities across space and time and an inability of watershed hydrologists to extrapolate findings and make predictions across regions and spatial scales might be remedied through the integration of hydrology with ecology and other related disciplines [*McDonnell et al.*, 2007]. The emerging discipline of hydropedology, or the integration of hydrology and soil science [*Lin et al.*, 2006], may provide a useful framework for examining hydrological and pedogenic processes that control heterogeneity and system complexity, and offer insight into hydrologic and biogeochemical function in headwater catchments.

Both topography and hydrological processes were long ago recognized as key factors affecting soil development [*Jenny*, 1941]. Soil moisture and hydrologic flowpaths have been shown to control soil composition and morphology [e.g., *Daniels et al.*, 1975; *Knuteson et al.*, 1989; *Pennock et al.*, 1987; *Zaslavsky and Rogowski*, 1969] and to be a principal cause of soil physical and chemical variability [*Norris*, 1972]. Other studies have related soil variability to landscape position [*Young and Hammer*, 2000] and topography [*Moore et al.*, 1993]. Traditional pedology tends to characterize water and solute transport through soils as vertical in nature [*Zaslavsky and Rogowski*, 1969]; thus, a typical representation of a soil profile reflects vertical percolation and translocation of minerals and organic material leading to horizontal layering. Yet, several recent studies documented lateral components to solute transport and water flow through soils [*McDaniel et al.*, 1992], podzolization [*Sommer et al.*, 2000] and pedogenic

processes in general [*Park and Burt*, 2002; *Sommer and Schlichting*, 1997]. Lateral translocation results in distinct soil morphology and composition and could provide the basis for enhanced understanding of hydrologic, pedogenic, and biogeochemical processes and patterns at the catchment level.

Over the past two decades, advancements in computer processing, remote sensing, and geospatial information technology have facilitated an evolution of digital approaches to soil mapping. The most common strategies fall under the broad umbrella of spatial inference models and generally require observed soil data and some sort of ancillary data related to one or more of the soil forming factors. *McBratney et al.* [2003] provide a detailed inventory of these models. Spatial inference models can be categorized into data mining approaches such as multiple regression models [*Moore et al.*, 1993] or classification trees [*Bell et al.*, 1992; 1994], geostatistical approaches such as regression kriging [*Odeh et al.*, 1994; 1995], and approaches utilizing the knowledge of soil surveyors with expertise in a given region [*Lagacherie et al.*, 1995; *Zhu et al.*, 1996].

Soils can be represented as discrete units with sharp boundaries or as fuzzy units with gradual transitions. Soils are continuous in nature, so their representation as discrete units involves uncertainty. This uncertainly can be reduced using a fuzzy logic approach. Fuzzy representations permit membership of more than one soil type for each map pixel, resulting in gradual transitions between soil units. Categorization, based on probability, can be used to estimate fuzzy membership. Probability that a given map pixel is covered by a given soil type can be determined using environmental predictor variables such as those related to topography and hydrological processes.

One fuzzy approach to digital soil mapping involves the use of logistic regression models. For example, *Campling et al*. [2002] used binomial logistic regression to predict soil drainage class using topographic metrics and vegetation indices. *Kempen et al*. [2009] used multinomial logistic regression (MNR) to update conventional soil survey maps. *Debella-Gilo and Etzelmuller* [2009] predicted soil groups using a variety of topographic metrics as predictors in an MNR model. Logistic regression models offer numerous benefits. Unlike multiple linear regression, logistic regression handles non-linear relationships in soil-landscape associations. MNR models can incorporate multiple prediction categories, the regressors may be continuous or categorical, and accuracy can be assessed by cross-validating the model against a set of data not used during model development. Logistic regression is also less demanding than other non-linear methods in terms of normality of the underlying data [*Real et al.*, 2006]. MNR is a common statistical method for predicting soil categories [*Bailey et al.*, 2003; *Debella-Gilo and Etzelmuller*, 2009; *Hengl et al.*, 2004; *Kempen et al.*, 2009].

While the previous studies demonstrated the utility of logistic regression as a quantitative approach to digital soil mapping, each made predictions using coarse DEMs of 25 m resolution. Logistic regression may also be appropriate for mapping soil units at a finer resolution, although such a method has not been reported in the literature. Recently, high-resolution DEMs (1 m to 10 m) derived from LiDAR data have become more accessible and their use for topographic analysis and topographic metric computation is increasingly commonplace. In pedogenic and geomorphologic applications such topographic analyses are often used as representations of spatial variation of hydrological processes and conditions [*Guntner et al.*, 2004; *Merot et al.*, 1995].

Previous research suggested that DEM resolution used to compute topographic metrics for hydrologic modeling must reflect the scale of features vital to the hydrologic response [*Quinn et al.*, 1991]. Furthermore, the finest grid resolution available may not be ideal for predicting soil-landscape relationships [*Wu et al.*, 2008b] or other soil/hydrologic phenomena [*Gillin et al.*, in review]. High-resolution DEMs may offer a level of landscape roughness greater than that controlling surface/near surface flow pathways that can interfere with the computation of some topographic metrics, including those related to hydrological processes. In such situations a DEM may be coarsened to a lower resolution or treated with a smoothing filter, both of which have the effect of mitigating landscape roughness. Common methods for DEM coarsening include nearest neighbor, bilinear or cubic convolution resampling and cell aggregation [e.g., *Band and Moore,* 1995; *Sorensen and Seibert*, 2007; *Wu et al.*, 2008a]. Smoothing filters mitigate landscape roughness [*Lillesand and Kiefer*, 2000] without generating a coarser DEM, thus maintaining greater topographic detail.

The relationship between landscape and both water and soil has been a critical component of research at the Hubbard Brook Experimental Forest (HBEF) [e.g., *Johnson et al.*, 2000; *Palmer et al.*, 2004; *Zimmer et al.*, 2012]. Soils at the HBEF have been characterized predominantly as Spodosols with considerable spatial heterogeneity of physical properties [*Johnson et al.*, 2000], yet current soil maps do not offer a complete picture of field observations [*Bailey et al.*, in review]. More recent investigations utilizing a hydropedologic framework indicated common development of a transient water table [*Detty and McGuire*, 2010] and a broad range in drainage class variability and horizontal hydrologic controls leading to lateral podzolization of HBEF soils [*Bailey et al.*, in review].

Field examination of soil morphological differences in Watershed 3 (WS3), one of the HBEF experimental watersheds, led to the conceptualization of functional soil units termed hydropedological units (HPUs). *Sommer et al*. [2000] suggested that podzolization processes facilitate soil unit development through distinct topography and subsurface flowpaths. In steep topography or mountainous regions, where subsurface heterogeneities facilitate lateral water movement, vertical podzolization tends to occur at the pedon scale, whereas lateral podzolization tends to occur at the hillslope or catena scale [*Sauer et al.*, 2007]. Following this work, researchers in WS3 hypothesized that soil morphological variability in WS3 results from variation in the direction and magnitude of subsurface water flow, and that soil differences occur in a predictable spatial distribution related to topography and hydrologic flowpaths [*Bailey et al.*, in review].

Five HPUs (each a variation of a podzol) have been identified in WS3. E podzols have thick greyish-colored E horizons (eluviated mineral soil of low organic matter content) and no B horizons (mineral soils) [*Sommer et al.*, 2000]. They occur in bedrock-controlled landscapes where lateral flowpaths dominate. Bhs podzols are found immediately downslope of E podzols where lateral flow continues to affect soil development [*Sommer et al.*, 2000]. These soils tend to lack an E horizon but have a thick dark reddish-brown Bhs horizon (illuviated material). Typical podzols, which have Bhs/Bs horizons but no Bh horizon (accumulated organic material), comprise a majority of soils in WS3 and are found on backslopes throughout the catchment. Their morphology indicates vertical flow influence on development. Bimodal podzols are a transitional HPU found at backslope-footslope locations below typical and above Bh podzols. These soils have an upper sequence resembling that of a typical podzol, but also contain a layer of illuviated organic material at the B-C interface where water tables develop seasonally. All

typical-Bh podzol transitions do not necessarily have a bimodal expression. Bh podzols occur in less steep areas, and in particular riparian areas (riparian Bh), but occasionally at upslope locations on hillslope benches (hillslope Bh) at least 10 m from the nearest stream. Bh podzols are influenced predominantly by lateral flow and are a result of transient water table development that reaches into the B horizon. They are comprised of thick, dark brown organic Bh horizons and typically lack an E horizon.

If topography and landscape shape affect hydrological processes that in turn influence soil development, then topographical information may be used to interpret hydrological processes and predict soil attributes and soil morphological variation. Furthermore, the use of topographic metrics for soil mapping, especially at the mesoscopic- and macroscopic-scale (i.e., catena- and watershed-scale) [*Lin*, 2003], may be preferable to techniques utilizing qualitative landform units that lack consistency of method [*Moore et al.*, 1993]. This study aimed to apply digital soil mapping techniques using topographic metrics computed from a high-resolution DEM as regressors in a logistic regression model to predict the spatial distribution of HPUs across a 42 ha catchment in the Hubbard Brook Experimental Forest. We propose that mapping process-based soil units will facilitate a better understanding of headwater catchment functionality in terms of hydrological processes, biogeochemistry, soil quality, and other management concerns such as forest nutrition and soil carbon storage.

3.2. Study location

The Hubbard Brook Experimental Forest (HBEF) (Figure 2.1), located in the White Mountains of New Hampshire (43°56’N, 71°45’W), is maintained by the United States Forest Service (USFS), Northern Research Station and is part of the National Science Foundation Long-Term Ecological Research (NSF LTER) network. Watershed Three (WS3), the hydrologic

reference catchment, is underlain by mica schist of the Silurian Rangeley formation [*Barton et al.*, 1997] and covered by glacial tills of varying thickness. Soils are predominantly Spodosols of sandy loam texture developed in glacial till parent material [*Likens and Bormann*, 1995]. Elevation ranges from 527 m to 732 m. The western side of the catchment is characterized by steep spurs flanking intermittent and perennial streams, while the eastern portion exhibits little or no evidence of channel formation. Bedrock outcrops are found in the upper portion of the catchment.

Climate at the HBEF is humid continental. Winters tend to be long and cold with an average January temperature of -9°C. Summers are mild with July temperatures averaging 19°C (temperature averages recorded at 450 m elevation). Annual precipitation averages 1400 mm, with about 30% falling as snow. Streamflow is high in the spring (nearly half of the 870 mm average annual runoff occurs during snowmelt) and very low in late summer/early autumn [*Bailey et al.*, 2003].

The catchment is dominated by second-growth northern hardwood forest including sugar maple (*Acer saccharum*), American beech (*Fagus grandifolia*), and yellow birch (*Betula alleghaniensis*) with shallow-to-bedrock areas dominated by red spruce (*Picea rubens*) and balsam fir (*Abies balsamea*) interspersed with mountain white birch (*Betula cordifolia*). The forest was harvested from 1880 to 1920 and damaged by a hurricane in 1938 [*Likens and Bormann*, 1995].

3.3. Methods

3.3.1. Soil characterization and HPU designation

A total of 172 soil characterization pits were dug throughout WS3 between 2008 and 2012 during several field campaigns (Figure 3.2). Pit locations were selected to include diverse

topography and landscape positions. Many pits were positioned at 3 m to 10 m intervals in down- or across-slope transects and grids to document fine-scale soil morphological changes and better understand the spatial extent of HPUs. Soils were characterized by horizon thicknesses, Munsell color, and texture. These data were used to designate genetic horizons, and HPU was identified for each pit location based on the presence and thickness of soil horizons (Figure 3.3). Horizon and HPU designations were cross-validated by two or more surveyors. HPU sample totals were 67 typical podzols, 38 Bh podzols, 29 Bhs podzols, 20 E podzols, and 18 bimodal podzols. We collected GPS locations for each pit using a Trimble Geo XT 2005 GPS unit equipped with a Trimble Hurricane Antenna. Data were differentially-corrected using Trimble Pathfinder software and Continuously Operating Reference Station (CORS) data from the National Geodetic Survey to obtain circa-one meter precision of horizontal positions.

3.3.2. LiDAR data collection and topographic metric computation

LiDAR (Light Detection and Ranging) data were collected for the USFS White Mountain National Forest (WMNF) in November 2010 and December 2012 by Photo Science, Inc. during leaf-off and snow-free conditions. Points classified as ground were used to interpolate a 1 m DEM using Terrasolids software (http://www.terrasolid.com). Ground return densities in WS3 were determined using LAS Tools software (http://www.cs.unc.edu/~isenburg/lastools) to be approximately 1.16 points per square meter.

We coarsened and filtered the native 1 m DEM. Coarsening was achieved through mean cell aggregation to a 5 m grid resolution. A 5 m grid resolution was selected after considering the spatial extent of smaller HPUs observed in the field (E and bimodal podzols) as well as the behavior of topographic metrics extracted from 5 m DEMs [*Gillin et al.*, in review]. The DEM was then treated with a low-pass smoothing filter over a nine-cell square neighborhood moving

window to smooth landscape roughness and facilitate computation of flow accumulation algorithms. A sink-filling algorithm [*Wang and Liu*, 2006] modified in System for Automated Geoscientific Analyses (SAGA) software (version 2.1.0) to maintain a downslope gradient was also applied to the DEM.

A variety of topographic metrics were computed (Table 3.1). All digital terrain analyses were conducted using ArcGIS (ArcMap version 10.1, ESRI, Redlands, CA) and SAGA. Two slope algorithms were calculated. The first (Slp) was calculated using the maximum slope algorithm [*Travis et al.*, 1975] and the second using the downslope index ($DI = d/L_d$; [*Hjerdt*, 2004]). UAA was computed using the Triangular Multiple Flow Direction algorithm [*Seibert and McGlynn*, 2007]. Subsequently, two versions of the TWI were computed – one using Slp and UAA, and the second using DI and UAA.

3.3.3. Ordination of soil data using non-metric multidimensional scaling

To identify topographic metrics for use as predictor variables in an MNR model, an ordination of presence/absence of genetic soil horizons and soil horizon thickness data using non-metric multidimensional scaling (NMS) was used to examine HPU similarity. We selected the Bray-Curtis dissimilarity [*Bray and Curtis*, 1957] as the measure of ecological distance. NMS is an iterative process – therefore, we examined the ordination of HPU data in both two and three dimensions to determine the number of dimensions required to reduce Kruskal's stress criterion [*Clarke*, 1993] (i.e., departure from monotonicity in the plot of distance in the original dissimilarity matrix and distance in the reduced ordination space). The Mantel R statistic was used to assess the fitted distances (i.e., the NMS model) vs. Bray-Curtis dissimilarities in the ordination. Finally, a biplot of the computed topographic metrics represented as Spearman

correlates was placed over the NMS ordination and correlation significance for each topographic metric were examined ($\alpha = 0.05$).

3.3.4. Multinomial logistic regression model development

The relationships between topographic metrics and soil type are often non-linear, yet building non-linear models to represent these relationships is complicated and linear models are generally preferred [*Debella-Gilo and Etzelmuller*, 2009]. Logistic regression belongs to the family of generalized linear models and is one of the most suitable linear models for handling non-linear relationships [*Real et al.*, 2006]. The method relates the natural logarithm of the odds ratio of a dependent categorical variable to independent variables (continuous or categorical), where the odds ratio represents the ratio of the probability of presence versus absence of each dependent categorical variable (i.e., HPU type).

HPU category represents the dependent (response) variable Y_i where $i = 1,\ldots, n$ and n = the total number of HPU types or categories identified in the field. The probability of occurrence of each category is $\pi_1,\ldots, \pi_n$. Logistic regression relates a given probability π_i to a set of predictor variables using the logit link function. To determine the probability of occurrence of category 1, Consider the following example where $n = 2$:

$$\text{Logit}(\pi_1) = \ln(\pi_1 / \pi_2) = \ln(\pi_1 / 1 - \pi_1) = \mathbf{x}'\boldsymbol{\beta} \quad (1)$$

where $\mathbf{x}$ represents a vector of predictor variables and $\boldsymbol{\beta}$ represents a vector of model coefficients. Equation 1 can be rewritten as:

$$\pi_1 / 1 - \pi_1 = \exp(\mathbf{x}'\boldsymbol{\beta}) = \exp(\eta) \quad (2)$$

where the quotient in Equation 2 is referred to as the *odds*. Equation 2 can be simplified as:

$$\pi_1 = \exp(\eta) / 1 + \exp(\eta) \quad (3)$$

The model described above, which is binomial (response variable is either 1 or 2), can be manipulated to handle multinomial situations. In the case of this study, *n* HPUs correspond with *m* response variables, each with a probability of occurrence $\pi_1,\ldots, \pi_n$ for a given set of predictor variables. Like the binomial logistic regression the odds $\pi_1 / \pi_n,\ldots, \pi_{n-1} / \pi_n$ may be modeled as $\exp(\eta_1),\ldots, \exp(\eta_{n-1})$, and it follows that:

$$\pi_i = \exp(\eta_i) / \exp(\eta_1) + \exp(\eta_2) + \ldots + \exp(\eta_n)$$

where $\eta_n = 0$, ensuring that all probabilities are in the range 0 to 1 and that the sum of all probabilities equals 1. So, for a given point on the landscape the MNR model will provide probabilities for HPU_1, HPU_2, HPU_3, HPU_4, and HPU_5, where the probability values sum to 1.

Logistic regression requires that one of the dependent variables be used as a reference to make comparisons with all other dependent variables. We selected typical podzols, which are the dominant HPU present in WS3, as the reference variable for which all other HPUs were compared. Model significance was examined using the likelihood ratio statistic [*Hosmer and Lemeshow*, 2004], the Akaike Information Criterion (AIC) [*Akaike*, 1973; *Campling et al.*, 2002], which is based on the likelihood ratio statistic but accounts for the number of observations and predictor variables, and McFadden's pseudo R^2 [*Menard*, 2000].

While dozens of topographic metrics may be computed using a DEM, it is likely that only a subset of all metrics is necessary to predict HPU distribution. Furthermore, logistic regression models may suffer from multicollinearity or fail to achieve model convergence if too many topographic metrics are used as predictor variables. The strongest correlations (positive and/or negative) between topographic metrics and NMS dimensions and uniqueness in NMS space were

used to identify candidate topographic metrics for multinomial logistic regression. Combinations of candidate topographic metrics were tested systematically during MNR model development. First, a metric exhibiting strong correlation was tested alone. Then, a second metric with strong correlation in a different direction was added and the model was re-tested. MNR models were evaluated using the aforementioned criteria (AIC, McFadden's pseudo R^2, and log-likelihood ratio test). This process was repeated until all plausible models were assessed and ranked.

3.3.5. Validation dataset and model accuracy

Twenty-five percent of the total number of pedons for each HPU type was randomly removed prior to MNR model development for use as a validation dataset. Model accuracy was assessed using an error matrix (probability threshold of 0.40) and a receiver operating characteristic (ROC) curve [*Fawcett*, 2006]. The error matrix was used to interpret two measures of categorical accuracy: 1) User accuracy indicates what the user interprets from map predictions; and 2) Overall accuracy indicates the number of field observations correctly classified as a percent of the total number of field observations. ROC curves are generated by plotting model true positive rate on the y-axis and false positive rate on the x-axis for a range of probability thresholds. The diagonal line y = x (when true positive rate equals false positive rate) represents random classification and the point (0, 1) represents perfect classification [*Fawcett*, 2006]. Models were thus evaluated by analyzing an ROC curve's maximization of true positive rate and minimization of false positive rate (i.e., tendency toward the point (0, 1)).

3.4. Results

3.4.1. HPU grouping and topographic metrics

NMS ordination indicated that all HPUs clustered into groups when two dimensions were examined, but bimodal podzols did not cluster when a third dimension was examined. Kruskal's

stress criterion for the two-dimensional ordination was 0.201. Stress decreased to 0.123 with the addition of the third dimension. Kruskal's stress criterion values should be less than 0.2, and ideally less than 0.1 to mitigate the risk of drawing false inferences [*Clarke*, 1993]. Examination of the NMS ordination of soil horizon and horizon thickness data in the first two dimensions showed E, Bhs, typical, Bh, and bimodal podzols separated into groups (Figure 3.4). E, Bhs, typical, and Bh podzols also exhibited clustering in dimensions 1 and 3, while bimodal podzols were scattered throughout the plot (Figure 3.4). The strongest topographic metric correlations were indicated by the length of the vector representing the Spearman correlation of each vector with ordination dimensions (Figure 3.4). All variable correlations except profile curvature (Prof) were significant in dimension 1, only Euclidean distance from stream (EDs) and planform curvature (Plan) correlations were significant in dimension 2, and all variable correlations except elevation above stream (EAS), maximum slope (Slp), and the downslope index (DI) were significant in dimension 3 ($\alpha = 0.05$). Overall, the strongest correlations for almost all topographic metrics occurred in dimensions 1 and 3. Of the variables with the strongest correlations and greatest significance, Euclidean distance from bedrock (EDb), both TWI variants, and UAA were positively correlated with Bh and bimodal podzols and negatively correlated with E, Bhs, and typical podzols (Figure 3.4). EDb, bedrock-weighted UAA (UAAb), EDs, flow distance from stream (FDs), and elevation (Elev) were positively correlated with E, Bhs, and typical podzols and negatively correlated with Bh and bimodal podzols (Figure 3.4).

3.4.2. Predicted soil spatial patterns

Bimodal podzols were excluded from MNR model development due to their lack of clustering in dimensions 1 and 3. After 25% of E, Bhs, typical, and Bh podzols were removed for model validation, a total of 116 pedons remained for model development. The subset of

topographic metrics that produced the best logistic regression model (highest R^2 and third-lowest AIC) included TWI with the downslope index for the tan β parameter (TWId), EDb, and UAAb. This model had an AIC of 156.32 and a McFadden's R^2 of 0.54 (likelihood ratio test statistic = 160.76, degrees of freedom = 9, p-value < 0.001). Table 3.2 provides MNR output for the best subset model. TWId was significant for predicting Bh podzols, EDb was significant for predicting E and Bhs podzols, and UAAb was significant for predicting Bhs and Bh podzols (α = 0.05). The odds ratio represents the likelihood for a given HPU compared to the reference HPU predicted by a given topographic metric for every one-unit increase in metric value. For example, for each 1 m increase in EDb there is an associated 76% decrease in likelihood that the HPU present will be an E podzol. Alternatively, each TWId increase of one unit is associated with a 3.6% increase in likelihood that the HPU present is a Bh podzol.

Graphical representation of HPU probabilities based on topographic metrics aids in the conceptualization of odds ratios (Figure 3.5) HPU graphical probability representations for each topographic metric are based on holding other metrics in the model at their mean values. EDb indicated that near bedrock outcrops HPU type is most likely E or Bhs podzol, and with increasing distance from bedrock HPU type is more likely typical podzol (Figure 3.5). TWId indicated that for lower TWI values HPU type is more likely typical podzol and with increasing TWI HPU type is more likely Bh podzol (Figure 3.5). Typical podzols were predicted for a range of log(UAAb) values while all other HPUs were not predicted by log(UAAb) with high probability (Figure 3.5).

Model coefficients (beta values; see equations 1 and 2) from the MNR model were used to create probabilistic prediction maps for the spatial distribution of HPUs in WS3 (Figure 3.6). E and Bhs podzols were predicted to occur only in the upper region of the catchment in the

bedrock-controlled landscape. Bh podzols were predicted with highest probability to occur near streams and in the southeast portion of the catchment where no streams are present but TWI values were high, with lower probability of occurrence in less steep areas near the catchment divide and no probability elsewhere. Typical podzols were predicted to occur at backslope positions as well as in areas of the bedrock-controlled portion of the catchment containing deeper soil inclusions.

3.4.3. Model validation and measures of categorical accuracy

Thirty-eight validation pedons, representing 25% of the total number of pedons (excluding bimodal podzols), were used for model validation. Typical podzol validation pedons achieved a mean prediction probability of 0.69 with a standard error (SE) of ±0.07, E podzol validation pedons achieved a mean of 0.49 (SE ±0.09), Bhs podzol validation pedons achieved a mean of 0.51 (SE ±0.08), and Bh podzol validation pedons achieved a mean of 0.69 (SE ±0.12) (Figure 3.7). The error matrix indicated user accuracies for typical podzols (0.83), E podzols (0.67), Bhs podzols (0.58), riparian Bh podzols (0.68), and hillslope Bh podzols (0.63) (Figure 3.8). Overall model accuracy, calculated by dividing the sum of all true positives by the total number of pedons in the error matrix, was 0.70. Note that 1 of 154 pedons used for MNR model development failed to achieve probability ≥ 0.40 for any HPU type and thus was not included in the error matrix (the pedon was identified as typical podzol in the field). ROC curves generated for each HPU indicated that at high probability thresholds (0.50 to 0.80) the model produced a true positive rate of 0.50 or less for E and Bhs podzols and 0.74 or less for typical and Bh podzols but also a false positive rate 0.09 or less for all HPUs (Figure 3.9). At lower probability thresholds (0.40 or less) the model produced a higher true positive rate for all HPUs (0.55 to 0.79) with only a small increase in false positive rate (0.04 to 0.14) (Figure 3.9).

3.5. Discussion

3.5.1. NMS ordination indicated clustering of most HPUs

We expected HPUs to cluster in the NMS ordination based on the tendency for each HPU to exhibit characteristic morphological attributes related to horizon presence/absence and thickness of each horizon. For instance, E podzols are comprised of a thick eluviated horizon with or without a thin Bhs horizon over bedrock. Bh podzols develop thick Bh horizons with high amounts of organic material. Indeed, the similarity of horizon presence and thickness for each HPU is reflected in the grouping indicated by the NMS ordination.

Bimodal podzols proved somewhat of an exception to HPU clustering in the NMS ordination, exhibiting clustering in dimensions 1 and 2 but not dimensions 1 and 3. While this HPU tends to exhibit a characteristic horizon sequence, it is perhaps the most variable in terms of thickness of horizons present. Furthermore, field investigations indicated that although bimodal podzols represent a transition HPU type linking typical and Bh podzols, the distance of the transition is variable and in some cases bimodal podzols are not present at all.

The lack of bimodal podzol clustering in the NMS ordination in dimensions 1 and 3 also precluded strong correlation with any of the topographic metrics in dimensions 1 and 3. This result was not entirely unexpected. While bimodal podzols occur most frequently near riparian areas, they can also be found away from streams at hillslope benches where water tables develop seasonally and persist for several weeks or longer. Field investigations indicated that the topography at landscape locations occupied by bimodal podzols is diverse and their morphological expression is variable, which could account for their lack of clustering in the NMS dimensions associated with a lower Kruskal's stress value. However, since bimodal podzols are associated with a typical podzol to Bh podzol transition, their expected location can

still be interpreted from the model by finding areas where typical podzols transition to Bh podzols on the HPU probability maps (Figure 3.6).

Neither planform nor profile curvature was correlated with HPU groups in dimensions 1, 2, or 3 compared with most of the other topographic metrics (0.26 and 0.29 max correlation, respectively). Previous researchers reported that planform and profile curvature are primary geomorphometric parameters important for understanding surface processes [*Schmidt et al.*, 2003]. However, previous analyses finding the importance of curvature utilized DEMs 10 m resolution or coarser. This study suggests that their importance may be less when using DEMs of resolution finer than 10 m for the mapping of soils in a hydrologic context or where subsurface features influence hydrologic process more than surface topography.

3.5.2. Predicted soil spatial patterns and HPU development

In general, HPU predictions match field observations and current understanding of HPU spatial occurrence in WS3. E podzols are predicted near bedrock, Bhs podzols are predicted downslope of E podzols, Bh podzols are predicted adjacent to streams, and typical podzols are predicted everywhere else (Figure 3.6). Bimodal podzols were excluded during model development, but can be interpreted to occur at the typical-Bh transition zone.

Variation in predicted probabilities among HPU types (Figures 3.7 and 3.8) has several possible explanations. MNR can be biased by a disproportionate number of samples [*Real et al.*, 2006]. In WS3, typical podzols are the dominant HPU and represent the largest number of pedons in the sample dataset used to develop the MNR model (followed by Bh, Bhs, and finally E podzols). The uneven number of samples has the potential to bias model predictions toward HPU types with higher samples. This may explain why typical and Bh podzols had a higher mean prediction probability than E or Bhs podzols. The inclusion of other environmental

ancillary data, such as categorical landform classes, may improve prediction probabilities. Furthermore, E and Bhs podzols are much smaller in spatial extent and their extent is variable compared to typical and bimodal podzols, so it can be expected that the probability of their predictions will be somewhat lower. However, lower mean probabilities do not tell the full story for E and Bhs podzol prediction accuracy using MNR. The error matrix indicated a user accuracy of 0.67 for E podzols (Figure 3.8), and the ROC curve indicated the highest true positive rate for Bhs podzols (0.79) at the lowest probability threshold (0.20) (Figure 3.9), suggesting that the model is able to predict E and Bhs podzols using lower probabilities than typical and Bh podzols.

Our model predicted with a user accuracy of 0.63 hillslope Bh podzols (Figure 3.8). Hillslope Bh podzols are perhaps the rarest HPU type in WS3. Field observations from this study noted that two HPUs characterized as hillslope Bh podzols located 25 m above the head of the nearest mapped stream and 25 m below a bedrock outcropping occurred adjacent to an area with evidence of ephemeral channel formation. Such evidence suggests that the mapped stream network needs refinement and that these two hillslope Bh podzols are likely riparian Bh podzols.

Five additional field-identified hillslope Bh podzols occurred in the southeast portion of the catchment where no streams are present, yet digital terrain analyses indicated high TWI and UAA values and flow accumulation algorithms suggested a dense channel network. Additionally, these Bh podzols did not occur on what could be identified as a hillslope bench, but rather on slopes of 10% to 20% and similar to surrounding topography. In this region, 4 of 5 Bh podzols were correctly mapped. The pedogenesis of Bh podzols is hypothesized to be related to lateral subsurface flow processes and the development of transient water tables at toeslope/footslope landscape positions. Frequently, such conditions are found within 5-10 m of a stream in riparian areas that wet up and remain saturated for some weeks following storm events

or snowmelt due to continuous water inputs from upslope locations. However, this does not explain the occurrence of Bh podzols at midslope locations. HBEF soils have been previously characterized as well-drained, but the Bh podzols located away from streams are likely related to heterogeneity of C horizon permeability that permits discontinuous transient water tables upslope of surficial channels that in turn facilitate Bh podzol development.

Although prediction probability of hillslope Bh podzols is not as strong as riparian Bh podzols (Figure 3.8), the model does show that Bh podzols are likely to occur throughout the catchment, both near and away from streams, and especially in lower portions of the catchment away from bedrock (Figure 3.6). This has significance for both research and management objectives. For example, HPU maps indicate soils that develop seasonal water tables that persist for several weeks or more. Trees growing in saturated soils may be at greater risk of blowdown in a windstorm than unsaturated soils. However, soils with higher plant available water may also enhance forest productivity, and so long as the risk of windthrow was low enough such areas could be targeted by forest managers for timber production. Additionally, the presence of a soil type often associated with riparian systems may also indicate the possible occurrence of biota typically associated riparian ecosystems away from streams.

HPU maps also suggest that there is much more carbon stored in HBEF soils (Bh and Bhs podzols) than indicated by previous studies [*Fahey et al.,* 2005; *Huntington et al.,* 1988], which has implications for soil carbon accounting and planning in the face of a changing climate. Long-term climate forecasts for New England have predicted that the region will experience a 3-5° C rise in temperature, increased evapotranspiration leading to as much as 31% reduction in streamflow, and a decrease in amount and duration of snow cover [*Moore et al.,* 1997]. Increased

temperatures, especially in autumn and winter, may promote increased decomposition of stored soil carbon.

In general, mapping the spatial distribution of HPUs offers novel insight into subsurface hydrologic dynamics and distribution. Areas that experience flashy lateral subsurface flow during storm events or snowmelt (E and Bhs podzols), areas that experience the development of seasonal water tables (Bh podzols), and areas that follow the more traditional view of water percolation through the soil (typical podzols) all can be interpreted from the HPU distribution maps (Figure 3.6).

3.6. Conclusions

In order to gain a better understanding of hydrological and biogeochemical functioning of headwater catchments, we used a hydropedological framework to map the distribution of functional soil units (HPUs) using topographic metrics as predictor variables in a multinomial logistic regression model. An NMS ordination of soil horizon data indicated the topographic wetness index, bedrock-weighted UAA, and Euclidean distance from bedrock exhibit the strongest correlations with HPU clustering. Our model indicated that in small headwater systems at the Hubbard Brook Experimental Forest, these three topographic metrics were well correlated to soil type classified by presence/absence and thickness of genetic horizons. However, other metrics, such as elevation above stream, Euclidean distance from stream, and plan curvature also exhibited correlations and should be considered when using topographic metrics to predict soil spatial patterns in a hydropedological framework.

HPU probability maps offer information about the spatial distribution of soils that can be used to interpret hydrological and biogeochemical function within a catchment. Subsurface flowpath, water table development, carbon storage in soils, and perhaps even ecological

communities and areas at increased risk of windthrow or greater productivity may be inferred from examination of the spatial pattern of HPUs. This type of soil map provides a more hydrological and biogeochemical context than traditional taxonomical surveys, and a more comprehensive understanding of spatial heterogeneity of soil and land management characteristics. However, HPUs are much narrower and less comprehensive in terms of specificity of soil physical and chemical properties than taxonomical units, and are not intended as a replacement. The methods used in this study can be calibrated to regions of differing climate without time and monetary inputs in the form of extensive fieldwork or specialized computer software. We recommend future investigations test the application of HPUs to regions outside the WMNF.

3.7. Acknowledgements

Financial support was provided by the National Science Foundation Long-Term Ecological Research (DEB 1114804) and Hydrologic Sciences (EAR 1014507) programs. LiDAR data were collected as part of the National Center for Airborne Laser Mapping seed award program for the hydropedology project and by Photo Science, Inc. for the White Mountain National Forest. Hubbard Brook Experimental Forest (HBEF) context map data courtesy of the Hubbard Brook Ecosystem Study. The HBEF is operated and maintained by the USDA Forest Service Northern Research Station and is part of the NSF Long-Term Ecological Research network.

Table 3.1. Topographic metrics used in a multinomial logistic regression model developed to predict HPU spatial distribution.

Metric	Variable	Method
Raw Elevation (meters)	Elev	Not applicable
Slope (%)	Slp	[*Travis et al.,* 1975]
Downslope Index (%)	DI	[*Hjerdt et al.,* 2004]
Planform Curvature	Plan	SAGA
Profile Curvature	Prof	SAGA
Elevation Above Stream (meters)	EAS	SAGA
Euclidean Distance from Stream (meters)	EDs	ArcMap 10.1
Flow Distance from Stream (meters)	FDs	ArcMap 10.1
Euclidean Distance from Bedrock (meters)	EDb	ArcMap 10.1
Topographic Wetness Index (Slope)	TWIs	[*Beven and Kirkby,* 1979]
Topographic Wetness Index (Downslope Index)	TWId	[*Beven and Kirkby,* 1979]; [*Hjerdt et al.,* 2004]
Upslope Accumulated Area	UAA	Seibert and McGlynn [2007]
Bedrock-weighted Upslope Accumulated Area	UAAb	Novel to this study

Table 3.2. MNR output for the best set of predictor topographic metrics (TWId, EDb, and UAAb). The odds ratio represents likelihood of a given soil type compared to the baseline soil type (typical podzols) when a given topographic metric is used for prediction. Model selection criteria included AIC = 156.3, McFadden's R^2 = 0.54, and likelihood ratio statistic = 160.8.

	Predictor	Beta	SE	t	P-value	Odds Ratio
E podzols	TWId	0.597	0.729	0.818	0.413	1.816
	EDb	-0.269	0.068	-3.970	0.000	0.764
	UAAb	0.306	0.426	0.719	0.472	1.358
Bhs podzols	TWId	1.351	0.692	1.952	0.051	3.862
	EDb	-0.046	0.020	-2.254	0.024	0.955
	UAAb	0.847	0.358	2.368	0.018	2.332
Bh podzols	TWId	1.287	0.286	4.502	0.000	3.623
	EDb	0.008	0.004	1.902	0.057	1.008
	UAAb	-1.774	0.763	-2.324	0.020	-0.170

Log-Likelihood = -69.161
AIC = 156.321
Likelihood ratio test = 160.759 (DF = 9, P-value = 0.000)
McFadden's pseudo R^2 = 0.538

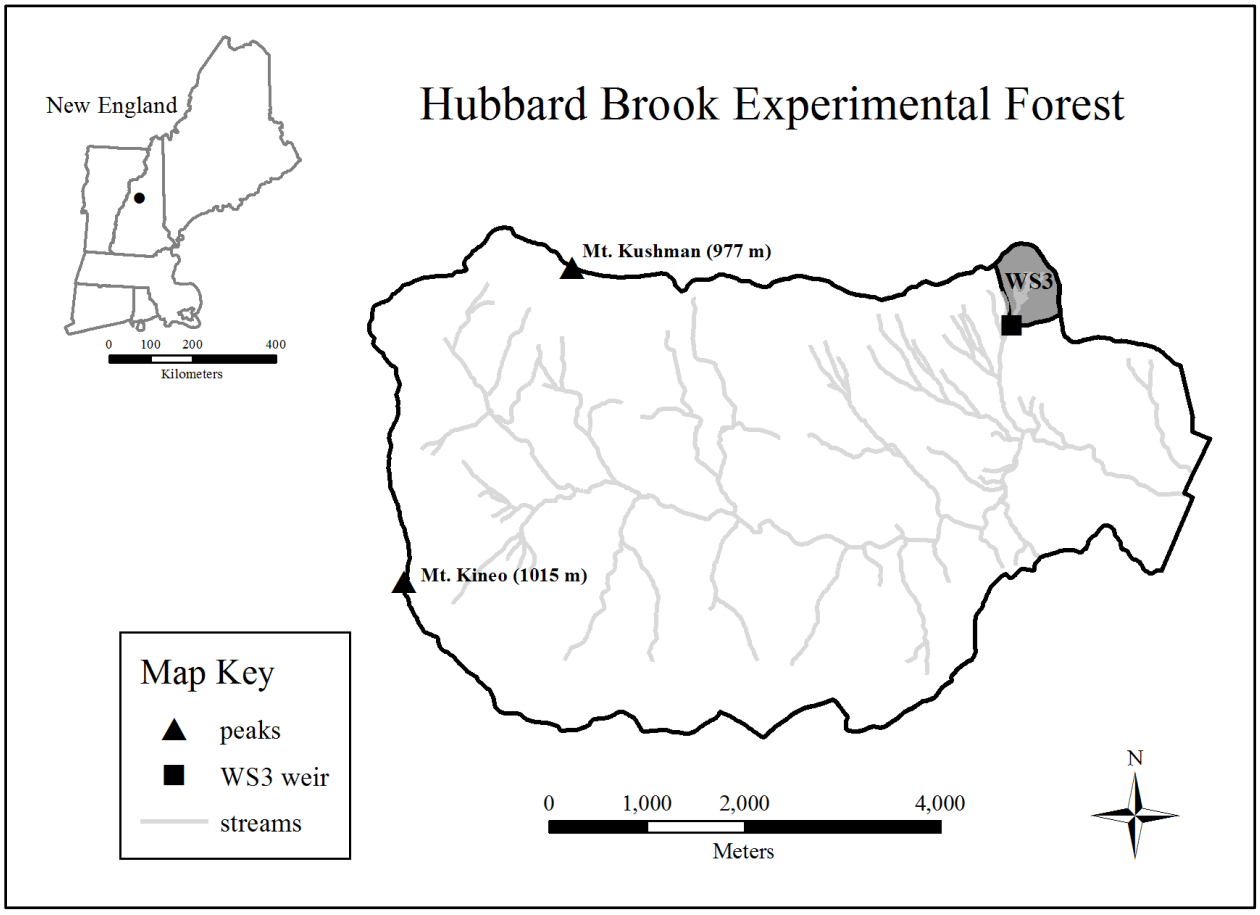

Figure 3.1. Map of Hubbard Brook Experimental Forest, WS3, and location within New England, United States. GIS data provided courtesy of the Hubbard Brook Ecosystem Study (public domain).

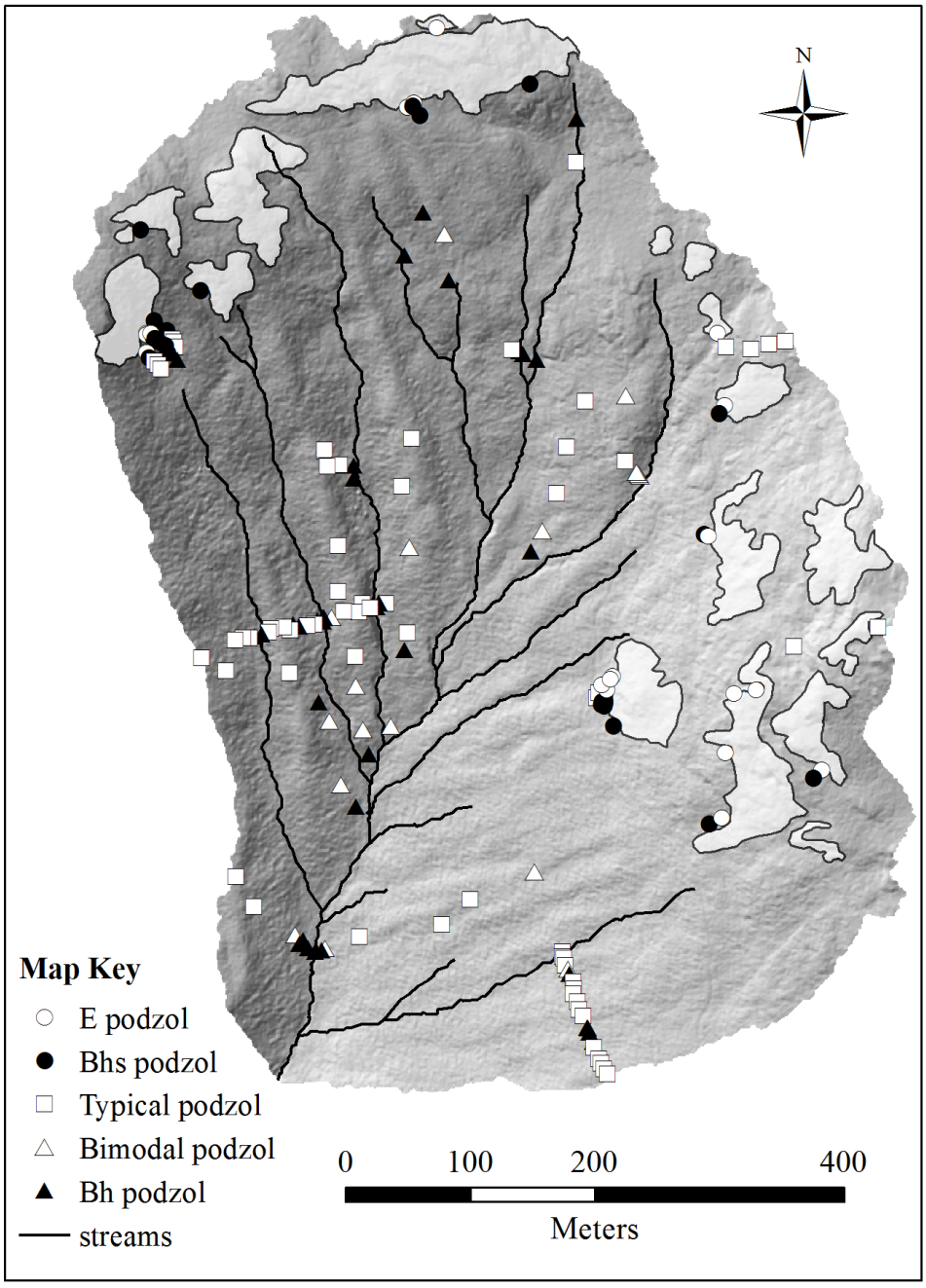

Figure 3.2. Map of soil pits, streams, and bedrock outcrops. A total of 172 soil pits were located in WS3. Soil characteristics, including horizon thicknesses, Munsell color values, and texture, were used to designate genetic soil horizons and infer HPU. Light grey-colored areas represent regions where bedrock is at or near the surface. DEM courtesy of the WMNF.

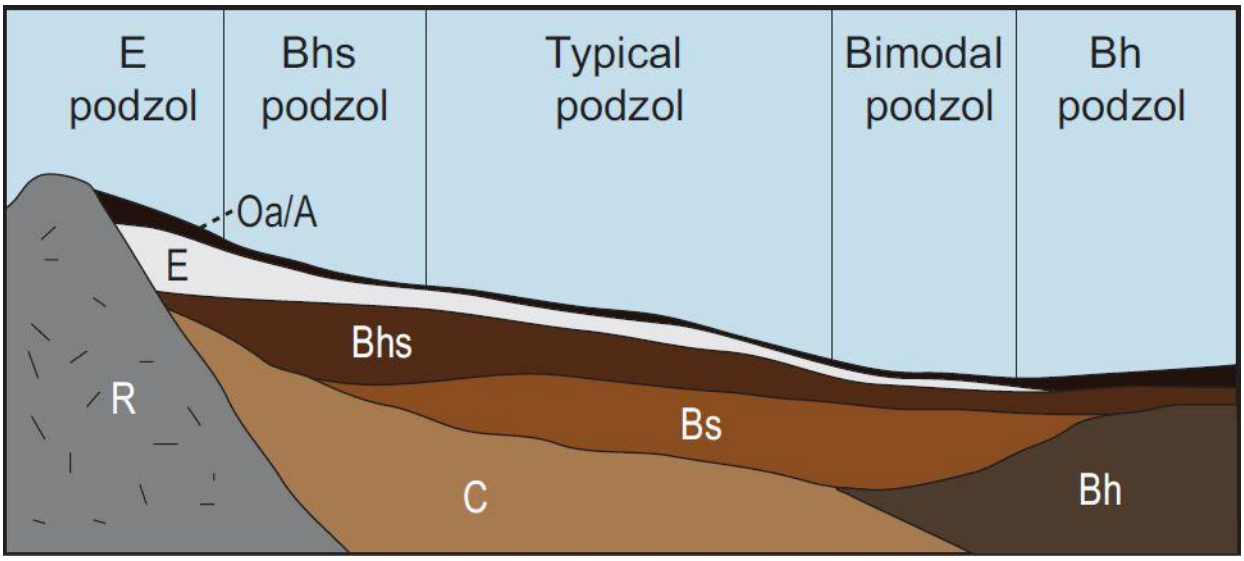

Figure 3.3. Conceptual representation of HPU locations along a hillslope toposequence (after *Bailey et al.*, [in review]). Oa layer is well-decomposed organic material. A horizon is uppermost mineral soil horizon but still contains a substantial amount of organic material. E horizon is mineral soil stripped of organic material by eluviation. Bhs is a mineral horizon containing deposited organic material removed from E layer. Bs is mineral horizon comprised with little organic material. Bh is a mineral horizon with substantial accumulation of organic material (more than Bhs but less than A).

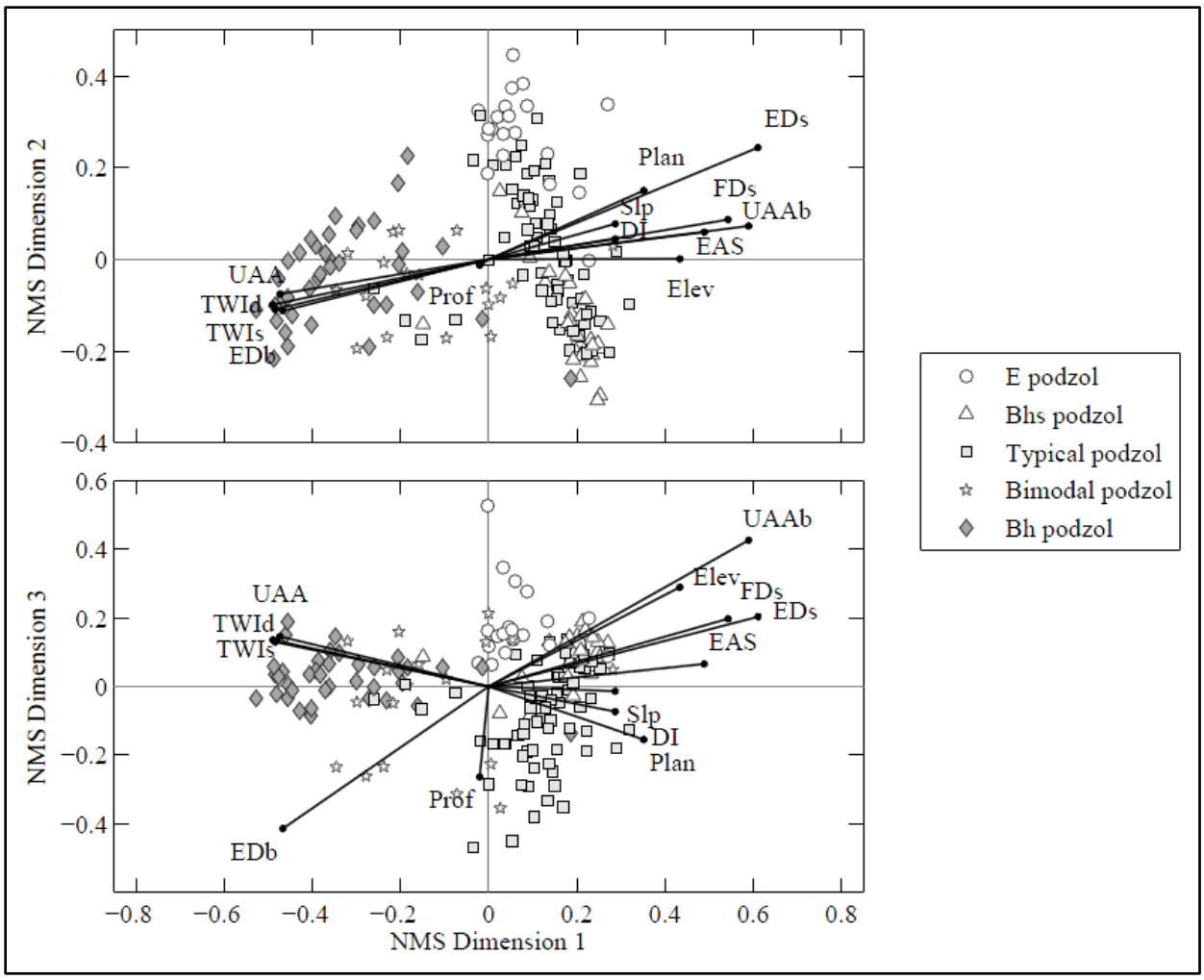

Figure 3.4. NMS ordination using the Bray-Curtis dissimilarity with topographic metrics overlain as Spearman correlates demonstrated clustering of E, Bhs, typical, and Bh podzols. bimodal podzols did not cluster and were excluded from MNR model development.

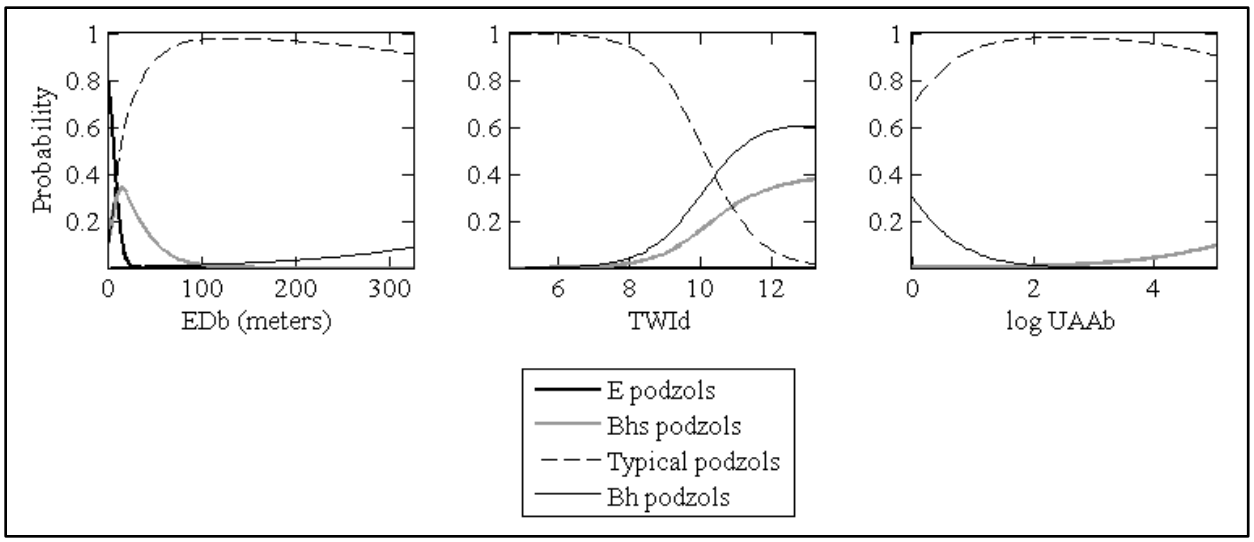

Figure 3.5. MNR probabilities for E, Bhs, typical, and Bh podzols predicted by EAS, EDb, UAA, and TWId. Bimodal podzols were not included in the MNR because NMS ordination indicated they did not correlate with any topographic metrics.

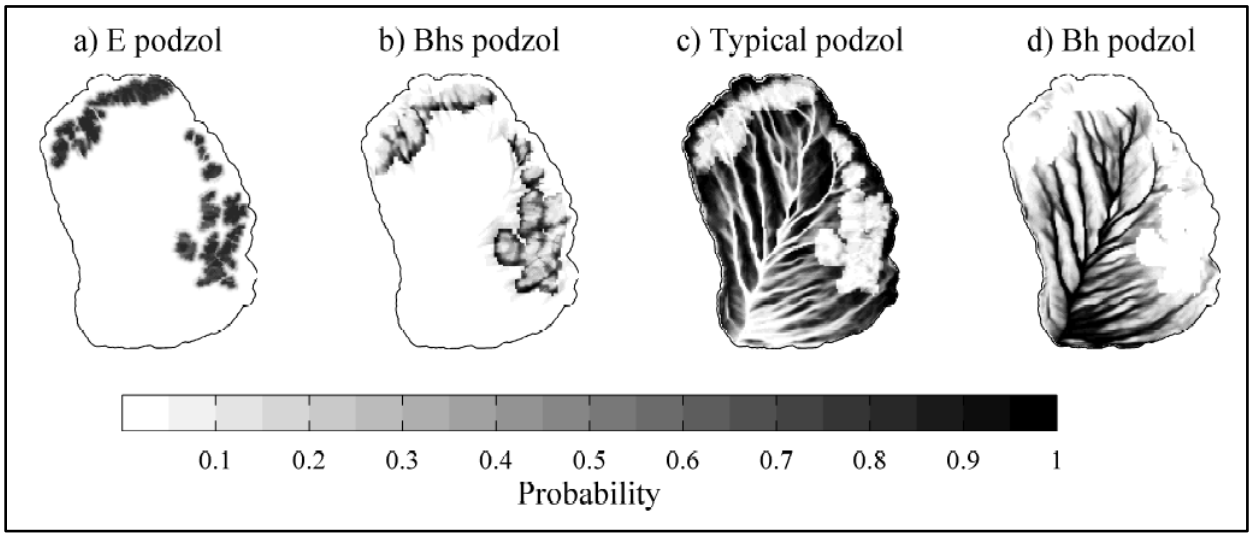

Figure 3.6. Probabilistic HPU maps in WS3 for E, Bhs, typical, and Bh podzols.

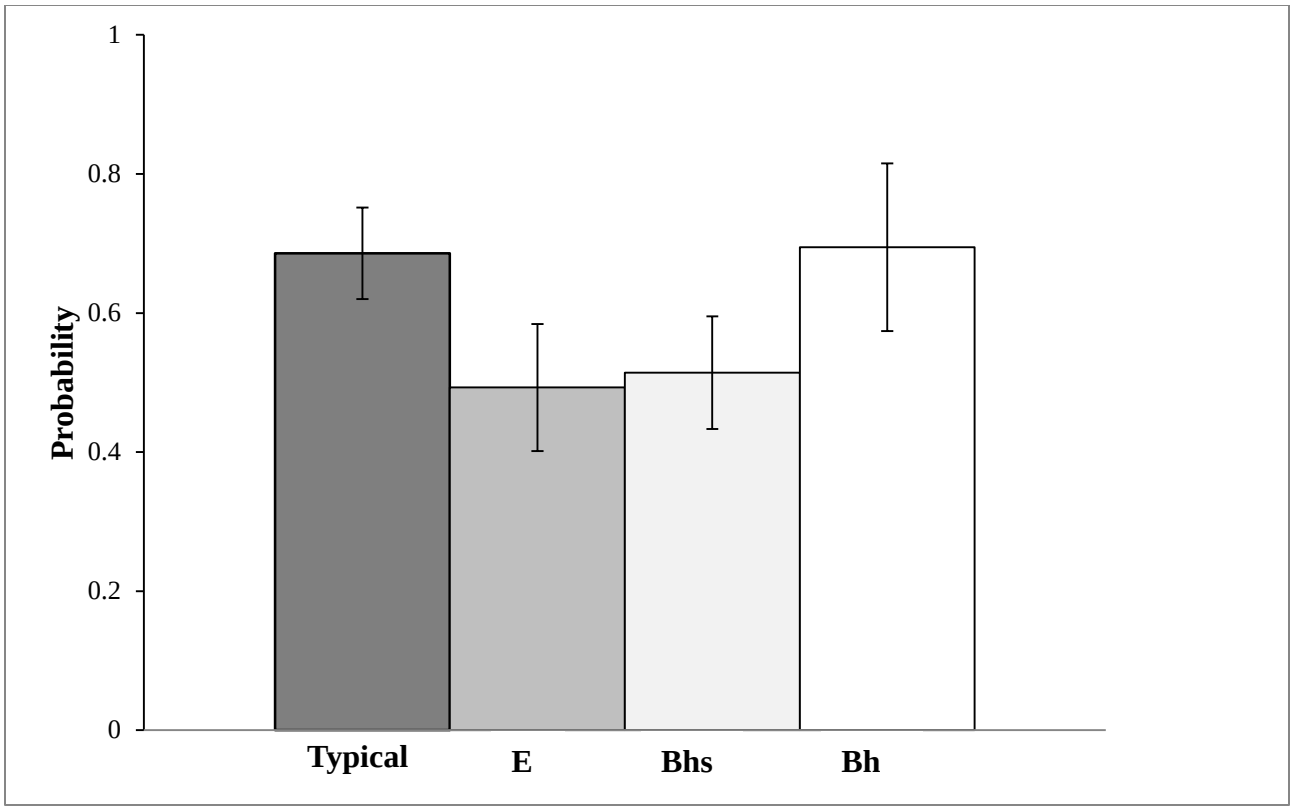

Figure 3.7. Mean probability and standard error for each set of validation HPUs. Validation pedons were excluded during MNR model development. Riparian and hillslope Bh podzols were grouped into a single category.

Classified Data (Mapped)	Reference Data (Field)						
	Typical	E	Bhs	Riparian Bh	Hillslope Bh	Total	User
Typical	44	0	0	7	2	53	0.83
E	0	12	6	0	0	18	0.67
Bhs	8	8	23	0	1	40	0.58
Riparian Bh	11	0	0	23	0	34	0.68
Hillslope Bh	2	0	1	0	5	8	0.63
Total	65	20	30	30	8	153	

Figure 3.8. Model accuracy assessed using an error matrix comparing field-identified HPUs with HPUs classified by the logistic regression model. Reference data refers to field observations and classified data refers to model predictions. Values indicate agreement/disagreement between field observations and model predictions. For instance, 44 pits identified as Typical podzols in the field were also classified as Typical podzols by the model, but 9 were incorrectly classified as Bh podzols. Overall accuracy (sum of correctly mapped HPUs divided by sum of total mapped HPUs) was 0.70.

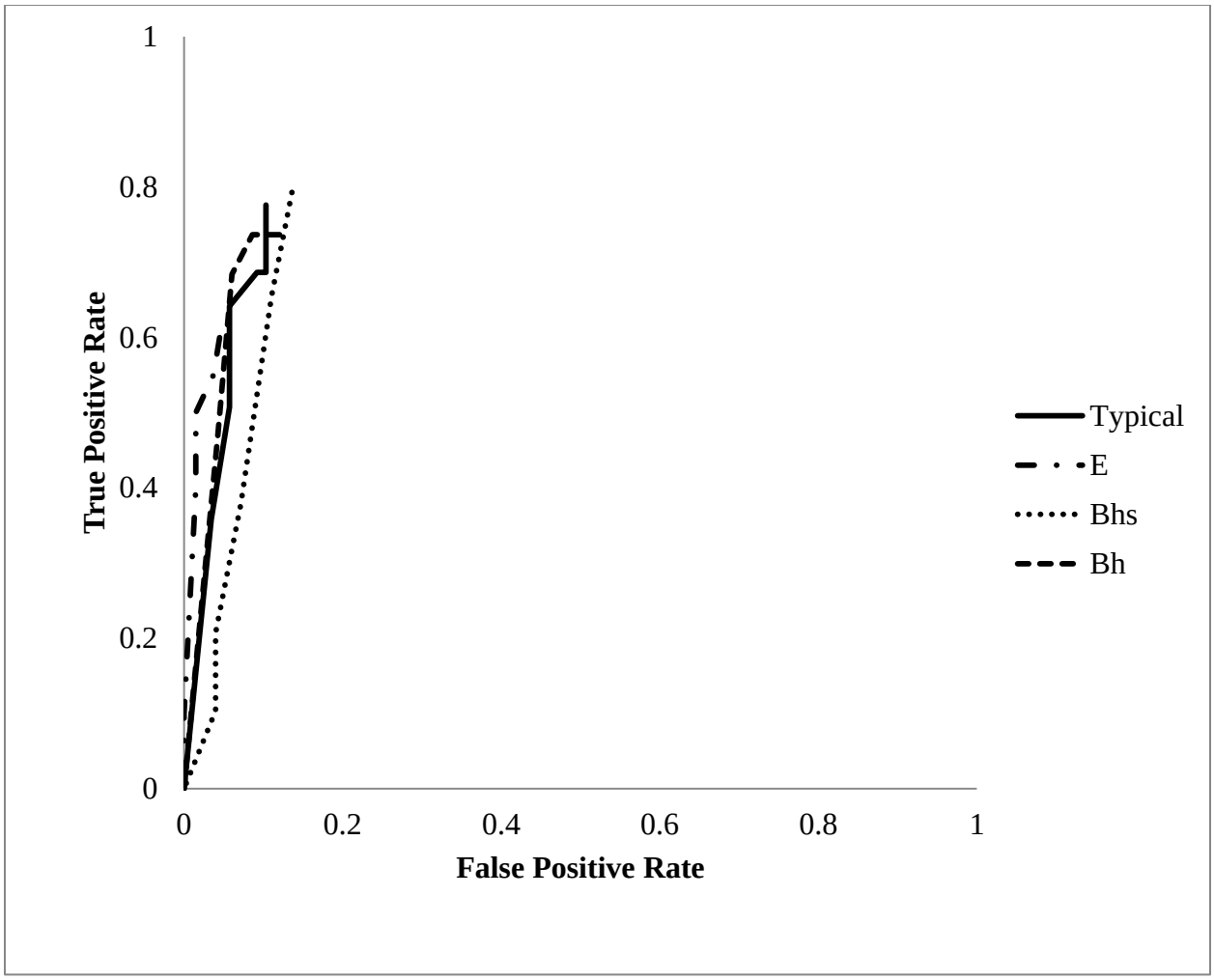

Figure 3.9. ROC curves for typical, E, Bhs, and Bh podzols were generated by computing true positive rate (y-axis) and false positive rate (x-axis) for probability thresholds ranging from 0.20 to 0.80.

3.8. References

Akaike, H. (1973), Information theory and an extension of the maximum likelihood principle, Proceedings of the Second International Symposium on Information Theory, Budapest, 267-281.

Bailey, A. S., J. W. Hornbeck, J. L. Campbell, and C. Eagar (2003), Hydrometeorological database for Hubbard Brook Experimental Forest: 1955-2000Rep., 36 pp, USDA Forest Service, Northeastern Research Station.

Bailey, N., T. Clements, J. T. Lee, and S. Thompson (2003), Modelling soil series data to facilitate targeted habitat restoration: a polytomous logistic regression approach, Journal of Environmental Management, 67, 395-407.

Bailey, S. W., P. A. Brousseau, K. J. McGuire, and D. S. Ross (in review), Influence of hillslope position and shallow water table dynamics on soil development and carbon distribution in a steep, headwater catchment, Geoderma.

Band, L. E., and I. D. Moore (1995), Scale: Landscape attributes and geographical information systems, Hydrological Processes, 9, 401-422.

Barton, C. C., R. H. Camerlo, and S. W. Bailey (1997), Bedrock geologic map of Hubbard Brook Experimental Forest and maps of fractures and geology in roadcuts along Interstate-93, Grafton County, New Hampshire, Sheet 1, Scale 1:12,000; Sheet 002, Scale 001:200, US Geological Survey, Miscellaneous Investigations Series, Map I-2562.

Bray, J. R., and J. T. Curtis (1957), An ordination of upland forest communities of southern Wisconsin, Ecological Monographs, 27, 325-349.

Campling, P., A. Gobin, and J. Feyen (2002), Logistic modeling to spatially predict the probability of soil drainage classes, Soil Science Society of America Journal, 66, 1390-1401.

Clarke, K. R. (1993), Non-parametric multivariate analyses of changes in community structure, Australian Journal of Ecology, 18, 117-143.

Daniels, R. B., S. Gamble, S. Buol, and H. Bailey (1975), Free iron sources in an aquult-udult sequence from North Carolina, Soil Science Society of America Proceedings, 39, 335-340.

Debella-Gilo, M., and B. Etzelmuller (2009), Spatial prediction of soil classes using digital terrain analysis and multinomial logistic regression modeling integrated in GIS: Examples from Vestfold County, Norway, Catena, 77, 8-18.

Detty, J. M., and K. J. McGuire (2010), Threshold changes in storm runoff generation at a till-mantled headwater catchment, Water Resources Research, 46, W07525.

Fahey, T. J., T. G. Siccama, C. T. Driscoll, G. E. Likens, J. L. Campbell, C. E. Johnson, J. J. Battles, J. D. Aber, J. J. Cole, M. C. Fisk, P. M. Groffman, S. P. Hamburg, R. T. Holmes, P. A. Schwarz, and R. D. Yanai, (2005), The biogeochemistry of carbon at Hubbard Brook, Biogeochemistry, 75, 109-176.

Fawcett, T. (2006), An introduction to ROC analysis, Pattern Recognition Letters, 27, 861-874.

Gillin, C. P., K. J. McGuire, S. W. Bailey, and S. P. Prisley (in review), Evaluation of LiDAR-derived DEMs through terrain analysis and field comparison, Photogrammetric Engineering & Remote Sensing.

Guntner, A., J. Seibert, and S. Uhlenbrook (2004), Modeling spatial patterns of saturated areas: An evaluation of different terrain indices, Water Resources Research, 40(5).

Hengl, T., N. Toomanian, H. I. Reuter, and M. J. Malakouti (2007), Methods to interpolate soil categorical variables from profile observations: Lessons from Iran, Geoderma, 140, 417-427.

Hjerdt, K. N. (2004), A new topographic index to quantify downslope controls on local drainage, Water Resources Research, 40, doi: W05602.

Hosmer, D. and S. Lemeshow (2004), Applied logistic regression, Wiley-Interscience, New York.

Huntington, T. G., D. F. Ryan, and S. P. Hamburg (1988), Estimating soil nitrogen and carbon pools in a northern hardwood forest ecosystem, Soil Science Society of America Journal, 52, 1162-1167.

Jenny, H. (1941), Factors of Soil Formation: A System of Quantitative Pedology, 320 pp., McGraw-Hill, New York.

Johnson, C. E., C. T. Driscoll, T. G. Siccama, and G. E. Likens (2000), Element Fluxes and Landscape Position in a Northern Hardwood Forest Watershed Ecosystem, Ecosystems, 3, 159-184.

Kempen, B., D. Brus, G. Heuvelink, and J. Stoorvogel (2009), Updating the 1:50,000 Dutch soil map using legacy soil data: A multinomial logistic regression approach, Geoderma, 151, 311-326.

Knuteson, J., J. Richardson, D. Patterson, and L. Prunty (1989), Pedogenic carbonates in a calciaquoll associated with a recharge wetland, Soil Science Society of America Journal, 53, 495-499.

Lagacherie, P., J. P. Legros, and P. A. Burrough (1995), A soil survey procedure using the knowledge of soil pattern established on a previously mapped reference area, Geoderma, 65, 283-301.

Likens, G. E., and F. H. Bormann (1995), Biogeochemistry of a forested ecosystem, 159 pp., Springer-Verlag, New York.

Lillesand, T. M., and R. W. Kiefer (2000), Remote Sensing and Image Interpretation, Fourth ed., John Wiley and Sons, Inc., New York.

Lin, H. S. (2003), Hydropedology: Bridging disciplines, scales, and data, Vadose Zone Journal, 2, 1-11.

Lin, H. S., J. Bouma, Y. Pachepsky, A. Western, J. Thompson, R. van Genuchten, H. Vogel, and A. Lilly (2006), Hydropedology: Synergistic integration of pedology and hydrology, Water Resources Research, 42, W05301.

McBratney, A. B., M. L. Mendonça Santos, and B. Minasny (2003), On digital soil mapping, Geoderma, 117, 3-52.

McDaniel, P. A., G. R. Bathke, S. W. Buol, D. K. Cassel, and A. L. Falen (1992), Secondary manganese iron ratios as pedochemical indicators of field-scale throughflow water-movement, Soil Science Society of America Journal, 56, 1211-1217.

McDonnell, J. J., et al. (2007), Moving beyond heterogeneity and process complexity: A new vision for watershed hydrology, Water Resources Research, 43, W07301.

Menard, S. (2000), Coefficients of determination for multiple logistic regression analysis, The American Statistician, 54, 17-24.

Merot, P., B. Ezzahar, C. Walter, and P. Aurousseau (1995), Mapping waterlogging of soils using digital terrain models, Hydrological Processes, 9(1), 27-34.

Moore, I. D., P. E. Gessler, G. A. Nielsen, and G. A. Petersen (1993), Soil attribute prediction using terrain analysis, Soil Science Society of America Journal, 57, 443-552.

Moore, M. V., M. L. Pace, J. R. Mather, P. S. Murdoch, R. W. Howarth, C. L. Folt, C. Y. Chen, H. F. Hemond, P. A. Flebbe, and C. T. Driscoll (1997), Potential effects of climate change on freshwater ecosystems of the New England/Mid-Atlantic region, Hydrological Processes, 11, 925-947.

Norris, J. M. (1972), The application of multivariate analysis to soil studies. Soil variation., Journal of Soil Science, 23, 62-75.

Odeh, I., A. McBratney, and D. Chittleborough (1994), Spatial prediction of soil properties from landform attributes derived from a digital elevation model, Geoderma, 63, 197-214.

Odeh, I., A. McBratney, and D. Chittleborough (1995), Further results on prediction of soil properties from terrain attributes: heterotrophic cokriging and regression kriging, Geoderma, 67, 215-226.

Palmer, S. M., C. T. Driscoll, and C. E. Johnson (2004), Long-term trends in soil solution and stream water chemistry at the Hubbard Brook Experimental Forest: relationship with landscape position, Biogeochemistry, 68, 51-70.

Park, S. J., and T. P. Burt (2002), Identification and characterization of pedogeomorphological processes on a hillslope, Soil Science Society of America Journal, 66, 1897-1910.

Pennock, D. J., B. J. Zebarth, and E. Dejong (1987), Landform classification and soil distribution in hummocky terrain, Saskatchewan, Canada, Geoderma, 40, 297-315.

Quinn, P., K. Beven, P. Chevallier, and O. Planchon (1991), The prediction of hillslope flow paths for distriubted hydrological modelling using digital terrain models, Hydrological Processes, 5, 59-79.

Real, R., A. M. Barbosa, and J. M. Vargas (2006), Obtaining environmental favourability functions from logistic regression, Environmental and Ecological Statistics, 13, 237-245.

Sauer, D., H. Sponagel, M. Sommer, L. Giani, R. Jahn, and K. Stahr (2007), Podzol: Soil of the year 2007. A review on its genesis, occurrence, and functions, Journal of Plant Nutrition and Soil Science, 170, 581-597.

Schmidt, J., I. Evans, and J. Brinkmann (2003), Comparison of polynomial models for land surface curvature calculation, International Journal of Geographical Information Science, 17, 797-814.

Seibert, J., and B. L. McGlynn (2007), A new triangular multiple flow direction algorithm for computing upslope areas from gridded digital elevation models, Water Resources Research, 43, W04501.

Sivapalan, M. (2005), Pattern, process and function: elements of a unified theory of hydrology at the catchment scale, in Encyclopedia of Hydrologic Sciences, edited by M. G. Anderson, pp. 193-220, John Wiley and Sons, Inc., Chichester, UK.

Sommer, M., and E. Schlichting (1997), Archetypes of catenas in respect to matter - A concept for structuring and grouping catenas, Geoderma, 76, 1-33.

Sommer, M., D. Halm, U. Weller, M. Zarei, and K. Stahr (2000), Lateral podzolization in a granite landscape, Soil Science Society of America Journal, 64, 1434-1442.

Sorensen, R., and J. Seibert (2007), Effects of DEM resolution on the calculation of topographical indices: TWI and its components, Journal of Hydrology, 347, 79-89.

Travis, M. R., G. H. Elsner, W. D. Iverson, and C. G. Johnson (1975), VIEWIT: computation of seen areas, slope, and aspect for land-use planning, in USDA General Technical Report PSW-11/1975, edited, Berkely, California, USA.

Wang, L., and H. Liu (2006), An efficient method for identifying and filling surface depressions in digital elevation models for hydrologic analysis and modelling, International Journal of Geographical Information Science, 20, 193-213.

Wu, S., J. Li, and G. H. Huang (2008a), A study on DEM-derived primary topographic attributes for hydrologic applications: Sensitivity to elevation data resolution, Applied Geography, 28, 210-223.

Wu, W., Y. Fan, Z. Wang, and H. Liu (2008b), Assessing effects of digital elevation model resolutions on soil–landscape correlations in a hilly area, Agriculture, Ecosystems & Environment, 126, 209-216.

Young, F. J., and R. D. Hammer (2000), Defining geographic soil bodies by landscape position, soil taxonomy, and cluster analysis, Soil Science Society of America Journal, 64, 989-998.

Zaslavsky, D., and A. S. Rogowski (1969), Hydrologic and morphologic implications of anisotropy and infiltration in soil profile development, Soil Science Society of America Proceedings, 33, 594-599.

Zhu, A. X., L. E. Band, B. Dutton, and T. J. Nimlos (1996), Automated soil inference under fuzzy logic, Ecological Modelling, 90, 123-145.

Zimmer, M. A., S. W. Bailey, K. J. McGuire, and T. D. Bullen (2012), Fine scale variations of surface water chemistry in an ephemeral to perennial drainage network, Hydrological Processes, doi: 10.1002/hyp.

Chapter Four

4.0. Conclusions, future research, and implications

Headwater catchments exhibit tremendous heterogeneity and complexity of landscape properties, making prediction of hydrologic and biogeochemical response to natural and anthropogenic forcing an immense challenge. However, researchers argue that there is also structure and organization within the landscape. When understood, landscape structure may help explain catchment complexity and functionality. One useful framework for examining catchment complexity is hydropedology. Research conducted during this study utilized a hydropedological framework for delineating process-based functional soil units, called hydropedological units (HPUs), which are hypothesized to develop as a result of distinct topography and hydrologic flowpaths. Results indicate that HPUs may be predicted and mapped using topographic metrics. HPU maps provide insight into hillslope- and catchment-scale hydrologic flowpaths, subsurface heterogeneities, and offer a more comprehensive picture of biogeochemical functionality of headwater catchments.

4.1. Conclusions: LiDAR and DEM error evaluation

Topographic metrics computed using high-resolution digital elevation models (DEMs) derived from two different light detection and ranging (LiDAR) datasets exhibited similar distribution statistics. Maximum slope values decreased and topographic wetness index values (TWI) (minimum, median, and maximum) increased with DEM coarsening. Plan curvature variance was smaller for DEMs treated with a low-pass filter than for unfiltered DEMs. Distribution statistics tended to stabilize around the 3 m – 5 m transition. Watershed boundaries delineated using DEMs from the different LiDAR datasets were most similar for filtered and unfiltered 3 m and 5 m resolutions, both in terms of morphology and area. Slope values

computed from the different DEMs provided a reasonable estimate of values determined in the field. While the National Center for Airborne Laser Mapping (NCALM) light LiDAR dataset was collected using higher-precision methodology and contains nearly three times the number of ground points per square meter, total station surveys indicated that the White Mountain National Forest (WMNF) dataset suffers from lower error.

This study is the first to assess LiDAR-derived DEMs focusing explicitly on high-resolution data. Results of the investigation highlight two important conclusions. First, filtered and unfiltered 3 m and 5 m DEMs are most suitable for evaluating environmental phenomena related to soils and hydrologic processes. Second, although previous research suggested that higher ground return density yields better accuracy, results from this investigation indicate that LiDAR data with a ground return density of about one point per square meter generated fewer errors than LiDAR data with over three ground returns per square meter.

4.2. Conclusions: Topographic metrics to predict soil spatial patterns

A variety of topographic metrics were computed for a filtered 5 m DEM and were used as independent variables in a multinomial logistic regression (MNR) model predicting the spatial distribution of HPUs. The best metrics for predicting HPUs were Euclidean distance from bedrock, bedrock-weighted upslope accumulated area, and the topographic wetness index using the downslope index for the slope parameter. Typical and Bh podzols were predicted with greater mean probabilities than E and Bhs podzols, likely a result of the smaller spatial extent and greater variability of the later HPU types. Nonetheless, MNR proved a useful tool for predicting soil spatial patterns that will help elucidate hydrological and biogeochemical functionality of headwater catchments. Probabilities may be improved if other ancillary data such as categorical landform classifications are included during MNR model development.

While the model predicted Bh podzols to occur predominately near streams, it also indicated a region of the catchment where they occur away from the mapped stream network (hillslope Bh podzols). These soils share morphological and biogeochemical characteristics with riparian Bh podzols, and the topographic predictor accounting for hillslope Bh podzols is the topographic wetness index. Additionally, flow accumulation and upslope accumulated area indicated a channel network where surface channels are not present but subsurface flow appears high. Morphological and biogeochemical similarity, as well as topographic metric commonality, suggest that hillslope and riparian Bh podzols not be considered distinct HPUs.

4.3. Implications: LiDAR and DEM error evaluation

- Better guidance developed for using high-resolution LiDAR-derived DEMs for examination of fine-scale environmental phenomena
- Potential for cost and time input reduction in LiDAR data collection and processing
- Demonstrated that special care must be taken to select DEM resolution reflecting topographic features affecting hydrologic response when modeling hydrological processes and soil properties

4.4. Implications: Topographic metrics to predict soil spatial patterns

- First demonstration that mapping hydropedological units (HPUs) is possible using only topographic metrics derived from a digital elevation model
- HPU maps can be used to interpret soil biogeochemistry, dominant subsurface flowpaths, and locations where water tables develop seasonally
- HPU maps also suggest that more carbon may be stored in Hubbard Brook Experimental Forest than previously thought, which could be of interest in carbon accounting under a changing climate

4.5. Future Research: LiDAR and DEM error evaluation

- Compare topographic metrics computed using high-resolution DEMs derived from LiDAR data with metrics computed using high-resolution DEMs interpolated from other sources such as aerial photos and topographic maps
- Conduct additional total station surveys in forest clearings to validate finding that clearings suffer fewer interpolation errors than areas with a forest canopy
- Test LiDAR datasets with lower ground return densities than 1.16 points per square meter to identify threshold density that results in a reduction of DEM accuracy
- Perform a similar study on the north-facing slopes of the Hubbard Brook Experimental Forest to determine if aspect and flight pattern interfere with error assessments

4.6. Future research: Topographic metrics to predict soil spatial patterns

- Utilize the Schwarz plots as a set of validation pits for testing the model in areas of the Hubbard Brook Experimental Forest outside of WS3
- Characterize pedons along transects covering the entire Hubbard Brook Valley for use as calibration pedons if necessary
- Incorporate landform classification as categorical predictor variable in MNR model predicting HPU spatial patterns
- Investigate how to reduce the variability of bimodal podzol data so that they may exhibit better clustering in an ordination and thus also correlate with topographic metrics, facilitating their inclusion in models predicting their spatial location
- Calibrate and test the model to different ecoregions to determine the applicability of the hydropedologic framework for evaluating hydropedologic spatial patterns

Appendices

A. Procedure for computing topographic metrics and generating random points

Procedure for Topographic Metric Computation and Random Point Generation to avoid Spatial Autocorrelation using ArcGIS and SAGA Spatial Analysis Software Packages

By Cody Gillin, Spring 2013

Topographic Metric Computation:

1. Convert all DEMs to ASCII in ArcMap
2. Import DEMs to SAGA
3. Fill Sinks (Liu and Wang method which fills depressions but also maintains downward slope to avoid broken channels or disappearance of flow; use smallest gradient allowed)
4. Compute topographic metrics (the following are example metrics used during this study)
    a. Slope (Maximum Slope from Travis et al. 1975)
    b. Plan curvature
    c. UAA (Parallel Catchment Area – Triangular Multiple Flow Direction)
        i. No linear flow
        ii. Set linear flow threshold to value higher than total possible flow for entire catchment to ensure linear flow is not computed
        iii. Leave convergence parameter at default setting (value of 1)
5. Export topographic metric raster layers
6. Give each topographic metric raster layer an appropriate spatial reference using ArcCatalog

Random Point Generation:

1. Use smallest watershed polygon (NCALM 1m) to generate a 20m negative buffer polygon
2. Check to make sure this polygon is fully contained within each regular watershed polygon
3. Determine number of grid cells if each DEM were 10m resolution
    a. Create new “double” field in each watershed polygon
    b. Use “calculate geometry” to determine area in hectares
    c. Create Excel spreadsheet with area values
    d. Use hectare values to compute approximate number of 10m square grid cells
    e. Find mean of 10m square grid cells for each DEM
    f. Use “create random points” tool to generate random points totaling 10% of value determined in 3e; use polygon created in 1 for extent in random point generation so all points are contained within each DEM

B. R pseudo code for projecting total station survey points

```
##import data
#data to be imported: horizontal angle and horizontal distance total station measurements for all
        total station survey points

#indicate benchmark location (location where total station machine was located during survey)
benchx <- 281577.47843
benchy <- 4870278.83859

#set x and y coordinate variables at 0,0 to center data at the origin of an XY plane
xcoord <- 0.0
ycoord <- 0.0

#set horizontal angle adjustment according to local magnetic declination where survey was
conducted
angle <- angle +/- #(insert angle here)
angle[angle>360] <- angle - 360
angle[angle<0] <- angle + 360

#locate total station survey points in XY plane according to quadrant and convert to radians
for (x in 1:max(point)){
        if (angle[x] > 0 & angle[x] < 90)
        {
                angle[x] <- angle[x] * pi/180 #radians
                xcoord[x] <- dist[x] * sin(angle[x])
                ycoord[x] <- sqrt(dist[x]^2 - xcoord[x]^2)

                xcoord[x] <- benchx + xcoord[x]
                ycoord[x] <- benchy + ycoord[x]
        }

        if (angle[x] > 90 & angle[x] < 180)
        {
                angle[x] <- angle[x] * pi/180 #radians
                xcoord[x] <- dist[x] * sin(angle[x])
                ycoord[x] <- sqrt(dist[x]^2 - xcoord[x]^2)

                xcoord[x] <- benchx + xcoord[x]
                ycoord[x] <- benchy - ycoord[x]
        }
```

```
        if (angle[x] > 180 & angle[x] < 270)
        {
                angle[x] <- angle[x] * pi/180 #radians
                xcoord[x] <- dist[x] * sin(angle[x])
                ycoord[x] <- sqrt(dist[x]^2 - xcoord[x]^2)

                xcoord[x] <- benchx - xcoord[x]
                ycoord[x] <- benchy - ycoord[x]
        }

        if (angle[x] > 270 & angle[x] < 360)
        {
                angle[x] <- angle[x] * pi/180 #radians
                xcoord[x] <- dist[x] * sin(angle[x])
                ycoord[x] <- sqrt(dist[x]^2 - xcoord[x]^2)

                xcoord[x] <- benchx - xcoord[x]
                ycoord[x] <- benchy + ycoord[x]
        }
}

#combine total station survey locations, now in radian values, into locational pairs
coords <- cbind(xcoord,ycoord)

#set the column names for the newly created coordinate pairs as X and Y
colnames(coords) <- c("X","Y")

#plot the total station survey coordinates and place a point for the total station machine
plot(xcoord,ycoord)
points(benchx,benchy,col="green")
```

C. Morphology and landscape position of HPUs identified in WS3

HPU ID	Description	Landscape Position
E podzol	Shallow greyish-colored soils dominated by an eluvial horizon (E – mineral particles stripped of organic matter, Fe, and Al)	Within and immediately downslope of areas of bedrock outcrops
Bhs podzol	Soils dominated by a brownish-colored illuvial horizon (Bhs – depositon of organic–Fe–Al complexes on mineral surfaces)	Immediately downslope of E podzols, near bedrock outcrops
Typical podzol	Deeper soils with thin E and Bhs horizons	Dominant in the portions of the catchment, with deeper glacial drift; typical of backslopes
Bimodal podzol	Deeper soils with a typical (thin E and Bhs) upper sequence and a zone of organic matter illuviation at the B/C interface	Breaks of slope (concave hillslope positions) and footslopes
Bh podzol	Dominated by dark brown or blackish-colored Bh horizons (accumulated organic material) typically lacking E and Bhs horizons	Toeslopes and streamside

D. Matlab pseudo code for NMS ordination and Spearman correlate biplot

```
%% import data
% data to be imported: soil horizon thickness (Oi/Oe/Oa combined, Oa, A, E, Bhs, Bh, Bs) as
        well as HPU type and coded numerical value for all soil pits

%% NMS computation:
% compute pairwise distances:
dis = f_dis(b,'bc'); % use Bray-Curtis (1957) or Euclidean distances from the FATHOM ver 2012

% use non-metric scaling to recreate data in 2D
mds = f_nmds(dis,3,1,1); % is essentially the same as Matlab's [Y,STRESS] = mdscale(dis,2);

%create biplot and correlation vectors
[biplot_Data,R12] = f_biplotEnv2_ver2([mds.scores(:,1)
mds.scores(:,2)],vars,1,perm,scale,offset,labels);
```

E. Matlab pseudo code for MNR model predicting HPU probabilities

```
% import data
% data to be imported: file where Typicals are given the largest class which makes MNR results
        relative to Typicals)
% data to be imported: file containing topographic metric values, HPU type, and coded HPU
        numerical value for all soil pits desired for MNR model development

% Run multinomial regression (MNR) and compute odds ratios
[B,dev,stats] = mnrfit(X,Y,'model','nominal');

% Calculation of odds ratio, Log-likelihoods, and other stats
[B0,dev0]       = mnrfit([],Y,'model','nominal');     %reduced or null model for testing
stats2.z        = stats.beta./stats.se;               %z values
stats2.OR       = exp(stats.beta); stats2.OR(1,:) = zeros(size(stats2.OR(1,:))); %odds ratios
stats2.OR_L     = exp(stats.beta-stats.se); stats2.OR_L(1,:) = zeros(size(stats2.OR_L(1,:)));
stats2.OR_U     = exp(stats.beta+stats.se); stats2.OR_U(1,:) = zeros(size(stats2.OR_U(1,:)));
stats2.LLnull   = -dev0/2;                            %Log-likelihood for null model (only the constant)
stats2.LLfull   = -dev/2;                             %Log-likelihood for full model
stats2.LRT      = -2*stats2.LLnull + 2*stats2.LLfull; %Likelihood ratio test, chi sq tested
stats2.df       = nX*(ymax-1);                        %degrees of freedom
stats2.pval     = 1-chi2cdf(stats2.LRT,stats2.df);    %p-value for LRT
stats2.McFaddensR2 = 1- stats2.LLfull/stats2.LLnull;  %McFadden's pseudo R-sq
stats2.AIC      = -2*stats2.LLfull + 2*stats2.df;     %Akaike Information Criterion

% Predict probabilities for each HPU type (phat)
[phat,DLO,DHI] = mnrval(B,X,[],stats); %with confidence limits on predicted probabilities
```